isvr Institute of Sound and Vibration Research

Driving Point and Transfer Mobility Matrices for Thin Plates Excited in Flexure

P. Gardonio and S.J. Elliott

ISVR Technical Report No 277

August 1998

University of Southampton

SCIENTIFIC PUBLICATIONS BY THE ISVR

Technical Reports are published to promote timely dissemination of research results by ISVR personnel. This medium permits more detailed presentation than is usually acceptable for scientific journals. Responsibility for both the content and any opinions expressed rests entirely with the author(s).

Technical Memoranda are produced to enable the early or preliminary release of information by ISVR personnel where such release is deemed to the appropriate. Information contained in these memoranda may be incomplete, or form part of a continuing programme; this should be borne in mind when using or quoting from these documents.

Contract Reports are produced to record the results of scientific work carried out for sponsors, under contract. The ISVR treats these reports as confidential to sponsors and does not make them available for general circulation. Individual sponsors may, however, authorize subsequent release of the material.

UNIVERSITY OF SOUTHAMPTON

INSTITUTE OF SOUND AND VIBRATION RESEARCH

SIGNAL PROCESSING & CONTROL GROUP

Driving Point and Transfer Mobility Matrices for Thin Plates Excited in Flexure

by

P. Gardonio and S.J. Elliott

ISVR Technical Report No. 277

August 1998

Authorised for issue by
Prof S J Elliott
Group Chairman

ABSTRACT

In this report a methodical presentation of mobility functions for thin plates excited in flexure is given. Both driving point and transfer mobilities are analysed considering either infinite or finite plates. The mobilities related to all kinematic (linear and angular velocities) and to all dynamic (force and moment excitations) parameters are considered. The matrix representation for a single point connection or for a multiple point connection plate system is also given. The main properties of the driving-point and transfer mobility matrices are analysed and it is shown that: the driving point mobility of an infinite plate gives approximately the mean response of the driving point mobility of a finite rectangular plate; the driving point mobility matrix of an infinite plate is a 3×3 *diagonal matrix while the driving point mobility matrix of a finite rectangular plate is a fully populated* 3×3 *matrix except in the particular case of considering the centre position of the plate in which case also for a finite plate the driving point mobility matrix is diagonal; the real part of the diagonal terms of the driving point mobility matrix of a finite rectangular plate are all positive; for reciprocity, if the system is linear, the transfer matrix between position* P_1 *and* P_2 *is equal to the transpose of the transfer mobility matrix between positions* P_2 *and* P_1 *and finally as a consequence of point c and d the driving point or driving multi-point mobility matrix is positive definite.*

INDEX

1. INTRODUCTION

Seismic vibration - structure borne sound

The vibration analysis of a mechanical system is usually classified in two categories: first, the "mechanical or seismic vibration" field and, second, the "structure borne sound" field [1]. The structure borne sound field deals with the generation and propagation of very small time-wise varying motions and forces in a solid body and with the radiated sound in the medium surrounding the solid body. This type of vibration is defined for periodic motions occurring in a frequency range between 16 and 16.000 Hz: the audible frequency range. In the majority of cases the study of structure borne sound transmission is related to problems of noise control, radiation of sound in water and "sonic" structural fatigue. Studies of engineering materials or musical instruments are more rare. Alternatively the mechanical vibration field deals with periodic vibrations at frequencies lower than 16 Hz. However, in many cases vibrations of mechanical systems occurring at relatively low frequencies, below 100 Hz, are also treated as seismic vibrations so that the system is modelled with a finite number of lumped elements (springs, rigid masses and dissipative elements).

Time-variation response to harmonic, periodic and transient excitations

When the excitation of the system is harmonic the system response is characterised by a transient part where the response is composed by an harmonic function that decays exponentially with time and by an harmonic function with constant amplitude. After a period of time the first component can be neglected and the steady-state response is then given only by the harmonic function with constant amplitude. If the harmonic excitations have the form $F(t) = \mathrm{Re}\{F_o \exp(j\omega t)\}$, where ω is the circular frequency, than the steady state response is also harmonic so that the displacement could be written as: $x(t) = \mathrm{Re}\{x_o \exp(j\omega t)\}$ where x_o is complex. The displacement $x(t)$ is related to the harmonic excitation via a linear relation of the following form [2,3]:

$$x(t) = \mathrm{Re}\{\alpha(\omega) F_o e^{j\omega t}\} \tag{1.1}$$

where $\alpha(\omega)$ is a complex function of frequency called the frequency response function (FRF) of the system that in this particular case is the system receptance (for more details see the following references: [4] sec. 1.5, [5] sec. 2.1, [2] sec. 3.5).

In many cases the excitation acting on the mechanical system is periodic with period T but not harmonic. In this case the excitation can be regarded as a summation of an infinite number of harmonic functions, whose circular frequency is an integer multiple of the fundamental one $\omega_n = n\omega_o = 2n\pi/T$, by means of a *Fourier series* $f(t) = \sum_{-\infty}^{+\infty} F_n \exp(jn\omega_o t)$ ([6] Ch. 7, pp 367-370). The steady-state response of a linear system can therefore be found by superposing the harmonic responses due to each of the exciting harmonic forces so that ([5] Sec2.9 pp 75-76 [6] Sec. 7.6, Examples 1 and 2 pp 370-374):

$$x(t) = \mathrm{Re}\left\{\sum_{n=-\infty}^{+\infty} \alpha_n(\omega) F_n e^{jn\omega_o t}\right\} \tag{1.2}$$

Even if the time variation of the excitation is not periodic the response of a linear system to that type of forcing can be treated as a superposition of an infinite continuous number of harmonic motions. In this case the Fourier series of the excitation is replaced by an integration

of harmonic motions by means of a *Fourier integral* $f(t)=\int_{-\infty}^{+\infty}F(\omega)\exp(j\omega t)d\omega$ ([6] Ch. 7 pp 380-388). The Fourier integral represents a continuous function in the frequency domain also called *spectrum* since it provides a measure of the intensity of f in the frequency interval between ω and $\omega+d\omega$. In this case the system response is not periodic and depend on the forcing variation in time although still it is characterised by the appropriate system frequency response function $\alpha(\omega)=X(\omega)/F(\omega)$ where $X(\omega)$ is the Fourier transform of the response $x(t)$ ([5] Sec2.9 pp 76-77 [6] Sec. 7.8 Example 1 pp 390-392):

$$x(t)=\mathrm{Re}\left\{\int_{-\infty}^{+\infty}\alpha(\omega)F(\omega)\cdot e^{j\omega t}d\omega\right\} \tag{1.3}$$

From this brief description of the three typical problems of forced vibration the picture that can be drawn is that the frequency response function of a mechanical system gives a lot of information about the vibration dynamics of a mechanical system apart from the type of excitation to which the system is forced. Most of the engineering vibration problems are therefore studied by considering the frequency response function rather than deriving the response of the system for a specific type of excitation. In the case of transient excitations, the specific effects on the response of the excitation time history are evaluated independently to the real system dynamics by considering the maximum peak response of a single degree of freedom oscillator as a function of the natural frequency of the oscillator itself, i.e. by considering the *response spectrum* [2] sec. 4.6.

Frequency Response Function forms

The frequency response function can assume different formats depending on the variable used to describe the response of the mechanical system: displacement, velocity or acceleration. For each of the defined frequency response functions it is possible to derive the inverse function which could also be defined as a frequency response function although these latter formats are discouraged as they can generate some confusion when muti-degrees-of-freedom systems are considered. The following table summarises the three standard definitions of frequency response function and the equivalent inverse functions.

Response Parameter	Standard Frequency Response Function		Inverse Frequency Response Function	
	Formula	Name	Formula	Name
displacement	$\alpha(\omega)=\frac{\tilde{x}(\omega)}{\tilde{F}(\omega)}$	Receptance Admittance Compliance Dynamic flexibility	$K(\omega)=\frac{\tilde{F}(\omega)}{\tilde{x}(\omega)}$	Dynamic stiffness
velocity	$Y(\omega)=\frac{\dot{\tilde{x}}(\omega)}{\tilde{F}(\omega)}$	Mobility	$Z(\omega)=\frac{\tilde{F}(\omega)}{\dot{\tilde{x}}(\omega)}$	Mechanical impedance
acceleration	$A(\omega)=\frac{\ddot{\tilde{x}}(\omega)}{\tilde{F}(\omega)}$	Inertance Accelerance	$M(\omega)=\frac{\tilde{F}(\omega)}{\ddot{\tilde{x}}(\omega)}$	Apparent mass

Mechanical-electrical analogies - Network theory

The vibration analysis of mechanical systems is also characterised by the geometry of the system. In general, the vibration analysis of complex mechanical structures is reduced to the analysis of a network of flexible elements connected at point-, line- or surface-junctions. The analysis is therefore reduced to two problems. First, the definition of the differential equation of motion of each element of the mechanical system at the junction points and at eventual positions of interest due to both the external excitations acting on the element (known parameters) and the reactive excitations produced by the elements directly connected to that under consideration (unknown parameters). Second, using the *equilibrium* and *compatibility* conditions at the junction positions, a system of equation is built from which the response of the entire system can be derived.

Thus, the vibration study of a mechanical system is reduced to the vibration analysis of basic elements which are usually classified depending on their geometry. The most common structural elements are beams, plates and shell of various shapes (cylinders, spheres etc.). For these types of structures, the structure borne sound vibration is studied in terms of wave types that characterise the element motion. For example, for beams three types of waves are defined: first, longitudinal waves; second, torsional waves and third, bending waves. The study of the wave types associated with the aforementioned basic type of structure has been widely studied in the past and books are now available on the topic (see for example references [1,7,8,9]).

As discussed in the paragraph above the vibration of a mechanical system is usually studied in terms of its frequency response function; in this particular case the vibration analysis can follow a pre-defined standard approach which is based on the mechanical-electrical analogy method formulated by Firestone [Firestone 10,11,12]. This method consists of the following three steps.

- First, the mechanical system is divided into sub-systems that could be considered as "black boxes" with a number of terminals that identify the position and direction of all junctions dynamic parameters (force and moment excitations) and the corresponding kinematic parameters (linear and angular displacements or velocities or accelerations).
- Second, for each "black box" an immittance or transfer matrix [13-18] that relates the terminals variables is defined.
- Third, the "equivalent mechanical circuit" of the mechanical problem to be solved is drawn. In this way the vibration problem is reduced to a form similar to that of electrical circuits so that the system response to the primary excitations can be found by applying similar principles to those used in the electrical networks theory [19,20] (Kirchhoff's laws, superposition theorem, reciprocity theorem, Thévenin's and Norton's equivalent systems reductions).

This approach has been widely studied during the last 50 years [4,18,19,20] particularly with reference to seismic vibrational problems where the elements comprising the mechanical system can be modelled as lumped sub-systems.

The method is however not well developed with reference to problems of structure borne sound vibrations. First of all there is a lack of frequency response function formulations for distributed systems. Bishop and Johnson's book [4] presents a methodical formulation of frequency response functions in terms of receptances for finite length beams. Cremer et al [1] gives instead the frequency response functions for infinite beams in terms of mobilities. Moving to plate or shells, Soedel [21] has presented a general theory from which it is possible to derive the frequency response function for plates and shells. However no specific formulae of frequency response functions are derived for the most common types of plate or shell structures. For plate and shell structures the best reference giving frequency response functions of infinite structures is the book written by Cremer at al [1].

It is then possible to find short sections of books or reports (see for example ch. 26 of [22]) or technical reports (see for example [23] and [24]) that give some formulae for the driving point frequency response functions of specific structures.

In this report an attempt is made to give a systematic presentation of frequency response functions for thin plates excited in flexure. The frequency response functions are expressed in terms of mobilities. Both driving point and transfer mobilities are analysed considering either infinite or finite plates. The mobilities related to all kinematic (linear and angular velocities) and to all dynamic (force and moment excitations) parameters are considered. The matrix representation for a single point connection or for a multiple point connection plate system is also given and the main properties of driving point and transfer mobilities are examined.

2. MOBILITY FORMULAE FOR AN INFINITE PLATE EXCITED IN FLEXURE

2.1. Driving-point and transfer mobilities

When an infinite plate is excited in flexure four different types of mechanical mobilities could be defined in a similar way as in reference [1] (p 312). Figure 1 shows the vector notation used for the kinematics (translational w and angular θ_u displacements) and dynamics (force N_z and moment M_u excitations) parameters related to bending waves at two generic positions $P_1 = (x_1, y_1)$ and $P_2 = (x_2, y_2)$. These positions are defined considering a right handed Cartesian co-ordinate[1] main system of reference (o,x,y,z) which has the z axis orthogonal to the surface of the plate.

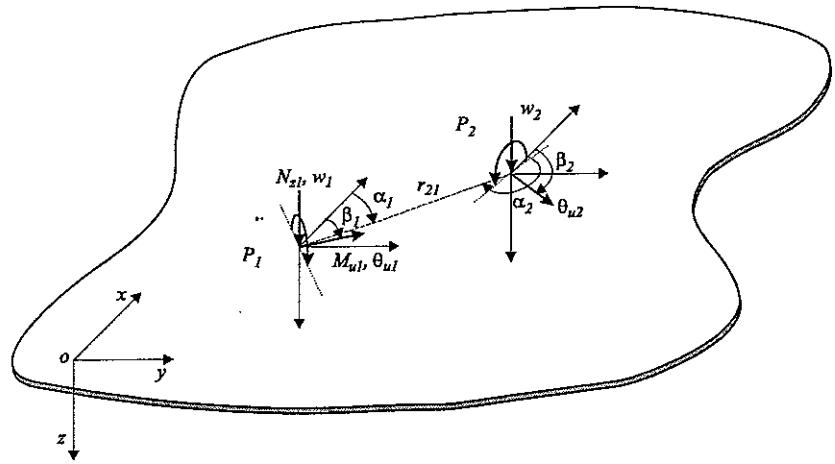

Fig. 1: *Notation of the displacement w and rotation θ_u at positions P_1 and P_2 when a plate is excited in flexure by a point force N_z and point moment M_u at position P_1.*

A flexural wave in an infinite plate can be generated at a specific point $P_1 = (x_1, y_1)$ by two independent types of excitations: first, a force $N_{z1}(t)$ in the z direction and second, a moment $M_{u1}(t)$ with the u_1 direction[2] in the plane of the plate (the u_1 direction is defined by the angle β_1 as shown in figure 1). If these two excitations are harmonic with time dependence of the form $\exp(j\omega t)$, where ω is the circular frequency, they can be represented by the real part of the phasors[3]

$$N_{z1}(t) = \mathrm{Re}\left\{\tilde{N}_{z1}(\omega)e^{j\omega t}\right\}, \qquad M_{u1}(t) = \mathrm{Re}\left\{\tilde{M}_{u1}(\omega)e^{j\omega t}\right\}. \tag{2.1,2}$$

When the infinite plate is excited by the harmonic force $N_{z1}(t)$ or by the harmonic moment $M_{u1}(t)$ the plate motion at the excitation position P_1 is equally harmonic and it can be

---

[1] According to reference [25] (p 443) a **Cartesian co-ordinate** system is called **right-handed** when the corresponding unit vectors **i**, **j**, **k** in the positive directions of the axes form a right-handed triple. Also from reference [25], a right-handed triple of vectors **i**, **j**, **k** is one in which the vectors assume, in the order given, the same sort of orientation as the index, middle finger and thumb, of the right hand when these three fingers are held in such a way to be orthogonal to each others.

[2] In reference [26] (p 237) the **positive direction** of a **moment** is defined as the direction to which points the thumb of the right hand when the fingers are curved in the direction of the rotation produced by applying the moment (right hand's rule).

[3] Neubert [18] describe a *phasor* as: "*a special vector in the complex plane having constant magnitude, with its tail anchored at the origin and rotating counter clockwise with angular velocity* ω".

represented respectively by the real part of the phasor of the translational velocity in the z direction and the real part of the phasors of the angular velocity in the u_1 direction[4]

$$\dot{w}_1(t) = \mathrm{Re}\left\{\tilde{\dot{w}}_1(\omega)e^{j\omega t}\right\}, \qquad \dot{\theta}_{u1}(t) = \mathrm{Re}\left\{\tilde{\dot{\theta}}_{u1}(\omega)e^{j\omega t}\right\}. \tag{2.3,4}$$

The force/moment excitation parameters $\tilde{N}_{z1}(\omega)$, $\tilde{M}_{u1}(\omega)$, and the linear/angular velocity parameters $\tilde{\dot{w}}_1(\omega)$, $\tilde{\dot{\theta}}_{u1}(\omega)$ are all complex numbers whose absolute values and phases denote respectively the amplitude and phase of the harmonic variation in time at the driving frequency ω. Considering the four parameters of equations 1 to 4, two *mechanical driving-point mobilities* could be defined as follow [1,24]:

$$Y^{11}_{wN_z}(\omega) = \frac{\tilde{\dot{w}}_1(\omega)}{\tilde{N}_{z1}(\omega)} \qquad Y^{11}_{\theta_u M_u}(\omega) = \frac{\tilde{\dot{\theta}}_{u1}(\omega)}{\tilde{M}_{u1}(\omega)}\ , \tag{2.5,6}$$

where the superscript "11" indicates that both the excitations and the velocities are taken at position $P_1 = (x_1, y_1)$. These driving-point mobilities are grouped together in a 2×2 *driving-point mobility matrix* $\mathbf{Y}^{11}(\omega)$ of the form [1,15,19]

$$\mathbf{Y}^{11}(\omega) = \begin{bmatrix} Y^{11}_{wN_z}(\omega) & 0 \\ 0 & Y^{11}_{\theta_u M_u}(\omega) \end{bmatrix} \tag{2.7}$$

so that the vector $\mathbf{v}_1(\omega) = \left\{\tilde{\dot{w}}_1(\omega) \quad \tilde{\dot{\theta}}_{u1}(\omega)\right\}^T$ is related to the vector $\mathbf{f}_1(\omega) = \left\{\tilde{N}_{z1}(\omega) \quad \tilde{M}_{u1}(\omega)\right\}^T$ by the driving-point mobility matrix as follow [1,15,19]

$$\mathbf{v}_1(\omega) = \mathbf{Y}^{11}(\omega)\cdot\mathbf{f}_1(\omega). \tag{2.8}$$

If the kinematic parameters (translational and angular velocity) are taken at position $P_2 = (x_2, y_2)$ four *mechanical transfer mobilities* could be then defined as follow [1,24]:

$$Y^{21}_{wN_z}(\omega) = \left.\frac{\tilde{\dot{w}}_2(\omega)}{\tilde{N}_{z1}(\omega)}\right|_{M_u=0} \qquad Y^{21}_{wM_u}(\omega) = \left.\frac{\tilde{\dot{w}}_2(\omega)}{\tilde{M}_{u1}(\omega)}\right|_{N_z=0}$$
$$Y^{21}_{\theta_u N_z}(\omega) = \left.\frac{\tilde{\dot{\theta}}_{u2}(\omega)}{\tilde{N}_{z1}(\omega)}\right|_{M_u=0} \qquad Y^{21}_{\theta_u M_u}(\omega) = \left.\frac{\tilde{\dot{\theta}}_{u2}(\omega)}{\tilde{M}_{u1}(\omega)}\right|_{N_z=0} \tag{2.9-12}$$

where the u_2 direction is defined by the angle β_2 as it is shown in figure 1. These four mobility terms could be grouped in a new mobility matrix $\mathbf{Y}^{21}(\omega)$ which is called the *transfer mobility matrix* [1,15,19]:

[4] Reference [26] (pp 237) defines the **positive direction** of an **angular velocity** along the axis of rotation in the direction of progression of a right-handed screw turned in the same way as that produced by the angular velocity.

$$\mathbf{Y}^{21}(\omega)=\begin{bmatrix} Y^{21}_{wN_z}(\omega) & Y^{21}_{wM_u}(\omega) \\ Y^{21}_{\theta_u N_z}(\omega) & Y^{21}_{\theta_u M_u}(\omega) \end{bmatrix}, \tag{2.13}$$

so that the velocity vector $\mathbf{v}_2(\omega)=\left\{\dot{\tilde{w}}_2(\omega) \quad \dot{\tilde{\theta}}_{u2}(\omega)\right\}^T$ is related to the vector of forces $\mathbf{f}_1(\omega)$ in the following way:

$$\mathbf{v}_2(\omega)=\mathbf{Y}^{21}(\omega)\cdot\mathbf{f}_1(\omega). \tag{2.14}$$

It is important to underline that the four transfer mobilities of equations (2.9) to (2.12) are defined for either a point force N_{z1} excitation when the moment M_{u1} is set to zero or for a point moment M_{u1} excitation when the force N_{z1} is set to zero [18]. The definition of the driving point mobilities in equations (2.5) and (2.6) has not specified this condition simply because the force N_{z1} or moment M_{u1} excitations do not produce respectively angular $\dot{\theta}_{u1}$ or linear $\dot{w}_1$ velocities at the excitation position P_1 [1,24]. This is a peculiar characteristic of the bending wave in an infinite plate that implies a diagonal driving point mobility matrix.

In the following sub-sections the formulae for the *mechanical driving-point* and *transfer mobilities* are derived for thin plates excited by a force or moment acting on a small rigid indenter with a circle base of radius a fixed to the plate.

2.2. Linear and angular velocities of bending waves generated by an out-of-plane force acting on a small rigid indenter fixed to an infinite thin plate

Flexural waves in a thin plate excited by a uniform distributed force $p_z(x,y,t)$ over the plate surface are described by a 4th order wave equation of the form [1] (p 286)

$$B\left(\frac{\partial^4 w}{\partial x^4}+2\frac{\partial^4 w}{\partial x^2\partial y^2}+\frac{\partial^4 w}{\partial y^4}\right)+m\frac{\partial^2 w}{\partial t^2}=-p_z(x,y,t). \tag{2.15}$$

where $B=EI/(1-\nu^2)$ is the bending stiffness, E is the Young's modulus of elasticity, ν is the Poisson ratio and $I=h^3/12$ is the cross sectional area moment of inertia. h is the thickness of the plate, $m=\rho h$ is the mass per unit area and ρ is the density of the material. Equation (2.15) is valid for plates whose thickness is much smaller than the bending wavelength. Also, equation (15) does not account for the effects produced by internal shear stress and rotary inertia component.

If the plate is excited by an harmonic point force excitation $N_z(t)=\mathrm{Re}\left\{\tilde{N}_z(\omega)e^{j\omega t}\right\}$, the steady state[5] linear velocity $\dot{w}(t)$ can be derived from equation (2.15) by considering the following boundary conditions [1] (pp 286-290):

- a the out-of-plane displacement w must be axially symmetric;
- b at the excitation point, the angular displacements θ must vanish;
- c at the excitation point the sum of the shear forces must be equal to the exciting force N_z;
- d the solution must satisfy the Sommerfeld "radiation condition", so that the displacements at large distances from the excitation point must behave like a decaying wave.

[5] The steady state response of a system harmonically excited does not account for the onset of vibrations (the transient part) induced by the excitation.

A possible set of solutions that satisfy equation (2.15) and the boundary conditions *a* to *d* is given by zero-order cylindrical functions; therefore, it has been chosen to formulate the solution of the problem in terms of a cylindrical system of co-ordinates (o,r,α,z), assuming the origin "o" coincident to the excitation point.

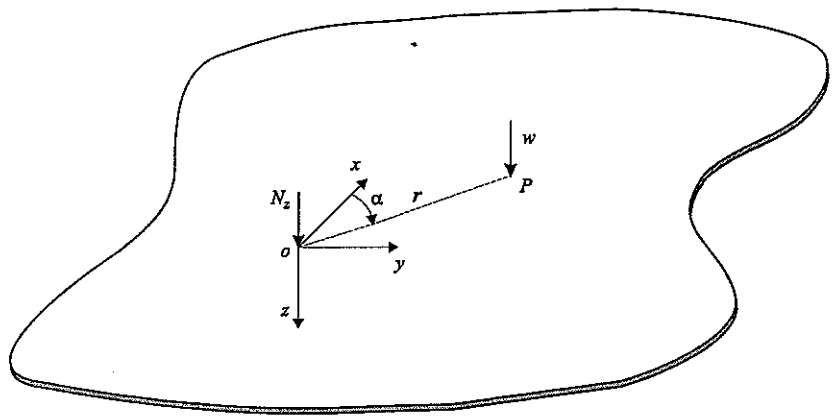

Fig. 2: *Notation of the displacement w at position P when the infinite plate is excited in flexure by a point force N_z applied at the origin of the system of reference.*

If the harmonic point force $N_z(t)$ is acting on a massless small rigid indenter with a circle base of radius a fixed to the plate and the plate thickness is small compared to the dimensions of the area of the indenter, the out-of-plane steady state velocity $\dot{w}(t)$ at any position P at distance $r = const$ from the origin is given by [1] (p 290):

$$\dot{w}(r,\alpha,t) = \mathrm{Re}\left\{\tilde{\dot{w}}(\omega)e^{j\omega t}\right\} = \mathrm{Re}\left\{\frac{\omega\tilde{N}_z(\omega)}{8Bk_B^2}\left[H_0^{(2)}(k_B r) - j\frac{2}{\pi}K_0(k_B r)\right]e^{j\omega t}\right\} \tag{2.16}$$

where $H_i^{(2)}(k_B r)$ is the second kind of Hankel function of the ith order and $K_i(k_B r)$ is the second kind of modified Bessel function of the ith order[6]. $k_B = \omega/c_B$ is the flexural wave number and $c_B = \sqrt[4]{B/m}\sqrt[2]{\omega}$ is the "*phase velocity*" of bending waves propagating in a plate.

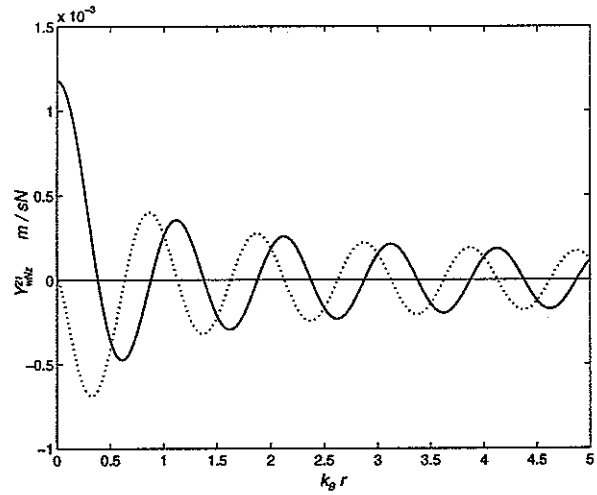

Fig. 3: *Real (solid) and Imaginary (dotted) part of the out-of-plane velocity phasor $\tilde{\dot{w}}$ when an infinite plate is excited by a unit out-of-plane force N_z ($k_B r = 0 \div 5$ and $\alpha = const$).*

[6] From reference [27]: $H_i^{(2)}(k_B r) = J_i(k_B r) - jY_i(k_B r)$ where $J_i(k_B r)$ and $Y_i(k_B r)$ are the Bessel functions respectively of the first kind and second kind of order i.

Figures 3 and 4 show the real and imaginary parts of the velocity phasor $\dot{\tilde{w}}(r,\alpha,\omega)$ due to a unit out-of-plane force $N_z(t)$ considering $k_B r = 0 \div 5$ and assuming $\alpha = const$ in figure 3, or assuming $\alpha = 90^o \div 360^o$ in figure 4. Both figures 3 and 4 show that for small values of $k_B r$ the real part of the velocity phasor is dominated by a strong near-field component which decays rapidly as $k_B r$ rises while the imaginary part of the velocity phasor tends to zero for $k_B r \to 0$.

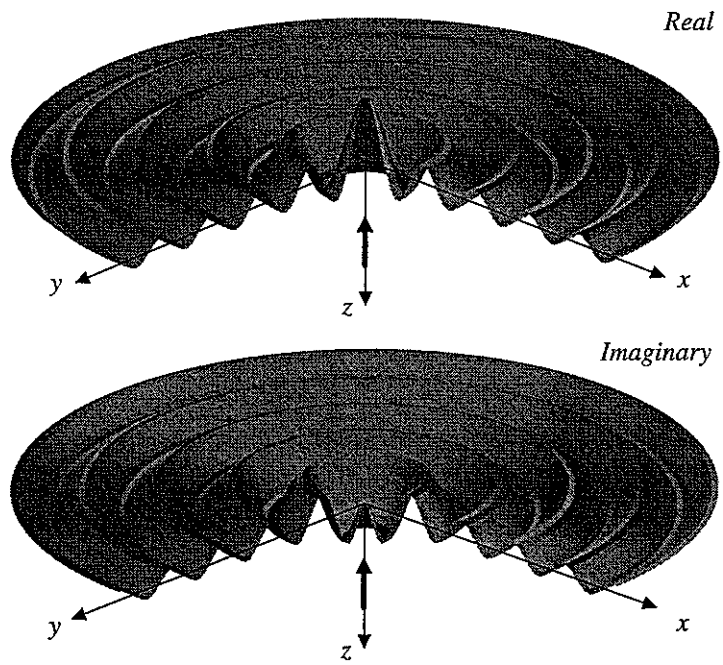

Fig. 4: *Real (top) and Imaginary (bottom) part of the out-of-plane velocity phasor $\dot{\tilde{w}}$ when an infinite plate is excited by a unit out-of-plane force -N_z (α=90°÷360° and $k_B r = 0 \div 5$).*

The steady state angular velocity $\dot{\theta}_u(t)$ with u orientation at a generic position P related to the bending wave generated by the out-of-plane harmonic force $N_z(t)$ acting on a small rigid indenter fixed to the plate could be calculated by making some geometrical considerations on the vibrating field generated by the force $N_z(t)$.

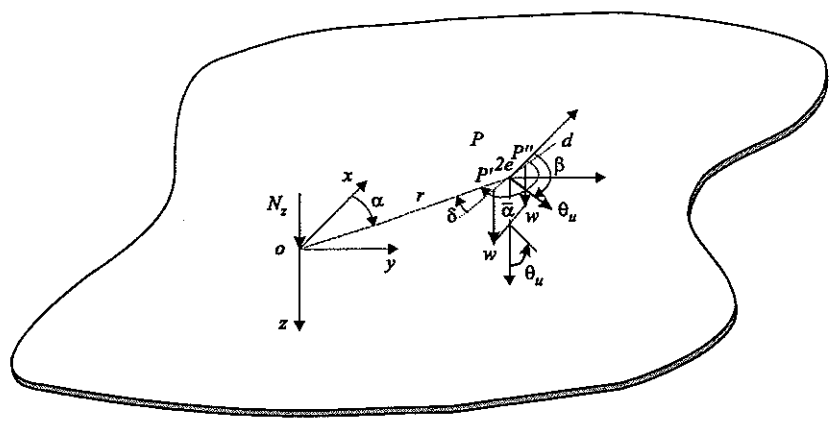

Fig. 5: *Notation of the angular displacement θ_u at position P of u orientation when the infinite plate is excited in flexure by a point force N_z applied at the origin of the system of reference.*

With reference to figure 5, the angular displacement θ_u with u orientation evaluated at position $P = (r,\alpha)$ could be derived by taking the following limit

$$\tan\{\theta_u(P)\} = \lim_{e\to 0} \frac{w(P') - w(P'')}{2e}, \tag{2.17}$$

where the out-of-plane displacements w are taken at two positions P' and P'' placed along a line d which is normal to the angular velocity direction u and at distance e apart from P. For small values of θ_u $\tan\{\theta_u(P)\} \cong \theta_u(P)$ and therefore the steady state angular velocity is given by the following limit

$$\dot{\theta}_u(r,\alpha,t) \cong \lim_{e\to 0} \frac{\dot{w}(r',\alpha,t) - \dot{w}(r'',\alpha,t)}{2e}. \tag{2.18}$$

The velocity phasors $\tilde{\dot{w}}(r',\alpha,\omega)$ and $\tilde{\dot{w}}(r'',\alpha,\omega)$ can be calculated from equation (2.16):

$$\tilde{\dot{w}}(r',\alpha,\omega) = \frac{\omega \tilde{N}_z(\omega)}{8Bk_B^2}\left[H_0^{(2)}(k_B r') - j\frac{2}{\pi}K_0(k_B r')\right], \tag{2.19}$$

$$\tilde{\dot{w}}(r'',\alpha,\omega) = \frac{\omega \tilde{N}_z(\omega)}{8Bk_B^2}\left[H_0^{(2)}(k_B r'') - j\frac{2}{\pi}K_0(k_B r'')\right]. \tag{2.20}$$

Therefore, with reference to equation (2.18), the angular velocity phasor is given by

$$\tilde{\dot{\theta}}_u(r,\alpha,\omega) = \lim_{e\to 0} \frac{\omega \tilde{N}_z(\omega)}{8Bk_B^2}\left[\frac{T_0(k_B r') - T_0(k_B r'')}{2e}\right], \tag{2.21}$$

where

$$T_0(k_B r) = H_0^{(2)}(k_B r) - j\frac{2}{\pi}K_0(k_B r). \tag{2.22}$$

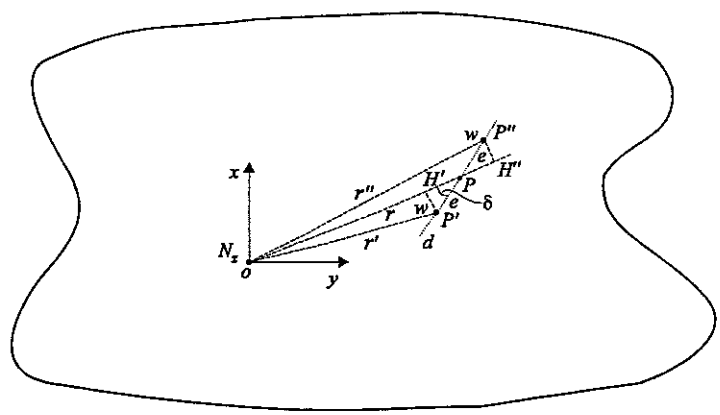

Fig. 6: *Top view showing the geometrical parameters relating the out of plane displacements $w(P')$ and $w(P'')$ to the out-of-plane point force N_z applied at the origin of the system of reference.*

Considering the sketch of figure 6, if $r >> e$ the distances $r' = OP'$ and $r'' = OP''$ could be assumed approximately equal to $r' = OH'$ and $r'' = OH''$ respectively, so that:

$$r' = r - e\cos\delta \qquad\qquad r'' = r + e\cos\delta \tag{2.23}$$

where, according to figure 5, $\delta = \overline{\alpha} - (\beta + \pi/2)$. Equation (2.21) then becomes

$$\dot{\tilde{\theta}}_u(r,\alpha,\omega) = \frac{\omega \tilde{N}_z(\omega)}{8Bk_B^2}\left\{\frac{T_0[k_B(r - e\cos\delta)] - T_0[k_B(r + e\cos\delta)]}{2e}\right\} \tag{2.24}$$

which, after defining $\varepsilon = e\cos\delta$, could be written as

$$\dot{\tilde{\theta}}_u(r,\alpha,\omega) = \lim_{\varepsilon\to 0} -\frac{\omega \tilde{N}_z(\omega)\cos\delta}{8Bk_B^2}\left\{\frac{T_0[k_B(r+\varepsilon)] - T_0[k_B(r-\varepsilon)]}{2\varepsilon}\right\}. \tag{2.25}$$

The term in curly brackets is the first derivative of $T_0(k_B r)$ with respect to r, hence

$$\dot{\tilde{\theta}}_u(r,\alpha,\omega) = -\frac{\omega \tilde{N}_z(\omega)\cos\delta}{8Bk_B^2}\frac{\partial T_0(k_B r)}{\partial r}. \tag{2.26}$$

The first derivative of $T_0(k_B r)$ with respect to r is given by:

$$\frac{\partial T_0(k_B r)}{\partial r} = -k_B T_1(k_B r), \tag{2.27}$$

where

$$T_1(k_B r) = H_1^{(2)}(k_B r) - j\frac{2}{\pi}K_1(k_B r). \tag{2.28}$$

Therefore the steady state angular velocity is given by:

$$\dot{\theta}_u(r,\alpha,t) = \mathrm{Re}\left\{\dot{\tilde{\theta}}_u(\omega)e^{j\omega t}\right\} = \mathrm{Re}\left\{\frac{\omega \tilde{N}_z(\omega)\cos\delta}{8Bk_B}\left[H_1^{(2)}(k_B r) - j\frac{2}{\pi}K_1(k_B r)\right]e^{j\omega t}\right\} \tag{2.29}$$

and, because $\cos\delta = \cos(\overline{\alpha} - \beta - \pi/2) = \sin(\overline{\alpha} - \beta)$,

$$\dot{\theta}_u(r,\alpha,t) = \mathrm{Re}\left\{\frac{\omega \tilde{N}_z(\omega)\sin(\overline{\alpha} - \beta)}{8Bk_B}\left[H_1^{(2)}(k_B r) - j\frac{2}{\pi}K_1(k_B r)\right]e^{j\omega t}\right\}. \tag{2.30}$$

2.3. Mobilities relating linear or angular velocities to a force

The driving point mobility $Y_{wN_z}^{11}(\omega) = \dot{\tilde{w}}_1(\omega)/\tilde{N}_{z1}(\omega)$, evaluated at a point $P_1 = (x_1, y_1)$, could be derived directly from equation (2.16) by considering the response due to a force excitation $N_{z1}(t)$ when $r \to 0$, which gives [1]:

$$Y_{wF_z}^{11} = \frac{\omega}{8Bk_B^2} = \frac{1}{8\sqrt{Bm}} \tag{2.31}$$

Two important observations should be made considering equation (2.31): first, this point mobility parameter is independent of frequency and second, it is purely real. The transfer mobility $Y^{21}_{wN_z} = \dot{\tilde{w}}_2(\omega)/\tilde{N}_{z1}(\omega)$ could also be derived from equation (2.16) by considering the distance r_{21} given by:

$$r_{21} = \sqrt{(x_2 - x_1)^2 + (y_2 - y_1)^2} \tag{2.32}$$

so that

$$Y^{21}_{wN_z}(\omega) = \frac{\omega}{8Bk_B^2}\left[H_0^{(2)}(k_B r_{21}) - j\frac{2}{\pi}K_0(k_B r_{21})\right]. \tag{2.33}$$

Finally the transfer mobility $Y^{21}_{\theta_u N_z}(\omega) = \dot{\tilde{\theta}}_{u2}(\omega)/\tilde{N}_{z1}(\omega)$ is derived from equation (2.30) by considering the distance r_{21} and $\overline{\alpha} = \alpha_2$, $\beta = \beta_2$ so that

$$Y^{21}_{\theta_u N_z}(\omega) = \frac{\omega \sin(\alpha_2 - \beta_2)}{8Bk_B}\left[H_1^{(2)}(k_B r_{21}) - j\frac{2}{\pi}K_1(k_B r_{21})\right]. \tag{2.34}$$

It is important to underline that these three mobility formulae are derived assuming the out-of-plane force $N_{z1}(t)$ acting on a small rigid indenter which transmits to the plate a uniform force distributed over a small circle of radius a (see Cremer et al [1] p 289). Moreover it is assumed that the plate thickness is small compared to both the bending wavelength and to the dimensions of the area of the indenter.

2.4. Linear and angular velocities of bending waves generated by a point moment acting on a small rigid indenter fixed to an infinite thin plate

If, instead, a point force N_z, a point moment $M_u = \mathrm{Re}\left\{\tilde{M}_u(\omega)\exp(j\omega t)\right\}$ of u direction is acting on a small indenter with a circle base of radius a fixed to the plate and the plate thickness is small compared to the dimensions of the area of the indenter, the translational velocity $\dot{w}(t)$ at any position P at distance $r = const$ from the origin could be calculated by adding the effects produced by a pair of opposite phase force excitations $N'_z(t) = +N_z(t)$ and $N''_z(t) = -N_z(t)$ acting along a line d, orthogonal to u, at distance e from the origin, as is shown in figure 7.

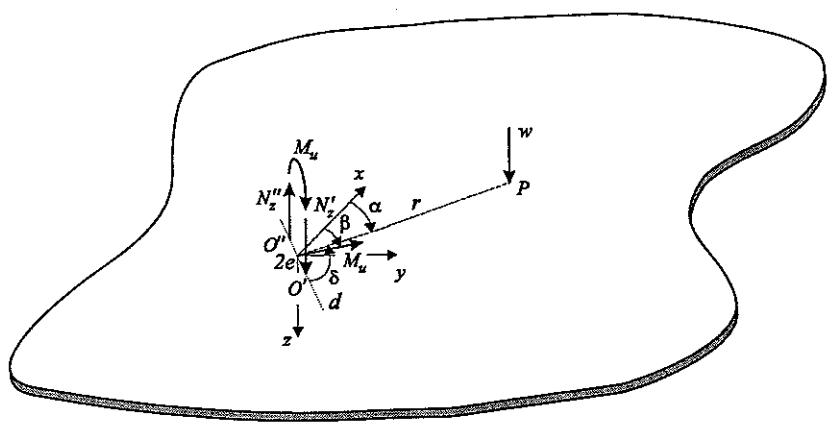

Fig. 7: *Notation of the displacement w at position P when a plate is excited in flexure by a point moment M_u with u orientation, applied at the origin of the system of reference.*

In fact, if the distance $2e$ between the two forces is reduced to zero, the two opposite phase forces N_z' and N_z'' generate a moment with u direction which is given by:

$$M_u(t) = \lim_{e\to 0} 2eN_z(t). \tag{2.35}$$

The steady state translational velocity at position P generated by the two point forces acting at positions O' and O'' could be calculated by means of equation (2.16) with reference to the distances $r' = O'P$ and $r'' = O''P$. Considering the sketch of figure 8, if $r >> e$ the distances $r' = O'P$ and $r'' = O''P$ could be assumed equal to $r' = H'P$ and $r'' = H''P$, so that:

$$r' = r - e\cos\delta \qquad\qquad r'' = r + e\cos\delta\,. \tag{2.36}$$

where according to figure 7, $\delta = \alpha - (\beta + \pi/2)$. Therefore the phasors of the translational velocities $\dot{w}'(t)$ and $\dot{w}''(t)$ at position P due respectively to $N_z'(t)$ and $N_z''(t)$, are given by:

$$\tilde{\dot{w}}'(r',\alpha,\omega) = \frac{\omega\tilde{N}_z(\omega)}{8Bk_B^2}\left[H_0^{(2)}(k_B r') - j\frac{2}{\pi}K_0(k_B r')\right] \tag{2.37}$$

$$\tilde{\dot{w}}''(r'',\alpha,\omega) = -\frac{\omega\tilde{N}_z(\omega)}{8Bk_B^2}\left[H_0^{(2)}(k_B r'') - j\frac{2}{\pi}K_0(k_B r'')\right] \tag{2.38}$$

so that, in the limiting case of $e \to 0$, the phasor of the total velocity at position P generated by the two point forces acting at positions O' and O'' is given by

$$\tilde{\dot{w}}(r,\alpha,\omega) = \lim_{e\to 0}\left[\tilde{\dot{w}}'(r',\alpha,\omega) + \tilde{\dot{w}}''(r'',\alpha,\omega)\right] \tag{2.39}$$

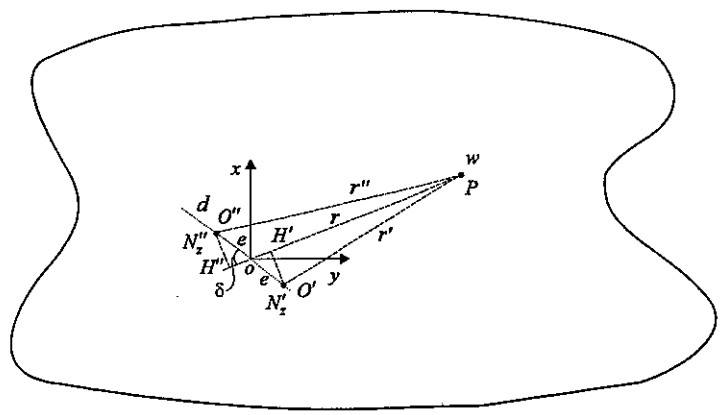

Fig. 8: *Top view showing the geometrical parameters relating the out of plane forces N_z' and N_z'' to the out-of-plane displacement w at position P.*

Equation (2.39) can be rearranged in the following way

$$\tilde{\dot{w}}(r,\alpha,\omega) = \lim_{e\to 0}\frac{\omega\tilde{N}_z(\omega)}{8Bk_B^2}\left[T_0(k_B r') - T_0(k_B r'')\right] \tag{2.40}$$

where $T_0(k_B r)$ is given by equation (2.22). Considering the expression (2.35) given for the

moment M_u, equation (2.40) can be written as follows:

$$\dot{\tilde{w}}(r,\alpha,\omega)=\lim_{e\to 0}\frac{\omega\tilde{M}_u(\omega)\cos\delta}{8Bk_B^2}\left\{\frac{T_0[k_B(r-e\cos\delta)]-T_0[k_B(r+e\cos\delta)]}{2e\cos\delta}\right\} \tag{2.41}$$

that, after defining $\varepsilon = e\cos\delta$, becomes

$$\dot{\tilde{w}}(r,\alpha,\omega)=\lim_{\varepsilon\to 0}-\frac{\omega\tilde{M}_u(\omega)\cos\delta}{8Bk_B^2}\left\{\frac{T_0[k_B(r+\varepsilon)]-T_0[k_B(r-\varepsilon)]}{2\varepsilon}\right\}. \tag{2.42}$$

The term in curly brackets is the first derivative of $T_0(k_Br)$ with respect to r, hence the expression for the translational velocity phasor is given by

$$\dot{\tilde{w}}(r,\alpha,\omega)=-\frac{\omega\tilde{M}_u(\omega)\cos\delta}{8Bk_B^2}\cdot\frac{\partial T_0(k_Br)}{\partial r}\ . \tag{2.43}$$

The first derivative of $T_0(k_Br)$ with respect to r is given in equations (2.27) and (2.28) so that the steady state linear velocity is given by:

$$\dot{w}(r,\alpha,t)=\mathrm{Re}\left\{\dot{\tilde{w}}(\omega)e^{j\omega t}\right\}=\mathrm{Re}\left\{\frac{\omega\tilde{M}_u(\omega)\cos\delta}{8Bk_B}\left[H_1^{(2)}(k_Br)-j\frac{2}{\pi}K_1(k_Br)\right]e^{j\omega t}\right\} \tag{2.44}$$

and, because $\cos\delta=\cos(\alpha-\beta-\pi/2)=\sin(\alpha-\beta)$,

$$\dot{w}(r,\alpha,t)=\mathrm{Re}\left\{\frac{\omega\tilde{M}_u(\omega)\sin(\alpha-\beta)}{8Bk_B}\left[H_1^{(2)}(k_Br)-j\frac{2}{\pi}K_1(k_Br)\right]e^{j\omega t}\right\}. \tag{2.45}$$

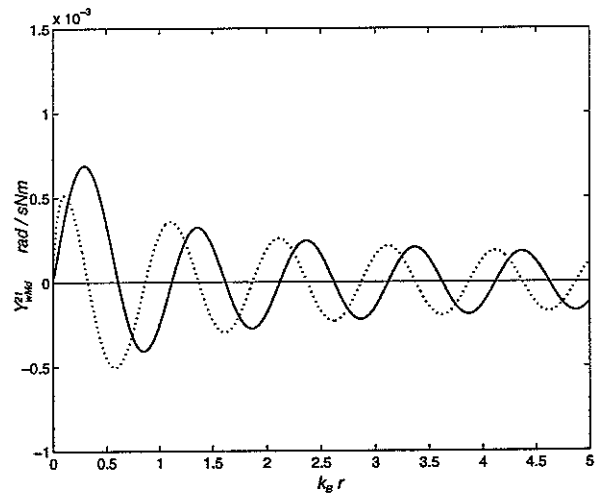

Fig. 9: *Real (solid) and Imaginary (dotted) part of the out-of-plane velocity phasor* $\dot{\tilde{w}}$ *when an infinite plate is excited by a unit moment* M_u *with u orientation (* $k_Br = 0 \div 5$ and $\alpha = 0^o$).

Figures 9 and 10 show the real and imaginary part of the velocity phasor $\dot{\tilde{w}}(r,\alpha,\omega)$ due to a unit moment $M_u(t)$ with direction u considering $k_B r = 0 \div 5$ and assuming $\alpha = 0^o$ in figure 9, or assuming $\alpha = 90^o \div 360^o$ in figure 10.

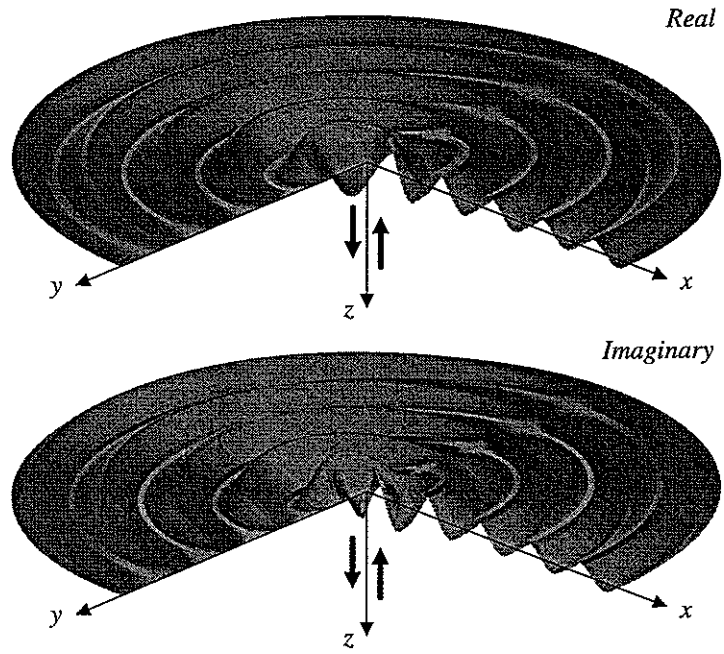

Fig. 10: *Real (top) and Imaginary (bottom) part of the out-of-plane velocity phasor* $\dot{\tilde{w}}$ *when an infinite plate is excited by a unit moment* M_u *with u orientation defined by* $\beta = 90^o$ ($\alpha = 90^o \div 360^o$ and $k_B r = 0 \div 5$).

The angular velocity $\dot{\theta}_{uP}$ with u_P orientation at a position $P = (r,\alpha)$ related to the bending wave generated by the point moment $M_u(t)$ of direction u acting at the origin o of the main system of reference (o,x,y,z) can be derived in a relatively simple way by defining a new set of cylindrical co-ordinates (o,r,γ,z).

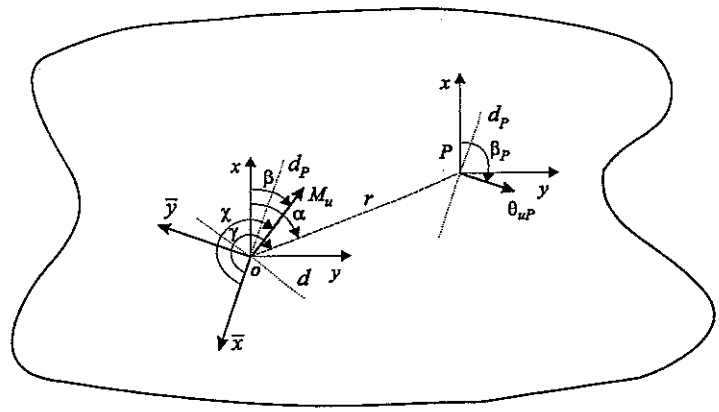

Fig. 11: *Top view showing the geometrical parameters relating the bending moment* M_u *of u direction to the angular displacement* θ_u *of u direction at position P.*

As shown in figure 11, the (o,r,γ,z) system of cylindrical co-ordinates is defined with reference to the main Cartesian system of reference rotated of $\beta_P+\pi/2$ around the z axis $(o,\bar{x},\bar{y},\bar{z})$ so that the $\bar{x}$ axis is parallel to the segment d_P. In this way

$$\bar{x}_P = r\cos\gamma \qquad\qquad \bar{y}_P = r\sin\gamma\ , \tag{2.46}$$

where

$$\gamma = 3/2\pi - \beta_P + \alpha\ , \qquad\qquad \chi = 3/2\pi - \beta_P + \beta\ . \tag{2.47,48}$$

The steady state translational velocity $\dot{w}$ at any position P at distance $r = const$ from the origin given by equation (2.45) can therefore be re-written in the following way:

$$\dot{w}(r,\gamma,t) = \mathrm{Re}\left\{\frac{\omega\tilde{M}_u(\omega)\sin(\gamma-\chi)}{8Bk_B}\left[H_1^{(2)}(k_B r) - j\frac{2}{\pi}K_1(k_B r)\right]e^{j\omega t}\right\}. \tag{2.49}$$

The steady state angular velocity $\dot{\theta}_{uP}(t)$ can be derived by differentiating $\dot{w}(r,\gamma,t)$ at $P=(r,\gamma)$ along the d_P direction, i.e. along the $\bar{x}$ direction:

$$\dot{\theta}_{uP}(r,\gamma,t) = \left.\frac{\partial\dot{w}(r,\gamma,t)}{\partial\bar{x}}\right|_{(r,\gamma)}. \tag{2.50}$$

This is the partial derivative along the $\bar{x}$ Cartesian co-ordinate of a function given in cylindrical co-ordinates. Therefore by using the "*chain rule*" for the derivation of a function (see reference [26] pp 186-190) it can be written in the following form

$$\dot{\theta}_{uP}(r,\gamma,t) = \frac{\partial\dot{w}(r,\gamma,t)}{\partial r}\frac{\partial r}{\partial\bar{x}} + \frac{\partial\dot{w}(r,\gamma,t)}{\partial\gamma}\frac{\partial\gamma}{\partial\bar{x}} \tag{2.51}$$

and, considering equation (2.46) (see reference [26], example 6 pp 165-167):

$$\dot{\theta}_{uP}(r,\gamma,t) = \cos\gamma\cdot\left.\frac{\partial\dot{w}(r,\gamma,t)}{\partial r}\right|_{(r,\gamma)} - \frac{\sin\gamma}{r}\cdot\left.\frac{\partial\dot{w}(r,\gamma,t)}{\partial\gamma}\right|_{(r,\gamma)}. \tag{2.52}$$

Because $\gamma = 3/2\pi - \beta_P + \alpha$, the cosine and sine terms in equation (2.52) become: $\cos(3/2\pi+\alpha-\beta_P) = \sin(\alpha-\beta_P)$ and $\sin(3/2\pi+\alpha-\beta_P) = -\cos(\alpha-\beta_P)$ so that equation (2.52) could be written in terms of the α and β_P angles as follow:

$$\dot{\theta}_{uP}(r,\gamma,t) = \sin(\alpha-\beta_P)\cdot\left.\frac{\partial\dot{w}(r,\gamma,t)}{\partial r}\right|_{(r,\gamma)} + \frac{\cos(\alpha-\beta_P)}{r}\cdot\left.\frac{\partial\dot{w}(r,\gamma,t)}{\partial\gamma}\right|_{(r,\gamma)}. \tag{2.53}$$

The first partial differentiation in equation (2.53) can be calculated directly from equation (2.49), so that:

$$\left.\frac{\partial \dot{w}(r,\gamma,t)}{\partial r}\right|_{(r,\gamma)} = \mathrm{Re}\left\{\frac{\omega M_u(\omega)\sin(\gamma-\beta)}{8Bk_B}\cdot\frac{\partial T_1(k_B r)}{\partial r}e^{j\omega t}\right\} \tag{2.54}$$

that because,

$$\frac{\partial T_1(k_B r)}{\partial r} = \frac{1}{r}T_1(k_B r) - k_B T_2(k_B r), \tag{2.55}$$

and

$$T_2(k_B r) = H_2^{(2)}(k_B r) - j\frac{2}{\pi}K_2(k_B r), \tag{2.56}$$

it becomes:

$$\begin{aligned}\left.\frac{\partial \dot{w}(r,\gamma,t)}{\partial r}\right|_{(r,\gamma)} = \mathrm{Re}\Bigg\{&\frac{\omega M_u(\omega)\sin(\gamma-\chi)}{8Bk_B}\Bigg[\frac{1}{r}\left(H_1^{(2)}(k_B r) - j\frac{2}{\pi}K_1(k_B r)\right) - \\ &-k_B\left(H_2^{(2)}(k_B r) - j\frac{2}{\pi}K_2(k_B r)\right)\Bigg]e^{j\omega t}\Bigg\}\end{aligned} \tag{2.57}$$

The second partial differentiation in equation (2.53) can also be calculated directly from equation (2.49), so that:

$$\left.\frac{\partial \dot{w}(r,\gamma,t)}{\partial \gamma}\right|_{(r,\gamma)} = \mathrm{Re}\left\{\frac{\omega \tilde{M}_u(\omega)\cos(\gamma-\chi)}{8Bk_B}\left[H_1^{(2)}(k_B r) - j\frac{2}{\pi}K_1(k_B r)\right]e^{j\omega t}\right\}. \tag{2.58}$$

In conclusion, substituting the expressions of γ and χ given by equations (2.47,48), equation (2.53) could be re-written in terms of the cylindrical co-ordinates r,α,z:

$$\begin{aligned}\dot{\theta}_{uP}(r,\alpha,t) = \mathrm{Re}\Bigg\{&\frac{\omega \tilde{M}_u(\omega)}{8Bk_B r}\Bigg\{\sin(\alpha-\beta_P)\sin(\alpha-\beta)\Bigg[\left(H_1^{(2)}(k_B r) - j\frac{2}{\pi}K_1(k_B r)\right) - \\ &-k_B r\cdot\left(H_2^{(2)}(k_B r) - j\frac{2}{\pi}K_2(k_B r)\right)\Bigg] + \cos(\alpha-\beta_P)\cos(\alpha-\beta)\left[H_1^{(2)}(k_B r) - j\frac{2}{\pi}K_1(k_B r)\right]\Bigg\}e^{j\omega t}\Bigg\}\end{aligned} \tag{2.59}$$

which can be written in a compact form as follows:

$$\begin{aligned}\dot{\theta}_{uP}(r,\alpha,t) = \mathrm{Re}\Bigg\{&\frac{\omega \tilde{M}_u(\omega)}{8Bk_B r}\Big\{\sin(\alpha-\beta_P)\sin(\alpha-\beta)\cdot\left[T_1(k_B r) - k_B r\cdot T_2(k_B r)\right] + \\ &+\cos(\alpha-\beta_P)\cos(\alpha-\beta)\cdot T_1(k_B r)\Big\}e^{j\omega t}\Bigg\}\end{aligned} \tag{2.60}$$

If the direction of the bending moment and angular velocity is the same or opposite such that $\beta = \beta_P$ or $\beta = \beta_P + \pi$ and the direction of the segment r is equal to those of the segments d and d_P so that $\beta = \beta_P = \alpha \pm \pi/2$ or $\beta = \alpha \pm \pi/2$ and $\beta_P = \alpha \mp \pi/2$ (i.e. the moment and angular velocity are "*aligned*") equation (2.60) assumes the simplified form:

$$\dot{\theta}_{uP}(r,\alpha,t) = \pm \mathrm{Re}\left\{ \frac{\omega \tilde{M}_u(\omega)}{8Bk_B r} \left[T_1(k_B r) - k_B r \cdot T_2(k_B r) \right] e^{j\omega t} \right\} \tag{2.61}$$

where the "+" sign is valid for the case $\beta = \beta_P = \alpha \pm \pi/2$ and the "—" sign is valid for the case $\beta = \alpha \pm \pi/2$ and $\beta_P = \alpha \mp \pi/2$.

2.5. Mobilities relating linear and angular velocity to a moment

The driving point mobility $Y^{11}_{\theta_u M_u}(\omega) = \dot{\tilde{\theta}}_{u1}(\omega) / \tilde{M}_{u1}(\omega)$, evaluated at any point $P_1 = (x_1, y_1)$, could be derived directly from equation (2.61) by taking the limit of $r \to 0$ [1]:

$$Y^{11}_{\theta_u M_u}(\omega) = \frac{\omega}{16B} \left\{ 1 - j\frac{4}{\pi} \ln(0.9 k_B a) \right\} \tag{2.62}$$

where a is the radius of the rigid indenter on which the moment excitation is applied. In this case the point mobility is characterised by both a real part and an imaginary part which are frequency dependent.

The transfer mobility $Y^{21}_{wM_u}(\omega) = \dot{\tilde{w}}_2(\omega) / \tilde{M}_{u1}(\omega)$ could be derived from equation (2.45) by considering the distance r_{21}

$$r_{21} = \sqrt{(x_2 - x_1)^2 + (y_2 - y_1)^2} \tag{2.63}$$

and $\alpha = \alpha_1$, $\beta = \beta_1$ so that:

$$Y^{21}_{wM_u}(\omega) = \frac{\omega \sin(\alpha_1 - \beta_1)}{8Bk_B} \left[H_1^{(2)}(k_B r_{21}) - j\frac{2}{\pi} K_1(k_B r_{21}) \right]. \tag{2.64}$$

Finally, the transfer mobility $Y^{21}_{\theta_u M_u}(\omega) = \dot{\tilde{\theta}}_{u2}(\omega) / \tilde{M}_{u1}(\omega)$ is derived from equation (2.60) by considering the distance r_{21} and $\alpha = \alpha_1$, $\beta = \beta_1$, $\beta_P = \beta_2$ so that:

$$Y^{21}_{\theta_u M_u}(\omega) = \frac{\omega}{8Bk_B r_{21}} \cdot \left\{ \sin(\alpha_1 - \beta_2) \sin(\alpha_1 - \beta_1) \left[\left(H_1^{(2)}(k_B r_{21}) - j\frac{2}{\pi} K_1(k_B r_{21}) \right) - k_B r_{21} \cdot \left(H_2^{(2)}(k_B r_{21}) - j\frac{2}{\pi} K_2(k_B r_{21}) \right) \right] + \right.$$
$$\left. + \cos(\alpha_1 - \beta_2) \cos(\alpha_1 - \beta_1) \left[H_1^{(2)}(k_B r_{21}) - j\frac{2}{\pi} K_1(k_B r_{21}) \right] \right\} \tag{2.65}$$

Also these three mobility formulae have been derived assuming the bending moment $M_{u1}(t)$ acting on a small rigid indenter which transmits to the plate a uniform distributed dipole excitation over a small circle of radius a (see Cremer et al [1] p 289). Moreover it is assumed

that the plate thickness is small compared to both the bending wavelength and to the dimensions of the area of the indenter.

2.6. Three by three point and transfer mobility matrix for a plate excited in flexure

The matrix equations (2.8) and (2.14) are often used to model the flexural vibration transmission of a complete mechanical system composed of a number of elements connected at point junctions. As for example described in reference [29], this type of matrix models define, for plate like elements, point and transfer mobility matrices of the same type of those of equations (2.7) and (2.13) except that the moment excitation $M_u(t)$ and the angular velocity $\dot{\theta}_u(t)$ at a specific point P are defined by two components in the x and y directions. As seen in previous sections, when the force and the two components of the moment excitation are harmonic with time dependence of the form $\exp(j\omega t)$, they can be represented by the real part of the phasors:

$$F_z(t) = \mathrm{Re}\left\{\tilde{F}_z(\omega)e^{j\omega t}\right\}, \qquad M_x(t) = \mathrm{Re}\left\{\tilde{M}_x(\omega)e^{j\omega t}\right\}, \qquad M_y(t) = \mathrm{Re}\left\{\tilde{M}_y(\omega)e^{j\omega t}\right\} \quad (2.66\text{-}68)$$

and the equivalent linear and angular components of the velocities are equally harmonic with time dependence of the form $\exp(j\omega t)$ so that

$$\dot{w}_x(t) = \mathrm{Re}\left\{\dot{\tilde{w}}_x(\omega)e^{j\omega t}\right\}, \qquad \dot{\theta}_x(t) = \mathrm{Re}\left\{\dot{\tilde{\theta}}_x(\omega)e^{j\omega t}\right\}, \qquad \dot{\theta}_y(t) = \mathrm{Re}\left\{\dot{\tilde{\theta}}_y(\omega)e^{j\omega t}\right\} \quad (2.69\text{-}71)$$

Therefore the force-moment excitation and the linear-angular velocity vectors are given by:

$$\mathbf{f}(\omega) = \begin{Bmatrix} \tilde{N}_z(\omega) \\ \tilde{M}_x(\omega) \\ \tilde{M}_y(\omega) \end{Bmatrix} \qquad \mathbf{v}(\omega) = \begin{Bmatrix} \dot{\tilde{w}}(\omega) \\ \dot{\tilde{\theta}}_x(\omega) \\ \dot{\tilde{\theta}}_y(\omega) \end{Bmatrix} \quad (2.72,73)$$

The positive direction of the moment excitations and angular displacements is shown in figure 12.

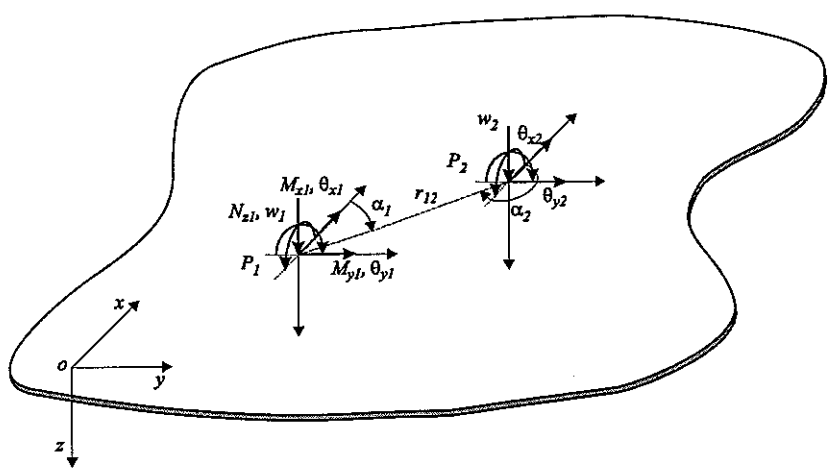

Fig. 12: *Notation of the displacement w and rotations θ_x and θ_y at positions P_1 and P_2 when a plate is excited in flexure by a point force N_z and point moments M_x and M_y at position P_1.*

The point $\mathbf{Y}^{11}(\omega)$ and transfer $\mathbf{Y}^{21}(\omega)$ matrices of equations (2.7) and (2.13) are therefore 3×3 matrices which are defined as follow:

$$\mathbf{Y}^{11}(\omega)=\begin{bmatrix} Y^{11}_{wN_z}(\omega) & 0 & 0 \\ 0 & Y^{11}_{\theta_x M_x}(\omega) & 0 \\ 0 & 0 & Y^{21}_{\theta_y M_y}(\omega) \end{bmatrix} \tag{2.74}$$

$$\mathbf{Y}^{21}(\omega)=\begin{bmatrix} Y^{21}_{wN_z}(\omega) & Y^{21}_{wM_x}(\omega) & Y^{21}_{wM_y}(\omega) \\ Y^{21}_{\theta_x N_z}(\omega) & Y^{21}_{\theta_x M_x}(\omega) & Y^{21}_{\theta_x M_y}(\omega) \\ Y^{21}_{\theta_y N_z}(\omega) & Y^{21}_{\theta_y M_x}(\omega) & Y^{21}_{\theta_y M_y}(\omega) \end{bmatrix} \tag{2.75}$$

where:

$$Y^{11}_{wN_z}(\omega)=\frac{\dot{\tilde{w}}_1(\omega)}{\tilde{N}_{z1}(\omega)} \qquad Y^{11}_{\theta_x M_x}(\omega)=\frac{\dot{\tilde{\theta}}_{x1}(\omega)}{\tilde{M}_{x1}(\omega)} \qquad Y^{11}_{\theta_y M_y}(\omega)=\frac{\dot{\tilde{\theta}}_{y1}(\omega)}{\tilde{M}_{y1}(\omega)}, \tag{2.76-78}$$

and:

$$\begin{aligned}
Y^{21}_{w_z F_z}(\omega)&=\left.\frac{\dot{\tilde{w}}_{z2}(\omega)}{\tilde{F}_{z1}(\omega)}\right|_{M_x,M_y=0} & Y^{21}_{w_z M_x}(\omega)&=\left.\frac{\dot{\tilde{w}}_{z2}(\omega)}{\tilde{M}_{x1}(\omega)}\right|_{F_z,M_y=0} & Y^{21}_{w_z M_y}(\omega)&=\left.\frac{\dot{\tilde{w}}_{z2}(\omega)}{\tilde{M}_{y1}(\omega)}\right|_{F_z,M_x=0} \\
Y^{21}_{\theta_x F_z}(\omega)&=\left.\frac{\dot{\tilde{\theta}}_{x2}(\omega)}{\tilde{F}_{z1}(\omega)}\right|_{M_x,M_y=0} & Y^{21}_{\theta_x M_x}(\omega)&=\left.\frac{\dot{\tilde{\theta}}_{x2}(\omega)}{\tilde{M}_{x1}(\omega)}\right|_{F_z,M_y=0} & Y^{21}_{\theta_x M_y}(\omega)&=\left.\frac{\dot{\tilde{\theta}}_{x2}(\omega)}{\tilde{M}_{y1}(\omega)}\right|_{F_z,M_x=0} \\
Y^{21}_{\theta_y F_z}(\omega)&=\left.\frac{\dot{\tilde{\theta}}_{y2}(\omega)}{\tilde{F}_{z1}(\omega)}\right|_{M_x,M_y=0} & Y^{21}_{\theta_y M_x}(\omega)&=\left.\frac{\dot{\tilde{\theta}}_{y2}(\omega)}{\tilde{M}_{x1}(\omega)}\right|_{F_z,M_y=0} & Y^{21}_{\theta_y M_y}(\omega)&=\left.\frac{\dot{\tilde{\theta}}_{x2}(\omega)}{\tilde{M}_{y1}(\omega)}\right|_{F_z,M_x=0}
\end{aligned} \tag{2.79-87}$$

The linear-velocity/force and the angular-velocity/moment mobilities of the point mobility matrix are the same as those derived in previous sections, thus:

$$Y^{11}_{wF_z}=\frac{\omega}{8Bk_B^2}=\frac{1}{8\sqrt{Bm}} \tag{2.88}$$

$$Y^{11}_{\theta_x M_x}(\omega)=Y^{11}_{\theta_y M_y}(\omega)=\frac{\omega}{16B}\left\{1-j\frac{4}{\pi}\ln(0.9k_B a)\right\}. \tag{2.89}$$

Also the transfer mobility matrix parameters are similar to those found in sections 2.3. and 2.5. In fact the transfer mobility $Y^{21}_{wN_z}(\omega)$ is given by the same formula as that of equation (2.33) so that:

$$Y^{21}_{wN_z}(\omega)=\frac{\omega}{8Bk_B^2}\left[H_0^{(2)}(k_B r_{21})-j\frac{2}{\pi}K_0(k_B r_{21})\right]. \tag{2.90}$$

The transfer mobilities relating an angular velocity to a force, $Y^{21}_{\theta_x N_z}(\omega)$ and $Y^{21}_{\theta_y N_z}(\omega)$, could be derived from equation (2.30) assuming respectively $\beta_2 = 0^o$ and $\beta_2 = 90^o$ and in both cases $\overline{\alpha} = \alpha_2$ so that:

$$Y^{21}_{\theta_x N_z}(\omega) = \frac{\omega \sin\alpha_2}{8Bk_B}\left[H_1^{(2)}(k_B r_{21}) - j\frac{2}{\pi}K_1(k_B r_{21})\right], \tag{2.91}$$

$$Y^{21}_{\theta_y N_z}(\omega) = -\frac{\omega \cos\alpha_2}{8Bk_B}\left[H_1^{(2)}(k_B r_{21}) - j\frac{2}{\pi}K_1(k_B r_{21})\right]. \tag{2.92}$$

Similarly, the transfer mobilities relating a linear velocity to a moment, $Y^{21}_{wM_x}(\omega)$ and $Y^{21}_{wM_y}(\omega)$, could be derived from equation (2.45) assuming respectively $\beta_1 = 0^o$ and $\beta_1 = 90^o$ and in both cases $\alpha = \alpha_1$ so that:

$$Y^{21}_{wM_x}(\omega) = \frac{\omega \sin\alpha_1}{8Bk_B}\left[H_1^{(2)}(k_B r_{21}) - j\frac{2}{\pi}K_1(k_B r_{21})\right], \tag{2.93}$$

$$Y^{21}_{wM_y}(\omega) = -\frac{\omega \cos\alpha_1}{8Bk_B}\left[H_1^{(2)}(k_B r_{21}) - j\frac{2}{\pi}K_1(k_B r_{21})\right]. \tag{2.94}$$

The four mobility terms relating angular velocity to a moment $Y^{21}_{\theta_x M_x}(\omega)$, $Y^{21}_{\theta_x M_y}(\omega)$, $Y^{21}_{\theta_y M_x}(\omega)$ $Y^{21}_{\theta_y M_y}(\omega)$ are derived from equation (2.59) assuming $\alpha = \alpha_1$ and assuming the following pairs of angles respectively: $(\beta_1 = 0 \quad \beta_2 = 0)$, $(\beta_1 = 90^o \quad \beta_2 = 0)$, $(\beta_1 = 0 \quad \beta_2 = 90^o)$ and $(\beta_1 = 90^o \quad \beta_2 = 90^o)$ so that:

$$Y^{21}_{\theta_x M_x}(\omega) = \frac{\omega}{8Bk_B r_{21}}\left\{\sin^2\alpha_1 \cdot \left[\left(H_1^{(2)}(k_B r_{21}) - j\frac{2}{\pi}K_1(k_B r_{21})\right) - k_B r_{21}\cdot\left(H_2^{(2)}(k_B r_{21}) - j\frac{2}{\pi}K_2(k_B r_{21})\right)\right] + \right.$$
$$\left. + \cos^2\alpha_1\left[H_1^{(2)}(k_B r_{21}) - j\frac{2}{\pi}K_1(k_B r_{21})\right]\right\} \tag{2.95}$$

$$Y^{21}_{\theta_y M_x}(\omega) = -\frac{\omega}{8Bk_B r_{21}}\left\{\cos\alpha_1 \sin\alpha_1 \cdot \left[\left(H_1^{(2)}(k_B r_{21}) - j\frac{2}{\pi}K_1(k_B r_{21})\right) - k_B r_{21}\cdot\left(H_2^{(2)}(k_B r_{21}) - j\frac{2}{\pi}K_2(k_B r_{21})\right)\right] - \right.$$
$$\left. - \sin\alpha_1 \cos\alpha_1\left[H_1^{(2)}(k_B r_{21}) - j\frac{2}{\pi}K_1(k_B r_{21})\right]\right\} \tag{2.96}$$

$$Y^{21}_{\theta_x M_y}(\omega) = -\frac{\omega}{8Bk_B r_{21}}\cdot\left\{\sin\alpha_1 \cos\alpha_1 \cdot \left[\left(H_1^{(2)}(k_B r_{21}) - j\frac{2}{\pi}K_1(k_B r_{21})\right) - k_B r_{21}\cdot\left(H_2^{(2)}(k_B r_{21}) - j\frac{2}{\pi}K_2(k_B r_{21})\right)\right] - \right.$$
$$\left. - \cos\alpha_1 \sin\alpha_1\left[H_1^{(2)}(k_B r_{21}) - j\frac{2}{\pi}K_1(k_B r_{21})\right]\right\} \tag{2.97}$$

$$Y^{21}_{\theta,M_y}(\omega)=\frac{\omega}{8Bk_Br_{21}}\left\{\cos^2\alpha_1\cdot\left[\left(H_1^{(2)}(k_Br_{21})-j\frac{2}{\pi}K_1(k_Br_{21})\right)-k_Br_{21}\cdot\left(H_2^{(2)}(k_Br_{21})-j\frac{2}{\pi}K_2(k_Br_{21})\right)\right]+\right.$$
$$\left.+\sin^2\alpha_1\left[H_1^{(2)}(k_Br_{21})-j\frac{2}{\pi}K_1(k_Br_{21})\right]\right\} \tag{2.98}$$

3. MOBILITY FORMULAE FOR RECTANGULAR PLATES EXCITED IN FLEXURE

3.1. Driving-point and transfer mobilities

In this section the driving point and transfer mobility matrices for a finite rectangular plate are derived. As shown in figure 13, a rectangular plate of dimensions $l_x \times l_y$ is considered and the main Cartesian co-ordinate system of reference (o,x,y,z) is placed at the bottom left corner of the plate with the z axis orthogonal to the surface of the plate.

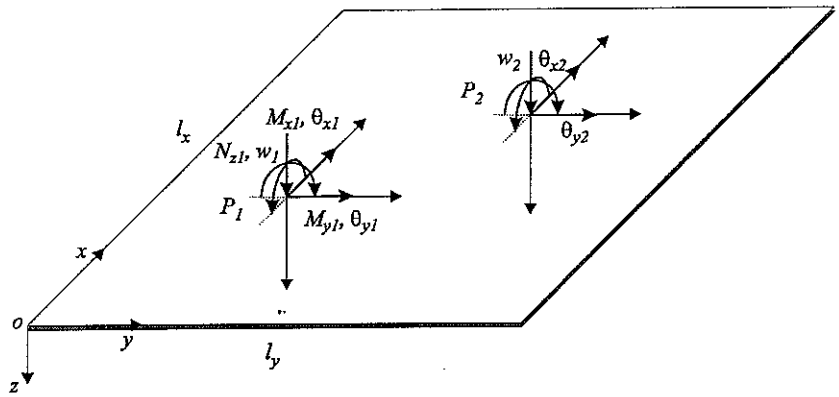

Fig. 13: *Notation of the displacement w and rotations θ_x, and θ_y, at positions P_1 and P_2 when a plate is excited in flexure by a point force N_z and point moments M_x, and M_y, at position P_1.*

The mobility terms relating the three kinematics (translational and angular velocities) and the three dynamic (force and moment excitations) parameters at two generic positions $P_1 = (x_1, y_1)$ and $P_2 = (x_2, y_2)$ are here derived using a modal superposition approach. Figure 13 shows the vector notation used for the force-moment excitation parameters at position P_1 and for the linear-angular velocity parameters at positions P_1 and P_2. Considering the flexural vibration harmonic with time dependence of the form $\exp(j\omega t)$, where ω is the circular frequency, the dynamic and kinematic parameters are represented by the real part of the phasors

$$F_z(t) = \mathrm{Re}\left\{\tilde{N}_z(\omega)e^{j\omega t}\right\}, \qquad M_x(t) = \mathrm{Re}\left\{\tilde{M}_x(\omega)e^{j\omega t}\right\}, \qquad M_y(t) = \mathrm{Re}\left\{\tilde{M}_y(\omega)e^{j\omega t}\right\} \tag{3.1-3}$$

$$\dot{w}_x(t) = \mathrm{Re}\left\{\dot{\tilde{w}}_x(\omega)e^{j\omega t}\right\}, \qquad \dot{\theta}_x(t) = \mathrm{Re}\left\{\dot{\tilde{\theta}}_x(\omega)e^{j\omega t}\right\}, \qquad \dot{\theta}_y(t) = \mathrm{Re}\left\{\dot{\tilde{\theta}}_y(\omega)e^{j\omega t}\right\}. \tag{3.4-6}$$

Nine mobility terms for any pair of points P_i and P_j could be defined as follows [1,18]:

$$Y^{ij}_{w_z F_z}(\omega) = \left.\frac{\dot{\tilde{w}}_{zi}(\omega)}{\tilde{N}_{zj}(\omega)}\right|_{M_x,M_y=0} \quad Y^{ij}_{w_z M_x}(\omega) = \left.\frac{\dot{\tilde{w}}_{zi}(\omega)}{\tilde{M}_{xj}(\omega)}\right|_{F_z,M_y=0} \quad Y^{ij}_{w_z M_y}(\omega) = \left.\frac{\dot{\tilde{w}}_{zi}(\omega)}{\tilde{M}_{yj}(\omega)}\right|_{F_z,M_x=0}$$

$$Y^{ij}_{\theta_x F_z}(\omega) = \left.\frac{\dot{\tilde{\theta}}_{xi}(\omega)}{\tilde{N}_{zj}(\omega)}\right|_{M_x,M_y=0} \quad Y^{ij}_{\theta_x M_x}(\omega) = \left.\frac{\dot{\tilde{\theta}}_{xi}(\omega)}{\tilde{M}_{xj}(\omega)}\right|_{F_z,M_y=0} \quad Y^{ij}_{\theta_x M_y}(\omega) = \left.\frac{\dot{\tilde{\theta}}_{xi}(\omega)}{\tilde{M}_{yj}(\omega)}\right|_{F_z,M_x=0} \tag{3.7-15}$$

$$Y^{ij}_{\theta_y F_z}(\omega) = \left.\frac{\dot{\tilde{\theta}}_{yi}(\omega)}{\tilde{N}_{zj}(\omega)}\right|_{M_x,M_y=0} \quad Y^{ij}_{\theta_y M_x}(\omega) = \left.\frac{\dot{\tilde{\theta}}_{yi}(\omega)}{\tilde{M}_{xj}(\omega)}\right|_{F_z,M_y=0} \quad Y^{ij}_{\theta_y M_y}(\omega) = \left.\frac{\dot{\tilde{\theta}}_{xi}(\omega)}{\tilde{M}_{yj}(\omega)}\right|_{F_z,M_x=0}$$

and therefore a 3×3 driving point or transfer mobility matrix could be defined as follows [18]:

$$\mathbf{Y}^{ij}(\omega)=\begin{bmatrix} Y^{ij}_{w_zN_z}(\omega) & Y^{ij}_{w_zM_x}(\omega) & Y^{ij}_{w_zM_y}(\omega) \\ Y^{ij}_{\theta_xN_z}(\omega) & Y^{ij}_{\theta_xM_x}(\omega) & Y^{ij}_{\theta_xM_y}(\omega) \\ Y^{ij}_{\theta_yN_z}(\omega) & Y^{ij}_{\theta_yM_x}(\omega) & Y^{ij}_{\theta_yM_y}(\omega) \end{bmatrix} \tag{3.16}$$

If $i=j$, i.e. $P_i \equiv P_j$, the matrix $\mathbf{Y}^{ij}(\omega)$ is a driving point mobility matrix while if $i\neq j$, i.e. $P_i \neq P_j$, the matrix $\mathbf{Y}^{ij}(\omega)$ is a transfer mobility matrix. For any pair of points P_i and P_j of the finite plate, including two coincident points $P_i \equiv P_j$, the force-moment excitation vector $\mathbf{f}_i(\omega)=\left\{\tilde{N}_{zi}(\omega) \quad \tilde{M}_{xi}(\omega) \quad \tilde{M}_{yi}(\omega)\right\}^T$ is related to the linear-angular velocity vector $\mathbf{v}_i(\omega)=\left\{\dot{\tilde{w}}_i(\omega) \quad \dot{\tilde{\theta}}_{xi}(\omega) \quad \dot{\tilde{\theta}}_{yi}(\omega)\right\}^T$ by the relation [18]:

$$\mathbf{v}_i(\omega)=\mathbf{Y}^{ij}(\omega)\cdot\mathbf{f}_j(\omega) \tag{3.17}$$

with $\mathbf{Y}^{ij}(\omega)$ always given by equation 3.16. So, unlike in the case of an infinite plate, the driving point mobility matrix is a fully populated matrix with off diagonal mobility terms that are called "*coupling mobilities*" [1,30].

The analytical expressions for the nine *transfer mobility* terms of equations 3.7 to 3.15 are derived in the following sections for a rectangular finite plate with three different types of boundary conditions: first, all edges *simply-supported*; second, all edges *free* and third, all edges *clamped*. The approach provided could be extended to plates of different geometry and/or different boundary conditions if analytic expressions are available for the natural frequencies and modes.

3.2. Modal expansion approach to calculate the steady-state translational velocity $\dot{w}_2(t)$ when the finite plate is driven by an harmonic point force $N_{z1}(t)$.

Flexural waves in a thin plate excited by a uniform distribution of force $p_z(x,y,t)=\mathrm{Re}\{\tilde{p}_z\exp(j\omega t)\}$ over the plate surface are described by a 4th order wave equation as given in equation (2.15). When the plate is finite, the distributed force excites all the natural modes[1] of the plate in different amounts so that, assuming the excitation harmonic with time dependence $\exp(j\omega t)$, the steady state velocity $\dot{w}_2(t)$ at position P_2 is given by [21] (pp 178)

$$\dot{w}_2(t)=\mathrm{Re}\left\{\dot{\tilde{w}}_2(\omega)e^{j\omega t}\right\}=\mathrm{Re}\left\{j\omega\sum_{m=1}^{\infty}\sum_{n=1}^{\infty}W_{mn}(t)\phi_{mn}(P_2)e^{j\omega t}\right\} \tag{3.18}$$

where $W_{mn}(t)$ is called the *modal participation factor* [21] and represents the amount of participation of each natural mode $\phi_{mn}(x,y)$ in the total dynamic response. The indices m and

[1] In reference [1] (Sec. II, 4) it is shown that there exist certain discrete preferred frequencies, the so called **natural frequencies**, at which a linear elastic distributed structure will tend to vibrate once it has been set into motion. At each natural frequency there is an associated **natural mode** which is a function over a structure describing the relative displacement of any point on the structure as the structure vibrates in that single mode.

n represent the number of half standing waves in the x and y directions for the mode ϕ_{mn}. If the plate has all the edges simply supported the kinematic *boundary conditions* are given by:

$$\begin{array}{lll} \text{for: } x=0 \text{ and } x=l_x & w=0 & \dfrac{\partial^2 w}{\partial x^2}=0 \\ \text{for: } y=0 \text{ and } y=l_y & w=0 & \dfrac{\partial^2 w}{\partial y^2}=0 \end{array} . \tag{3.19}$$

A set of *natural modes* that satisfy both the homogeneous flexural wave equation (2.15) and these boundary conditions could be [1,21]:

$$\phi_{mn}(x,y)=\sin\frac{m\pi x}{l_x}\sin\frac{n\pi y}{l_y}. \tag{3.20}$$

where $m=1,2,3,\ldots$ and $n=1,2,3,\ldots$ The *modal participation factor* is then given by [21] (pp 186):

$$W_{mn}(t)=\frac{F_{mn}(t)}{\left[\omega^2_{fmn}(1+j\eta)-\omega^2\right]} \tag{3.21}$$

where ω_{fmn} is the m,n-th natural frequency, η is the *hysteresis loss factor* [1] (Chapter 3). F_{mn} is the *modal force* which is given by

$$F_{mn}(t)=\frac{1}{\rho h N_{mn}}\int_0^{l_x}\int_0^{l_y}\phi_{mn}(x,y)\tilde{p}_z(x,y)dxdy \tag{3.22}$$

where, for a simply supported plate,

$$N_{mn}=\int_0^{l_x}\int_0^{l_y}\phi^2_{mn}(x,y)dxdy=\frac{l_x l_y}{4}. \tag{3.23}$$

For a simply supported plate, the m,n-th natural frequency of the flexural vibration ω_{fmn} is given by [1,21]

$$\omega_{fmn}=\sqrt{\frac{Eh^2}{12\rho(1-\nu^2)}}\left[\left(\frac{m\pi}{l_x}\right)^2+\left(\frac{n\pi}{l_y}\right)^2\right], \tag{3.24}$$

where ν is the Poisson ratio. Some references (see for example [21]) give the modal participation factor in the form:

$$W_{mn}(t)=\frac{F_{mn}(t)}{\left[(\omega^2_{fmn}-\omega^2)+2j\zeta_{mn}\omega_{mn}\omega\right]} \tag{3.25}$$

where ζ_{mn} is the *modal damping coefficient*. Chapter 14 of reference [21] presents a detailed description of the relation occurring between these two ways of describing the dissipative phenomena in a plate under harmonic excitations. The modal damping coefficient is related to

the hysteric loss factor via the expression

$$\zeta_{mn} = \frac{1}{2}\frac{\omega_{mn}}{\omega}\eta \tag{3.26}$$

thus at resonance, $\omega = \omega_{mn}$, the modal damping coefficient is half of the hysteresis loss factor $\zeta_{mn} = \eta/2$.

For the specific case of an harmonic point force excitation $N_{z1}(t) = \mathrm{Re}\left\{\tilde{N}_{z1}(\omega)\exp(j\omega t)\right\}$ at position P_1 the modal participation factor of equation (3.18) could be calculated by using the Dirac delta function δ so that the excitation is represented in the form $N_{z1}(t) = \delta(x-x_1)\delta(y-y_1)p_z(x,y,t)$, with $\left|p_z(x,y,t)\right| = \left|\tilde{N}_{z1}(\omega)\right|$, and therefore

$$W_{mn}(t) = \frac{\phi_{mn}(P_1)\tilde{N}_{z1}(\omega)}{\Lambda_{mn}\left[\omega_{fmn}^2(1+j\eta)-\omega^2\right]} \tag{3.27}$$

where, considering the simply supported plate

$$\Lambda_{mn} = \rho h N_{mn} = \rho h\int_0^{l_x}\int_0^{l_y}\phi_{mn}^2(x,y)dxdy = \frac{\rho h l_x l_y}{4}. \tag{3.28}$$

In reference [1] the parameter Λ_{mn} is reported as the *norm*. At this point it is possible to give an expression for the steady-state translational velocity $\dot{w}_2(t)$ due to an harmonic force excitation $N_{z1}(t)$

$$\dot{w}_2(t) = \mathrm{Re}\left\{\tilde{\dot{w}}_2(\omega)e^{j\omega t}\right\} = \mathrm{Re}\left\{j\omega\sum_{m=1}^{\infty}\sum_{n=1}^{\infty}\frac{\phi_{mn}(P_2)\phi_{mn}(P_1)}{\Lambda_{mn}\left[\omega_{fmn}^2(1+j\eta)-\omega^2\right]}\cdot\tilde{N}_{z1}(\omega)e^{j\omega t}\right\}. \tag{3.29}$$

3.3. Modal expansion approach to calculate the steady-state angular velocity $\dot{\theta}_{u2}(t)$ of arbitrary orientation u_2 when the finite plate is driven by an harmonic point force $N_{z1}(t)$.

The steady state angular velocity $\dot{\theta}_{u2}(t)$ of u_2 orientation at P_2 due to a point force excitation $N_{z1}(t)$ at P_1 could be evaluated with the same approach used in section 2.2. and using the modal formulation discussed in the previous section [21,28].

With reference to the sketch of figure 14, the angular displacement $\theta_{u2}(t)$ could be calculated from equation (2.17) considering the out-of-plane displacements $w_2'(t)$ and $w_2''(t)$, evaluated at two positions, $P_2' = (x_2 - e\sin\beta_2, y_2 + e\cos\beta_2)$ and $P_2'' = (x_1 + e\sin\beta_2, y_1 - e\cos\beta_2)$, placed along a line d_2 which is normal to the angular velocity direction u_2 and at distance e apart from P_2. Also in this case, for small values of θ_{u2} $\tan\{\theta_{u2}\} \cong \theta_{u2}$ and therefore the angular velocity is given by the following limit:

$$\dot{\theta}_{u2}(t) = \lim_{e\to 0}\frac{\dot{w}_2'(t) - \dot{w}_2''(t)}{2e}. \tag{3.30}$$

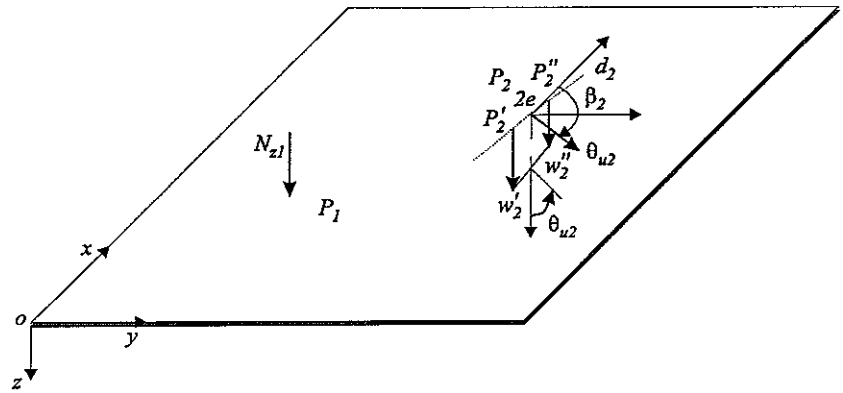

Fig. 14: *Notation of the angular displacement θ_u of u orientation at P_2 induced by a force N_z at P_1.*

The phasors of the linear velocities $\dot{w}_2'(t)$ and $\dot{w}_2''(t)$ can be derived from equation (3.18):

$$\dot{w}_2'(t) = j\omega \sum_{m=1}^{\infty}\sum_{n=1}^{\infty} W_{mn}(t)\phi_{mn}(P_2') \qquad \dot{w}_2''(t) = j\omega \sum_{m=1}^{\infty}\sum_{n=1}^{\infty} W_{mn}(t)\phi_{mn}(P_2'') \qquad (3.31,32)$$

By substituting equations (3.31) and (3.32) into equation (3.30) and after some mathematical manipulations it comes out that

$$\dot{\theta}_{u2}(t) = \mathrm{Re}\left\{\tilde{\theta}_{u2}(\omega)e^{j\omega t}\right\} = \mathrm{Re}\left\{ j\omega \sum_{m=1}^{\infty}\sum_{n=1}^{\infty} \frac{\psi_{mn}^{(u_2)}(P_2)\phi_{mn}(P_1)}{\Lambda_{mn}\left[\omega_{fmn}^2(1+j\eta)-\omega^2\right]} \cdot \tilde{N}_{z1}(\omega)e^{j\omega t} \right\} \qquad (3.33)$$

where

$$\psi_{mn}^{u_2}(x,y) = -\sin\beta_2 \frac{\partial\phi(x,y)}{\partial x} + \cos\beta_2 \frac{\partial\phi(x,y)}{\partial y}. \qquad (3.34)$$

3.4. Modal expansion approach to calculate the steady-state translational velocity $\dot{w}_2(t)$ when the finite plate is driven by an harmonic point moment $M_{u1}(t)$ with arbitrary orientation u_1.

If instead of a point force, an harmonic point moment $M_{u1}(t) = \mathrm{Re}\left\{\tilde{M}_{u1}(\omega)e^{j\omega t}\right\}$ with arbitrary orientation u_1 is exciting the plate at position P_1, the translational velocity $\dot{w}_2(t)$ at position P_2 could be evaluated with the same approach used in section 2.4. and by using the modal formulation discussed in section 3.2. [21,28]. In fact, as shown in figure 15, the moment could be substituted by a pair of forces with opposite phases $N_z'(t) = +N_z(t)$ and $N_z''(t) = -N_z(t)$ applied along the line d_1 which is normal to the moment direction u_1 and at distance e apart from P_1. If the distance $2e$ between the two forces is reduced to zero then the moment $M_{u1}(t)$ with orientation u_1 is given by:

$$M_{u1}(t) = \lim_{e\to 0} 2eN_z(t). \qquad (3.35)$$

The phasor of the translational velocities $\dot{w}_2'(t)$ and $\dot{w}_2''(t)$ due respectively to $N_z'(t)$ and $N_z''(t)$ could be evaluated by using equation (3.18):

$$\tilde{\dot{w}}_2'(t) = j\omega \sum_{m=1}^{\infty}\sum_{n=1}^{\infty} W_{mn}'(t)\phi_{mn}(P_2) \qquad \tilde{\dot{w}}_2''(t) = j\omega \sum_{m=1}^{\infty}\sum_{n=1}^{\infty} W_{mn}''(t)\phi_{mn}(P_2) \tag{3.36,37}$$

where $W_{mn}'(t)$ is given by equation (3.27) assuming $\phi_{mn} = \phi_{mn}(P_1')$ and $W_{mn}''(t)$ is also given by equation (3.27) assuming $\phi_{mn} = \phi_{mn}(P_1'')$ with $P_1' = (x_1 - e\sin\beta_1, y_1 + e\cos\beta_1)$ and $P_1'' = (x_1 + e\sin\beta_1, y_1 - e\cos\beta)$.

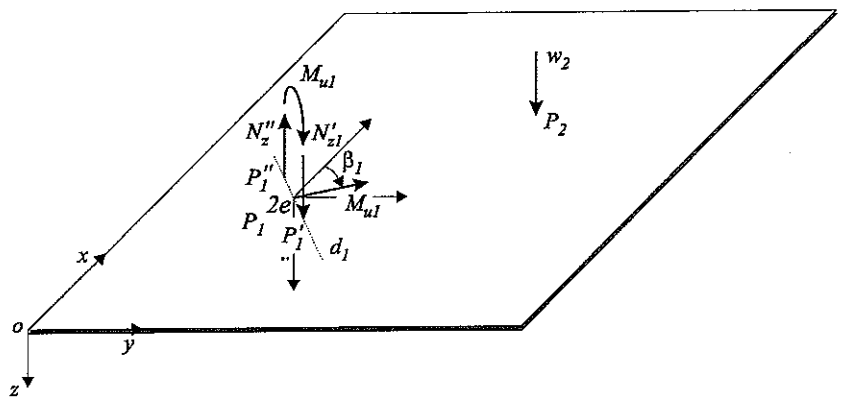

Fig. 15: *Notation of the translational displacement w at position P_2 induced by a moment M_{u1} at position P_1.*

Therefore the steady state translational velocity $\dot{w}_2(t)$ due to the moment $M_{u1}(t)$ is given by:

$$\dot{w}_2(t) = \mathrm{Re}\left\{\tilde{\dot{w}}_2(\omega)e^{j\omega t}\right\} = \lim_{e\to 0}\left[2e\dot{w}_2'(t) + 2e\dot{w}_2''(t)\right] = \mathrm{Re}\left\{ j\omega \sum_{m=1}^{\infty}\sum_{n=1}^{\infty} \frac{\phi_{mn}(P_2)\psi_{mn}^{(u_1)}(P_1)}{\Lambda_{mn}\left[\omega_{fmn}^2(1+j\eta) - \omega^2\right]} \cdot \tilde{M}_{u1}(\omega)e^{j\omega t} \right\} \tag{3.38}$$

where $\psi_{mn}^{(u_1)}(x,y)$ is given by equation (3.34) assuming $\beta = \beta_1$.

3.5. Modal expansion approach to calculate the steady-state angular velocity $\dot{\theta}_{u2}(t)$ of arbitrary u_2 orientation when the finite plate is driven by an harmonic point moment $M_{u1}(t)$ with arbitrary orientation u_1.

The steady state angular velocity $\dot{\theta}_{u2}(t)$ of orientation u_2 at P_2 due to a point moment $M_{u1}(t)$ excitation with arbitrary orientation u_1 at P_1 could be evaluated by using the same approach used in subsections 3.3. and 3.4. In fact, the angular velocity $\dot{\theta}_{u2}(t)$ can be calculated using equation (3.30) assuming that the translational velocities $\dot{w}_2'(t)$ and $\dot{w}_2''(t)$ are both due to a pair of forces with opposite phases $N_z'(t) = +N_z(t)$ and $N_z''(t) = -N_z(t)$ applied along the d_1 line at distance e from P_1 as it is shown in figure 15. The point moment excitation is then obtained by reducing to zero the distance $2e$ between the two forces. After some mathematical manipulations it comes out that

$$\dot{\theta}_{u2}(t) = \mathrm{Re}\left\{\tilde{\dot{\theta}}_{u2}(\omega)e^{j\omega t}\right\} = \mathrm{Re}\left\{ j\omega \sum_{m=1}^{\infty}\sum_{n=1}^{\infty} \frac{\psi_{mn}^{(u1)}(P_2)\psi_{mn}^{(u2)}(P_1)}{\Lambda_{mn}\left[\omega_{fmn}^2(1+j\eta)-\omega^2\right]} \cdot \tilde{M}_{u1}(\omega)e^{j\omega t} \right\}. \tag{3.39}$$

with both $\psi_{mn}^{(u1)}(x,y)$ and $\psi_{mn}^{(u2)}(x,y)$ given by equation (3.34) assuming respectively $\beta = \beta_1$ and $\beta = \beta_2$.

3.6. Mobility formulae for a finite rectangular plate excited in flexure.

Using the modal expansion approach described in previous subsections it is possible to derive an analytic formulation for the nine mechanical mobilities for either the driving-point or transfer mobility matrix of equation (3.16). Because the analytical formulae for the driving-point and transfer mobilities are the same, only the elements of the transfer mobility matrix are reported in here. The mobility term relating a translational velocity $\dot{w}_2(t)$ to a point force excitation $N_{z1}(t)$ can be derived directly by equation (3.29) so that

$$m_{wNz}^{21}(\omega) = \frac{\tilde{\dot{w}}_2(\omega)}{\tilde{N}_{z1}(\omega)} = j\omega \sum_{m=1}^{\infty}\sum_{n=1}^{\infty} \frac{\phi_{mn}(P_2)\phi_{mn}(P_1)}{\Lambda_{mn}\left[\omega_{fmn}^2(1+j\eta)-\omega^2\right]}. \tag{3.40}$$

The mobility terms relating a translational velocity $w_2(t)$ to the point moment excitations $M_{x2}(t)$ and $M_{y2}(t)$ can be derived from equation (3.38) assuming respectively $\beta_1 = 0^o$ or $\beta_1 = 90^o$ so that:

$$m_{wMx}^{21}(\omega) = \frac{\tilde{\dot{w}}_2(\omega)}{\tilde{M}_{x1}(\omega)} = j\omega \sum_{m=1}^{\infty}\sum_{n=1}^{\infty} \frac{\phi_{mn}(P_2)\psi_{mn}^{(x)}(P_1)}{\Lambda_{mn}\left[\omega_{fmn}^2(1+j\eta)-\omega^2\right]} \tag{3.41}$$

$$m_{wMy}^{21}(\omega) = \frac{\tilde{\dot{w}}_2(\omega)}{\tilde{M}_{y1}(\omega)} = j\omega \sum_{m=1}^{\infty}\sum_{n=1}^{\infty} \frac{\phi_{mn}(P_2)\psi_{mn}^{(y)}(P_1)}{\Lambda_{mn}\left[\omega_{fmn}^2(1+j\eta)-\omega^2\right]}. \tag{3.42}$$

where, assuming the plate simply supported so that the natural modes are given by equation (3.20), the two functions $\psi_{mn}^{(x)}(x,y)$ and $\psi_{mn}^{(y)}(x,y)$ assume the forms

$$\psi_{mn}^{(x)}(x,y) = \frac{n\pi}{l_y}\sin\frac{m\pi x}{l_x}\cos\frac{n\pi y}{l_y} \qquad \psi_{mn}^{(y)}(x,y) = -\frac{m\pi}{l_x}\cos\frac{m\pi x}{l_x}\sin\frac{n\pi y}{l_y}. \tag{3.43,44}$$

The mobility terms relating the angular velocities $\dot{\theta}_{x2}(t)$ and $\dot{\theta}_{y2}(t)$ to a point force excitation $N_{z1}(t)$ could be obtained from equation (3.33) assuming respectively $\beta_2 = 0^o$ or $\beta_2 = 90^o$ so that

$$m_{\theta xNz}^{21}(\omega) = \frac{\tilde{\dot{\theta}}_{x2}(\omega)}{\tilde{N}_{z1}(\omega)} = j\omega \sum_{m=1}^{\infty}\sum_{n=1}^{\infty} \frac{\psi_{mn}^{(x)}(P_2)\phi_{mn}(P_1)}{\Lambda_{mn}\left[\omega_{fmn}^2(1+j\eta)-\omega^2\right]} \tag{3.45}$$

$$m_{\theta yNz}^{21}(\omega) = \frac{\tilde{\dot{\theta}}_{y}(\omega)}{\tilde{N}_{z2}(\omega)} = j\omega \sum_{m=1}^{\infty}\sum_{n=1}^{\infty} \frac{\psi_{mn}^{(y)}(P_2)\phi_{mn}(P_1)}{\Lambda_{mn}\left[\omega_{fmn}^2(1+j\eta)-\omega^2\right]}. \tag{3.46}$$

Finally, the four mobility terms relating the angular velocities $\dot{\theta}_{x2}(t)$ and $\dot{\theta}_{y2}(t)$ to the point moment excitations $M_{x2}(t)$ and $M_{y2}(t)$ can be derived from equation (3.39) assuming also in this case $\beta_1 = 0^o$ or $\beta_1 = 90^o$ when $\beta_2 = 0^o$ or $\beta_2 = 90^o$ so that

$$m^{21}_{\theta xMx}(\omega) = \frac{\dot{\tilde{\theta}}_{x2}(\omega)}{\tilde{M}_{x1}(\omega)} = j\omega \sum_{m=1}^{\infty}\sum_{n=1}^{\infty} \frac{\psi^{(x)}_{mn}(P_2)\psi^{(x)}_{mn}(P_1)}{\Lambda_{mn}\left[\omega^2_{fmn}(1+j\eta)-\omega^2\right]} \tag{3.47}$$

$$m^{21}_{\theta xMy}(\omega) = \frac{\dot{\tilde{\theta}}_{x2}(\omega)}{\tilde{M}_{y1}(\omega)} = j\omega \sum_{m=1}^{\infty}\sum_{n=1}^{\infty} \frac{\psi^{(x)}_{mn}(P_2)\psi^{(y)}_{mn}(P_1)}{\Lambda_{mn}\left[\omega^2_{fmn}(1+j\eta)-\omega^2\right]} \tag{3.48}$$

$$m^{21}_{\theta yMx}(\omega) = \frac{\dot{\tilde{\theta}}_{y2}(\omega)}{\tilde{M}_{x1}(\omega)} = j\omega \sum_{m=1}^{\infty}\sum_{n=1}^{\infty} \frac{\psi^{(y)}_{mn}(P_2)\psi^{(x)}_{m,n}(P_1)}{\Lambda_{mn}\left[\omega^2_{fmn}(1+j\eta)-\omega^2\right]}. \tag{3.49}$$

$$m^{21}_{\theta yMy}(\omega) = \frac{\dot{\tilde{\theta}}_{y2}(\omega)}{\tilde{M}_{y1}(\omega)} = j\omega \sum_{m=1}^{\infty}\sum_{n=1}^{\infty} \frac{\psi^{(y)}_{mn}(P_2)\psi^{(y)}_{m,n}(P_1)}{\Lambda_{mn}\left[\omega^2_{fmn}(1+j\eta)-\omega^2\right]}. \tag{3.50}$$

The driving-point mobility terms could be evaluated using exactly the same formulae given by equations (3.42) to (3.50) just by assuming both natural mode functions evaluated at the position of the excitation P_1.

The formulae given here are valid for point force or moment excitations. If the excitation is acting over a rigid indenter of a relatively large area the effect of a distributed excitation should be included in the formulation. This could be done by calculating the modal force, given by equation (3.22), due to a uniform force $p_z(x,y,t) = \mathrm{Re}\{\tilde{p}_z(\omega)\exp(j\omega t)\}$ distributed over the indenter area S_{ind}

$$F_{mn}(t) = \frac{1}{\rho h N_{mn}} \int_{S_{ind}} \phi_{mn}(x,y)\tilde{p}_z(\omega)dS \cdot e^{j\omega t} \tag{3.51}$$

where $\tilde{p}_z(\omega) = \tilde{N}_z(\omega)/S_{ind}$ and the force acting on the indenter is given by $N_z(t) = \mathrm{Re}\{\tilde{N}_z(\omega)\exp(j\omega t)\}$. For a moment excitation the modal force is also evaluated using equation (3.51) but the uniform force over the indenter area S_{ind} has a dipole distribution oriented with reference to the moment orientation.

3.7. Approximate method for plates with all the four edges either free or clamped.

When a plate with four edges simply supported is considered, an exact solution of the wave equation and boundary condition equations can be found. This is not the case for plates with all four edges either free or clamped, thus an approximate solution must be used. Warburton [31] has derived formulae for the natural modes and natural frequencies by applying the Rayleigh method. He assumed that the natural modes of plates and beams are similar so that, for example, the natural modes of a plate of dimensions $l_x \times l_y$ with all edges clamped is the product of the natural modes of two beams of lengths l_x and l_y and with the ends clamped as well. A general description of the theory of this approximate method can be found in references [31,32].

From reference [31] the natural frequency for plates with all four edges either free or clamped can be calculated using the following equation

$$\omega_{fmn} = \sqrt{\frac{Eh^2}{12\rho(1-\nu^2)}} \cdot \left(\frac{\pi}{l_x}\right)^2 q_{ik} \tag{3.52}$$

where ω_{fmn} is in rad/s, $\underline{i = m+1}$, $\underline{k = n+1}$ and

$$q_{ik} = \sqrt{G_x^4(i) + G_y^4(k)\left(\frac{l_x}{l_y}\right)^4 + 2\left(\frac{l_x}{l_y}\right)^2 \left[\nu H_x(i)H_y(k) + (1-\nu)J_x(i)J_y(k)\right]}. \tag{3.53}$$

The constants G_x, G_y, H_x, H_y, J_x, J_y are summarised in tables 1 and 2 respectively for a plate with all four edges either free or clamped.

Table 1: *Values for the constants G_x, G_y, H_x, H_y, J_x, J_y when a rectangular plate have all four edges free (from reference [31]).*

i or k	$G_x(i)$ or $G_y(k)$	$H_x(i)$ or $H_y(k)$	$J_x(i)$ or $J_y(k)$
0	0	0	0
1	0	0	$12/\pi^2$
2	1.506	1.248	5.017
3,4,5,....	$i-\frac{1}{2}$	$\left(i-\frac{1}{2}\right)^2\left(1-\frac{4}{(2i-1)\pi}\right)$	$\left(i-\frac{1}{2}\right)^2\left(1+\frac{12}{(2i-1)\pi}\right)$

Table 2: *Values for the constants G_x, G_y, H_x, H_y, J_x, J_y when a rectangular plate have all four edges are clamped (from reference [31]).*

i or k	G_x or G_y	H_x or H_y	J_x or J_y
2	1.506	1.248	1.248
3,4,5,....	$i-\frac{1}{2}$	$\left(i-\frac{1}{2}\right)^2\left(1-\frac{4}{(2i-1)\pi}\right)$	$\left(i-\frac{1}{2}\right)^2\left(1-\frac{4}{(2i-1)\pi}\right)$

The plate natural modes $\phi_{mn}(x,y)$ are given by the product of the $\varphi_m(x)$ and $\varphi_n(y)$ beam functions

$$\phi_{mn}(x,y) = \varphi_i(x)\varphi_k(y). \tag{3.54}$$

The function $\varphi_i(x)$ represents the natural modes of a beam having the same boundary conditions of the plate under consideration at $y = 0$ and $y = l_y$ and, in the same way, the function $\varphi_k(y)$ represents the natural modes of a beam having the same boundary conditions of the plate under consideration at $x = 0$ and $x = l_x$. The boundary conditions for a plate with all edges free are given by [1,31]:

$$\begin{array}{lll} x=0 \text{ and } x=l_x & \dfrac{\partial^2 w}{\partial x^2}=0 & \dfrac{\partial^3 w}{\partial x^3}=0 \\ y=0 \text{ and } y=l_y & \dfrac{\partial^2 w}{\partial y^2}=0 & \dfrac{\partial^3 w}{\partial y^3}=0 \end{array} \tag{3.55}$$

The beam functions in the x-direction for a free-free beam are given by [31,32]:

$$\begin{aligned} \varphi_0(x) &= \sqrt{1/2} \\ \varphi_1(x) &= \sqrt{3/2}\left(1-\frac{2x}{l_x}\right) \\ \varphi_{2,4,6,\ldots}(x) &= \cos\gamma_i\left(\frac{x}{l_x}-\frac{1}{2}\right)+k_i\cosh\gamma_i\left(\frac{x}{l_x}-\frac{1}{2}\right) \\ \varphi_{3,5,7,\ldots}(x) &= \sin\gamma_i'\left(\frac{x}{l_x}-\frac{1}{2}\right)+k_i'\sinh\gamma_i'\left(\frac{x}{l_x}-\frac{1}{2}\right) \end{aligned} \tag{3.56}$$

where

$$k_i=-\frac{\sin(\gamma_i/2)}{\sinh(\gamma_i/2)} \qquad k_i'=\frac{\sin(\gamma_i'/2)}{\sinh(\gamma_i'/2)}. \tag{3.57,58}$$

and the constants γ_i and γ_i' are the i-th zeros of the two following implicit equations

$$\tan(\gamma_i/2)+\tanh(\gamma_i/2)=0 \qquad \tan(\gamma_i'/2)-\tanh(\gamma_i'/2)=0 \tag{3.59,60}$$

Bishop and Johnson's book [4] (p 389 and p 397) reports tables with the first 5 roots of these equations and gives approximate equations for the higher order roots.

Table 3: *Roots for the 2 equations (3.59) and (3.60). r=6,7,8,9,....*

$\gamma_2=4{,}7300$	$\gamma_3'=7{,}8532$
$\gamma_4=10{,}9956$	$\gamma_5'=14{,}1372$
$\gamma_6=17{,}2788$	$\gamma_7'=20{,}4204$
$\gamma_8=23{,}5620$	$\gamma_9'=26{,}7036$
$\gamma_{10}=29{,}8452$	$\gamma_{11}'=32{,}9868$
$\gamma_{12,14,\ldots}=(4r-1)\pi/2$	$\gamma_{13,15,\ldots}'=(4r+1)\pi/2$

In table 3 $r=6,7,8,\ldots$. The beam functions in the y-direction are same as those in the x-direction given by equation (3.56) which are all normalised so that

$$\int_0^{l_x}\varphi_i^2(x)dx=\frac{l_x}{2} \qquad \int_0^{l_y}\varphi_k^2(y)dy=\frac{l_y}{2}. \tag{3.61,62}$$

Therefore, considering a plate with four edges free, the norm Λ_{mn} given in equation (3.28) becomes

$$\Lambda_{mn} = \rho h \int_0^{l_x}\int_0^{l_y} \varphi_i^2(x)\varphi_k^2(y)dxdy = \rho h \frac{l_x l_y}{4}. \tag{3.63}$$

The first three natural modes for a plate with all edges free are rigid body modes and therefore the indices m and n have not the usual meaning, that is to represent the number of half standing waves in the x and y directions for the mode ϕ_{mn}. The first rigid body mode is for $i,k = 0,0$ (e.g. $m,n = -1,-1$) and represents a translational oscillation in the z direction of the plate. The second and third rigid body modes are for $i,k = 0,1$ and $i,k = 1,0$ (e.g. $m,n = -1,0$ and $m,n = 0,-1$ respectively) and represent rigid body angular oscillations around the x and y axes respectively. In this case the double summations in the mobility formulae of equations (3.40) to (3.50) should consider $m = -1,0,1,2,3,\ldots$ and $n = -1,0,1,2,3,\ldots$

The boundary conditions for a plate with all edges clamped are given by [1,31]:

$$\begin{aligned} &x = 0 \text{ and } x = l_x && w = 0 && \frac{\partial w}{\partial x} = 0 \\ &y = 0 \text{ and } y = l_y && w = 0 && \frac{\partial w}{\partial y} = 0 \end{aligned} \tag{3.64}$$

and the beam functions in the x-direction for a clamped-clamped beam, also given in references [31,32], are:

$$\begin{aligned} \varphi_{2,4,6,\ldots}(x) &= \cos\gamma_i\left(\frac{x}{l_x} - \frac{1}{2}\right) + k_i \cosh\gamma_i\left(\frac{x}{l_x} - \frac{1}{2}\right) \\ \varphi_{3,5,7,\ldots}(x) &= \sin\gamma_i'\left(\frac{x}{l_x} - \frac{1}{2}\right) + k_i' \sinh\gamma_i'\left(\frac{x}{l_x} - \frac{1}{2}\right) \end{aligned} \tag{3.65}$$

where in this case

$$k_i = \frac{\sin(\gamma_i/2)}{\sinh(\gamma_i/2)} \qquad k_i' = -\frac{\sin(\gamma_i'/2)}{\sinh(\gamma_i'/2)}. \tag{3.66,67}$$

and the constants γ_i and γ_i' are the i-th zeros of the two following implicit equations

$$\tan(\gamma_i/2) + \tanh(\gamma_i/2) = 0 \qquad \tan(\gamma_i'/2) - \tanh(\gamma_i'/2) = 0 \tag{3.68,69}$$

whose roots are summarised in table 3. Also in this case the beam functions in the y-direction are the same as those in the x-direction given by equation (3.65) and are all normalised so that the norm Λ_{mn} for a plate with all edges clamped is given by $\Lambda_{mn} = \rho h l_x l_y/4$.

The functions $\psi_{mn}^{(x)}(x,y)$ and $\psi_{mn}^{(y)}(x,y)$, which are required to derive the mobility equations (3.40) to (3.50) are given by equation (3.34) assuming $\beta = 0^o$ or $\beta = 90^o$ respectively. Since the natural modes are given by the product of beam functions as in equation (3.54), equation (3.34) can be written as follow:

$$\psi_{mn}^{(u)}(x,y) = -\sin\beta \cdot \varphi_k(y) \cdot \frac{\partial \varphi_i(x)}{\partial x} + \cos\beta \cdot \varphi_i(x) \cdot \frac{\partial \varphi_k(y)}{\partial y}, \tag{3.70}$$

therefore:

$$\psi_{mn}^{(x)}(x,y)=\varphi_i(x)\cdot\frac{\partial\varphi_k(y)}{\partial y}\qquad\qquad \psi_{mn}^{(y)}(x,y)=-\varphi_k(y)\cdot\frac{\partial\varphi_i(x)}{\partial x}. \tag{3.71,72}$$

Considering a beam with both ends free the term $\varphi_i'=\partial\varphi_i(x)/\partial x$ is given by

$$\begin{aligned}
&\varphi_0'(x)=0\\
&\varphi_1'(x)=-\sqrt{6}/l_x\\
&\varphi_{2,4,6,\ldots}'(x)=\frac{\gamma_i}{l_x}\left\{-\sin\gamma_i\left(\frac{x}{l_x}-\frac{1}{2}\right)+k_i\sinh\gamma_i\left(\frac{x}{l_x}-\frac{1}{2}\right)\right\}.\\
&\varphi_{3,5,7,\ldots}'(x)=\frac{\gamma_i'}{l_x}\left\{\cos\gamma_i'\left(\frac{x}{l_x}-\frac{1}{2}\right)+k_i'\cosh\gamma_i'\left(\frac{x}{l_x}-\frac{1}{2}\right)\right\}
\end{aligned} \tag{3.73}$$

and equal types of expression gives the $\varphi_k'=\partial\varphi_k(x)/\partial y$. For the beam with both ends clamped the term $\varphi_i'=\partial\varphi_i(x)/\partial x$ is given by

$$\begin{aligned}
&\varphi_{2,4,6,\ldots}'(x)=\frac{\gamma_i}{l_x}\left\{-\sin\gamma_i\left(\frac{x}{l_x}-\frac{1}{2}\right)+k_i\sinh\gamma_i\left(\frac{x}{l_x}-\frac{1}{2}\right)\right\}\\
&\varphi_{3,5,6,\ldots}'(x)=\frac{\gamma_i'}{l_x}\left\{\cos\gamma_i'\left(\frac{x}{l_x}-\frac{1}{2}\right)+k_i'\cosh\gamma_i'\left(\frac{x}{l_x}-\frac{1}{2}\right)\right\}
\end{aligned}. \tag{3.74}$$

and, also in this case, equal types of expression give the $\varphi_k'=\partial\varphi_k(x)/\partial y$.

The method described in this section to calculate the natural frequencies, modal amplitudes and modal slopes needed to calculate the driving point and transfer mobilities of finite plates (equations (3.40) to (3.3.50)) can be used for rectangular plates having any combination of the three basic edge boundary conditions, e.g. simply supported, freely supported and clamped. For example it could be used to study a plate with the two opposite edges in the x direction free and the other two opposite edges in the y direction clamped and simply supported respectively. In this case the beam function in the x direction $\varphi_i(x)$ is given by the mode shape of a clamped-simply supported beam and the beam function in the y direction $\varphi_k(y)$ is given by the mode shape of a free-free plate. The mode shapes for a beam with boundary conditions which differ from each other could be found in references [31,32] where the constants needed to calculate the natural frequency equation (3.52, 3.53) are also reported.

Figures 16 to 18 show the modal amplitude and the modal slope of the first four modes respectively for a simply supported beam, for a freely supported beam and for a clamped beam. From the plots of figure 17 it is clear that the first two modes (m=-1, m=0) of the freely suspended beam differ from the other modes (m=1, m=2) of the freely supported beam or from the model m=1,2,3,4,.... of the simply supported or clamped beams since they are not characterised by a deformation of the beam. These two peculiar modes are the so called "*rigid body modes*". The mode number m=-1 and m=0 have no meaning, they have been assigned in such a way to be consistent with the modal formulation adopted for the mobility formulae derived in section 3.6. The mode numbers, m=1,2,3,4,... have instead a precise meaning: they represent the number of half standing waves of the mode.

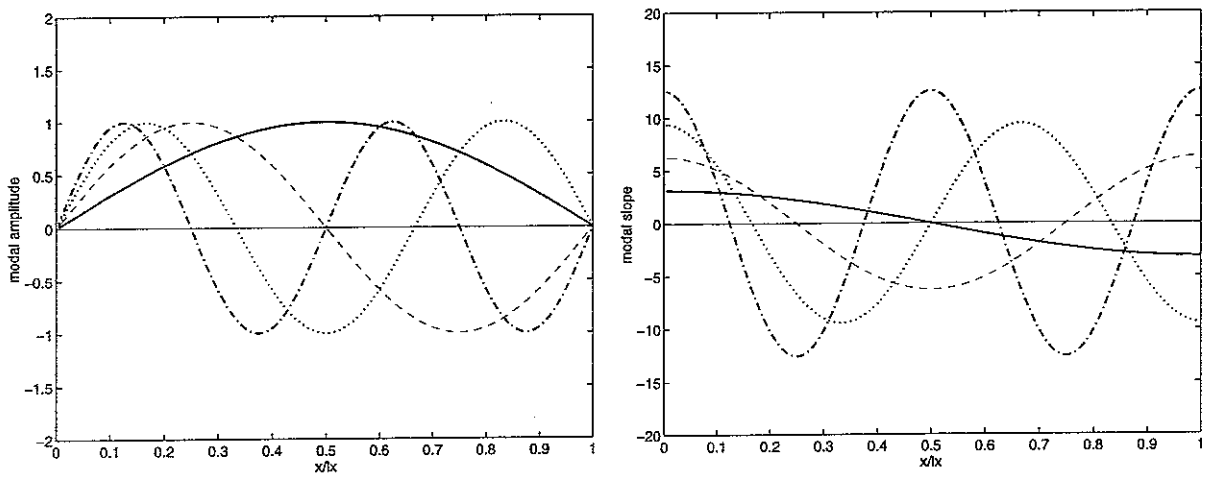

Fig.: 16: *Modal amplitude and modal slope of a simply supported beam. Solid line* m=1, *dashed line* m=2, *dotted line* m=3, *dash-dotted line* m=4.

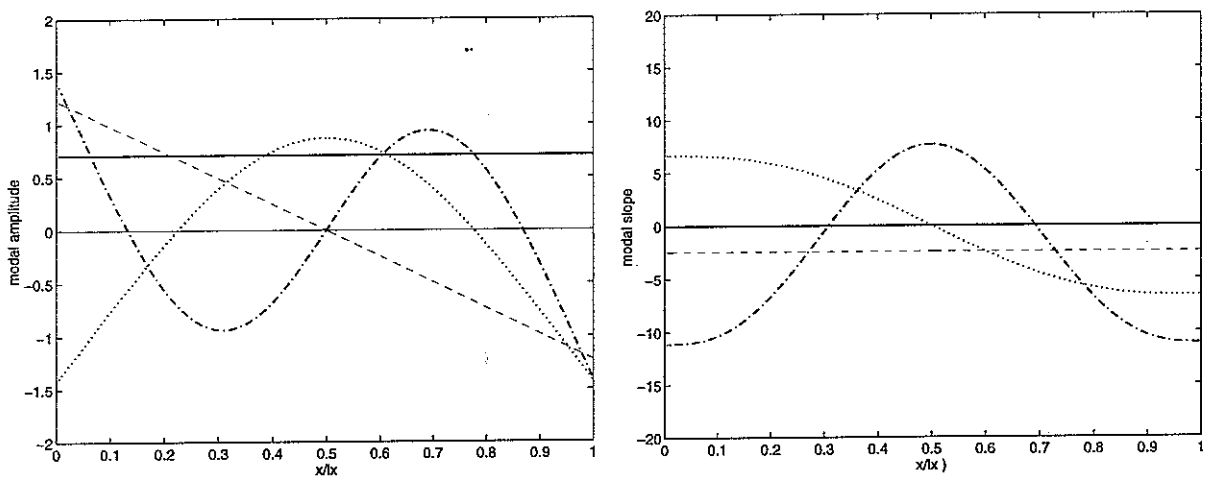

Fig.: 17: *Modal amplitude and modal slope of a freely supported beam. Solid line* m=-1 *(translational rigid body mode), dashed line* m=0 *(rocking rigid body mode), dotted line* m=1, *dash-dotted line* m=2.

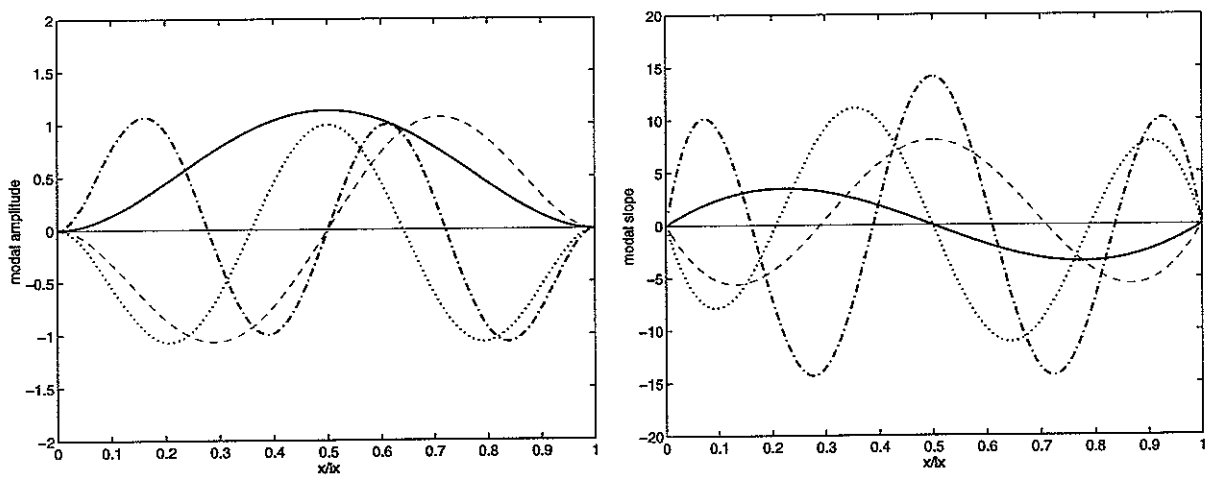

Fig.: 18: *Modal amplitude and modal slope of a clamped beam. Solid line* m=1, *dashed line* m=2, *dotted line* m=3, *dash-dotted line* m=4.

3.8. Frequency spectrum of the point and transfer mobility parameters

In this section the frequency spectrum between 0 and 1000 Hz of the nine driving point and transfer mobility parameters are plotted for the three cases of boundary conditions considered i.e. all edges simply supported, all edges free and all edges clamped.

The plate considered is made of aluminium with density $\rho = 2798$ Kg/m^3, Young's modulus of elasticity $E_s = 7.2 \times 10^{10}$ N/m^2, Poisson's ratio 0.33. The plate thickness is $h = 3$ mm and dimensions are $l_x = 0.48$ m, $l_y = 0.2$ m. The driving point mobility matrix is evaluated at position $P_1 = (0.30\ ,\ 0.15)$ while the transfer mobility matrix is evaluated between position P_1 (excitation position) and position $P_2 = (0.35\ ,\ 0.09)$ (velocity position).

The natural frequencies in the frequency range considered, i.e. 0-1000 Hz, of the three types of plate under consideration are given in tables 4,5,6.

Table 4: Natural frequencies of the simply supported plate.

m	*n*	*f* (Hz)
1	1	214.5
2	1	309.7
3	1	468.3
4	1	690.4
1	2	762.7
2	2	857.9
5	1	976.0
3	2	1016.6

Table 5: Natural frequencies of the freely supported plate.

m	*n*	*f* (Hz)
-1 t	-1 t	0
-1 t	0 r	0
0 r	-1 t	0
1	-1 t	71.96
0 r	0 r	107.2
2	-1 t	198.3
1	0 r	229.3
2	0 r	378.8
3	-1 t	388.7
-1 t	1	414.5
0 r	1	468.2
3	0 r	574.4
1	1	615.2
4	-1 t	642.5
2	1	814.3
4	0 r	827.8
5	-1	959.8

Table 6: Natural frequencies of the clamped plate.

m	*n*	*f* (Hz)
1	1	441.6
2	1	527.8
3	1	684.0
4	1	914.5

Note: in table 5 **t** stands for "*translational mode*" and **r** stands for "*rocking mode*"

For each type of boundary condition eleven plots are reported. The first one consists of a 3×3 matrix of plots showing the modulus of the nine driving point or transfer mobilities (figures 19, 30, 41). The second one shows the frequency spectrum of the driving point and transfer mobility $Y^{ij}_{wN_z}(\omega) = \tilde{\dot{w}}_{zi}(\omega) / \tilde{N}_{zj}(\omega)$ (figures 19, 31, 42). The other nine pictures consist of a 2×2 matrix of plots showing the real and imaginary parts of the nine driving point or transfer mobilities (figures 20-28, 31-39, 42-51).

Considering the plots of the modulus of the point and transfer mobilities given in figures 19-20, 30-31, 41-42 for the three types of boundary condition it can be seen that the mobility parameters of the plate with all edges simply supported or clamped (figures 19-20 and 41-42) present a similar frequency spectrum which is characterised by a spring like behaviour [19] at frequencies below the first resonance and by a mass like behaviour at higher frequencies [5]. The low frequency response of the plate is in fact dominated by the local stiffeness reaction of the plate while for frequencies above the first resonance, the spectrum tends to drift downwards with antiresonances occurring immediately before resonance which is the characteristic mobility trend shown by a system whose response is dominated by the inertia of its mass (see pages 154-156 of reference [5]). The modulus of the point and transfer mobilities derived for the plate with all edges free (figures 30 and 31) is characterised by a mass like behaviour in all frequency ranges. Unlikley the other two cases, at frequencies below the first

resonance is dominated by a mass like behaviour [19] since the plate is vibrating as a rigid body and therefore the response is controlled by the mass of the plate.

The nine plots showing the spectra of the real and imaginary parts of the point and transfer mobilities for the three types of plate considered show that the following conditions are valid for the driving point mobility matrices (top plots of figures 21-29, 32-40, 42-51):

$$\mathrm{Re}\left\{Y^{11}_{w_z N_z}(\omega)\right\} > 0 \qquad \mathrm{Re}\left\{Y^{11}_{\theta_x M_x}(\omega)\right\} > 0 \qquad \mathrm{Re}\left\{Y^{11}_{\theta_y M_y}(\omega)\right\} > 0 \quad (3.75\text{-}77)$$

and

$$Y^{11}_{\theta_x N_z}(\omega) = Y^{11}_{w_z M_x}(\omega) \qquad Y^{11}_{\theta_y N_z}(\omega) = Y^{11}_{w_z M_y}(\omega) \qquad Y^{11}_{\theta_y M_x}(\omega) = Y^{11}_{\theta_x M_y}(\omega) \quad (3.78\text{-}80)$$

In other words, the driving point mobility matrix $\mathbf{Y}^{11}(\omega)$ is positive definite [25,26] since it is symmetric and the real part of the diagonal terms is always positive. The transfer mobility matrix $\mathbf{Y}^{21}(\omega)$ is not positive definite, in fact, as shown in the bottom two plots of figures 21-29, 32-40 and 42-51 the following conditions hold:

$$-\infty < Y^{21}_{w_z N_z}(\omega) < +\infty \qquad -\infty < Y^{21}_{\theta_x M_x}(\omega) < +\infty \qquad -\infty < Y^{21}_{\theta_y M_y}(\omega) < +\infty \quad (3.81\text{-}83)$$

and

$$Y^{21}_{\theta_x N_z}(\omega) \neq Y^{21}_{w_z M_x}(\omega) \qquad Y^{21}_{\theta_y N_z}(\omega) \neq Y^{21}_{w_z M_y}(\omega) \qquad Y^{21}_{\theta_y M_x}(\omega) \neq Y^{21}_{\theta_x M_y}(\omega) \quad (3.84\text{-}86)$$

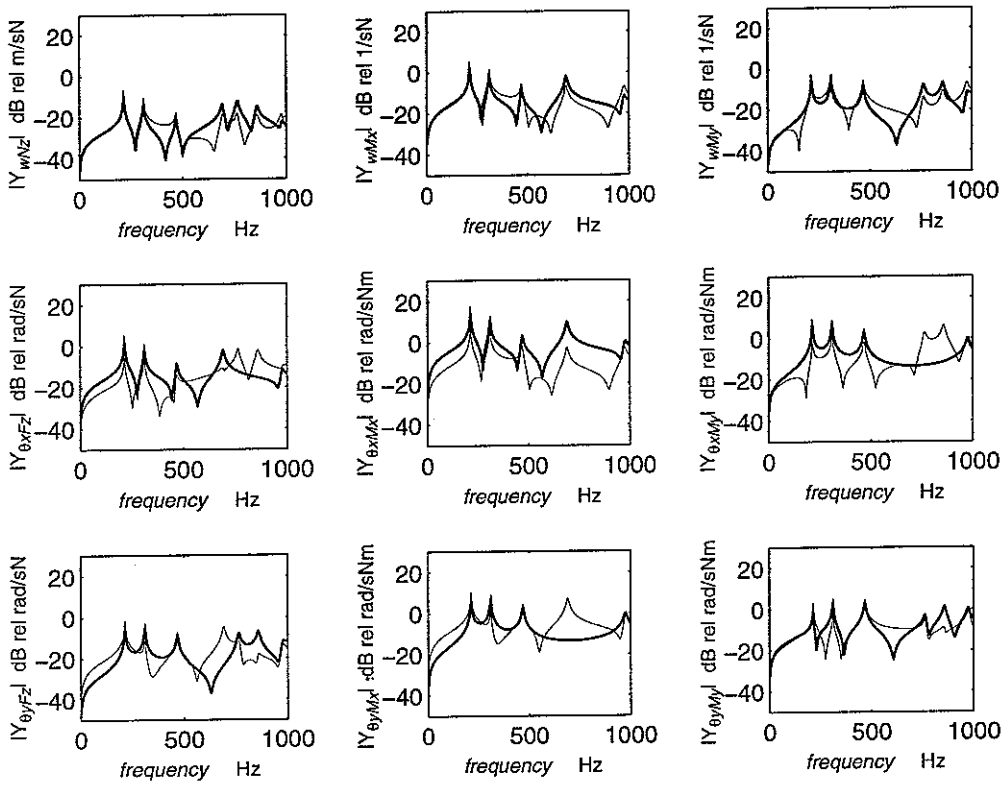

Fig. 19: *Modulus of the nine driving-point (solid line) and transfer (faint line) mobilities for a plate having all four edges simply supported.*

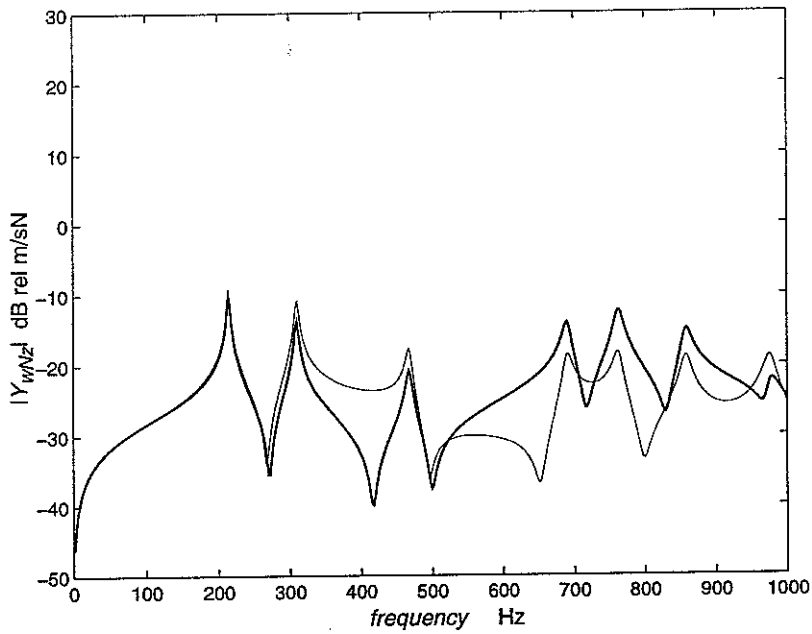

Fig. 20: *Modulus of the Y_{wFz} driving-point (solid line) and transfer (faint line) mobilities for a plate having all four edges simply supported.*

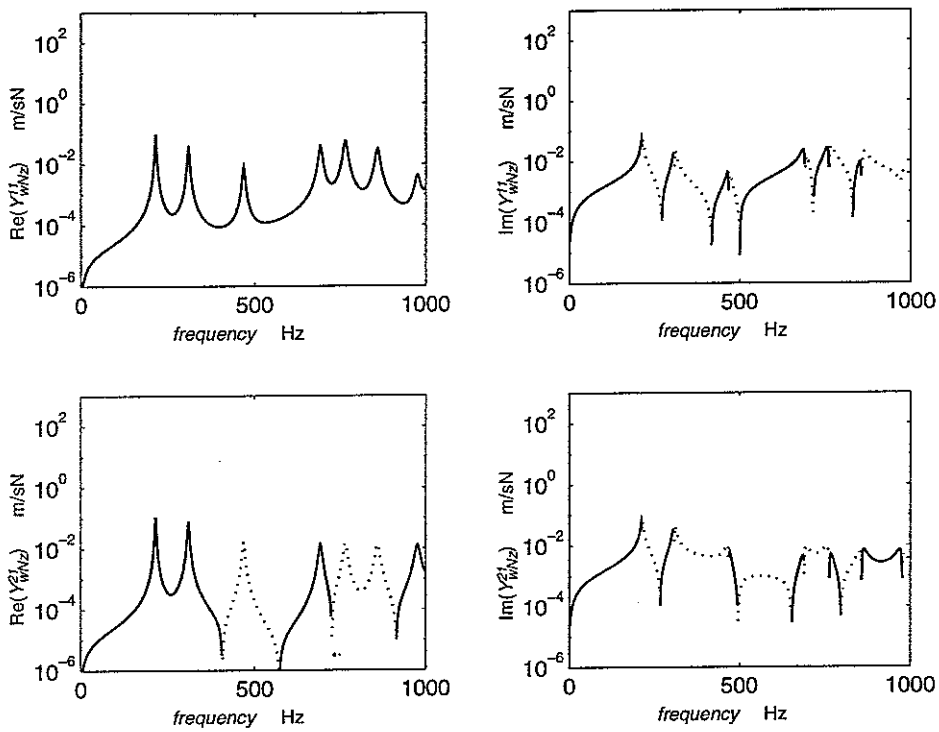

Fig. 21: *Real (left-side plots) and imaginary (right-side plots) part of the Y_{wFz} driving-point (top plots) and transfer (bottom plots) mobilities for a plate having all four edges simply supported. Solid line: positive values, dotted line: negative values.*

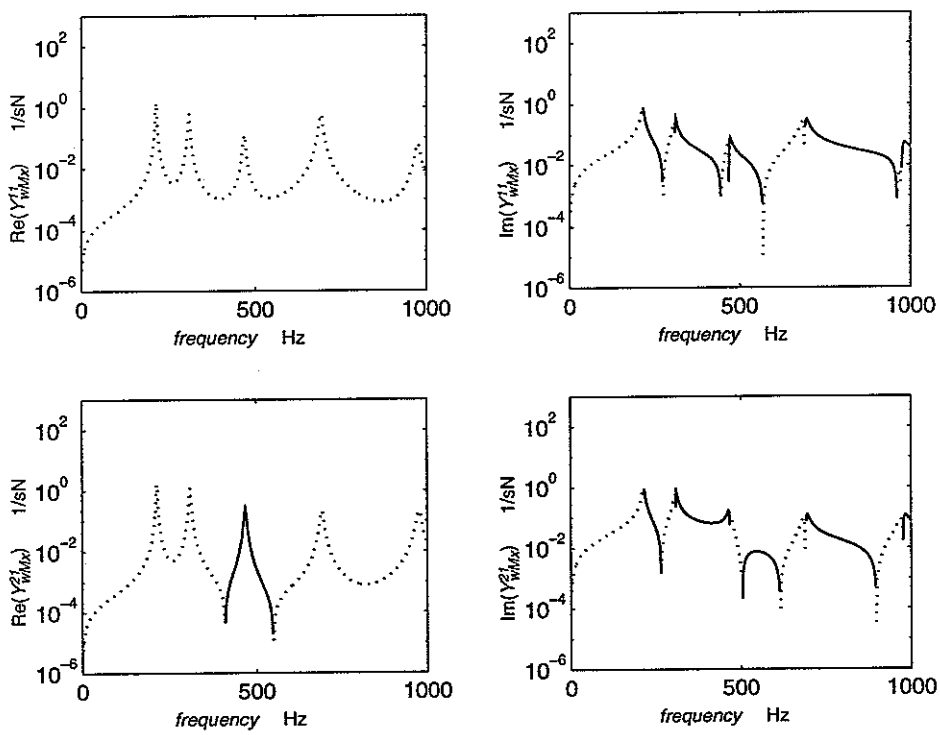

Fig. 22: *Real (left-side plots) and imaginary (right-side plots) part of the Y_{wMx} driving-point (top plots) and transfer (bottom plots) mobilities for a plate having all four edges simply supported. Solid line: positive values, dotted line: negative values.*

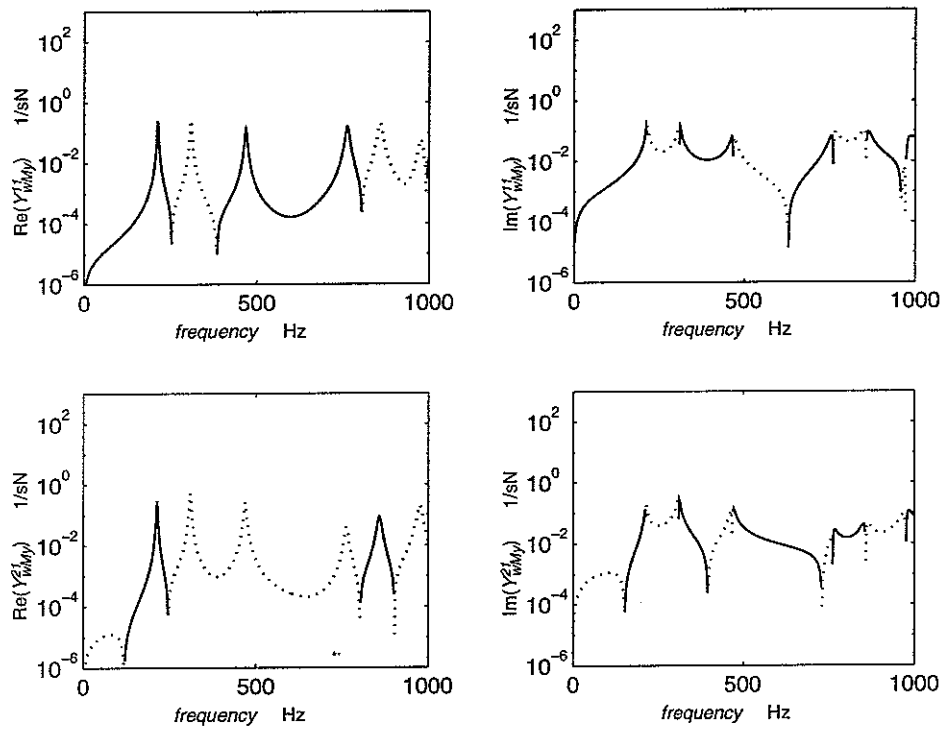

Fig. 23: *Real (left-side plots) and imaginary (right-side plots) part of the Y_{wMy} driving-point (top plots) and transfer (bottom plots) mobilities for a plate having all four edges simply supported. Solid line: positive values, dotted line: negative values.*

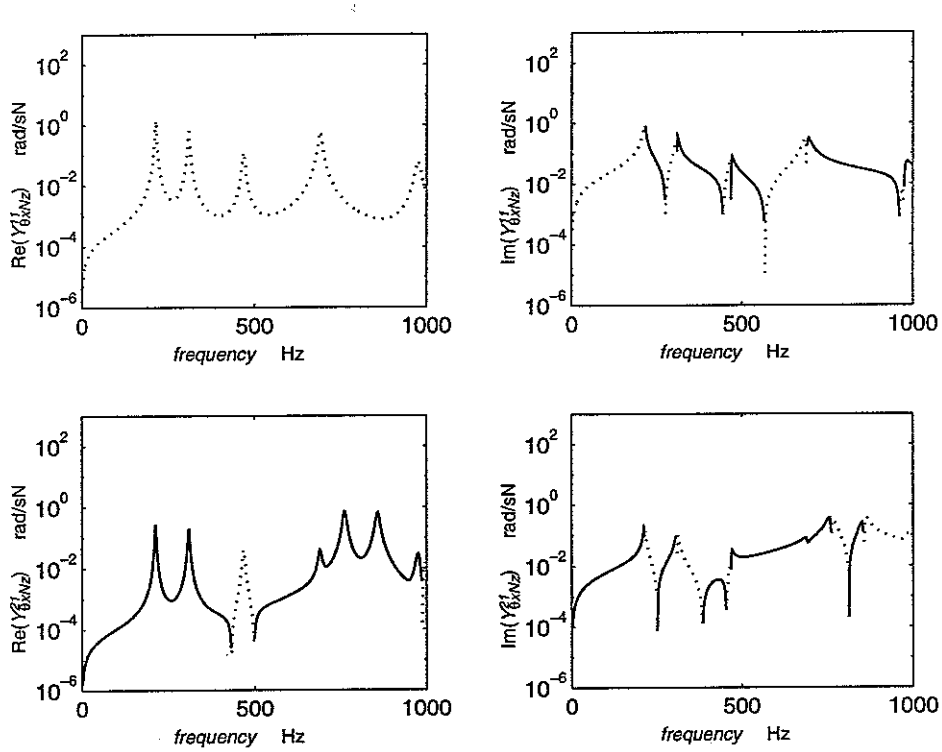

Fig. 24: *Real (left-side plots) and imaginary (right-side plots) part of the $Y_{\theta xFz}$ driving-point (top plots) and transfer (bottom plots) mobilities for a plate having all four edges simply supported. Solid line: positive values, dotted line: negative values.*

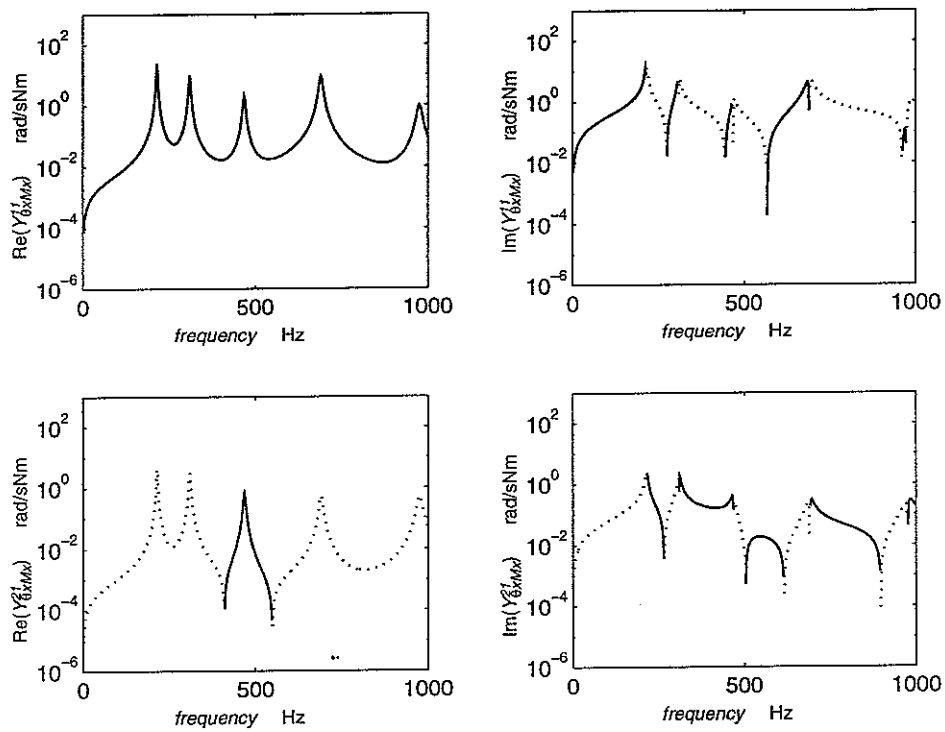

Fig. 25: *Real (left-side plots) and imaginary (right-side plots) part of the $Y_{\theta xMx}$ driving-point (top plots) and transfer (bottom plots) mobilities for a plate having all four edges simply supported. Solid line: positive values, dotted line: negative values.*

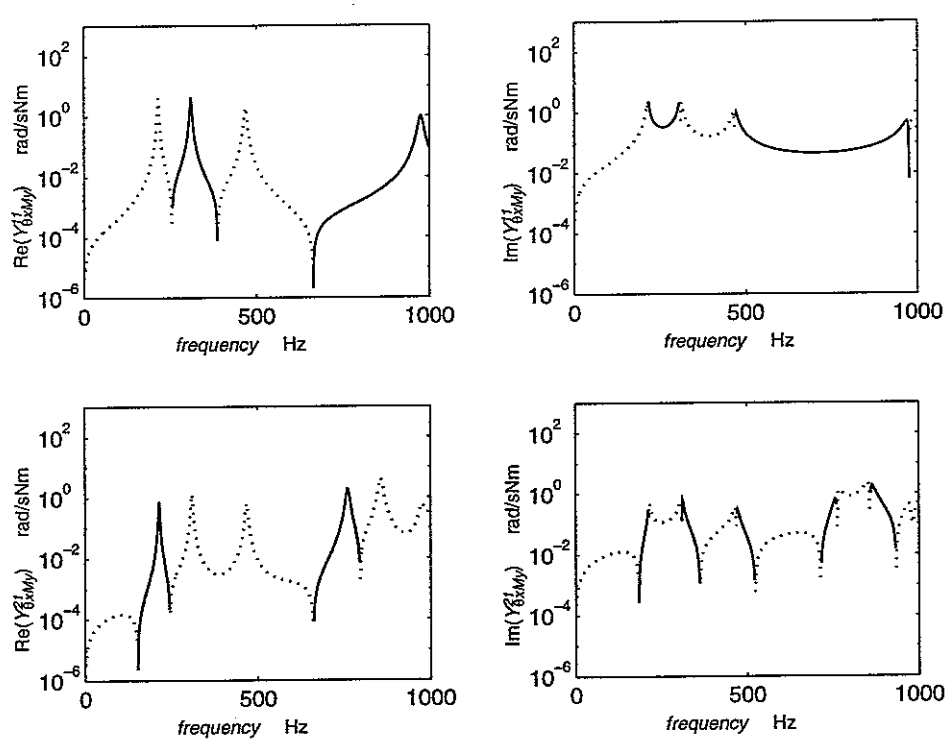

Fig. 26: *Real (left-side plots) and imaginary (right-side plots) part of the $Y_{\theta xMy}$ driving-point (top plots) and transfer (bottom plots) mobilities for a plate having all four edges simply supported. Solid line: positive values, dotted line: negative values.*

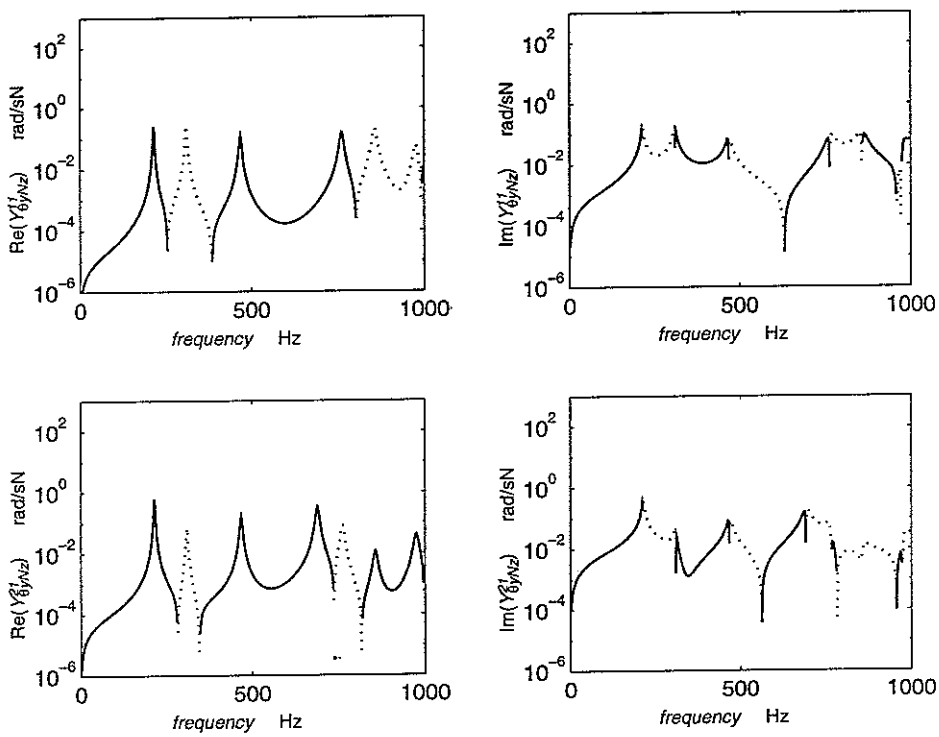

Fig. 27: *Real (left-side plots) and imaginary (right-side plots) part of the $Y_{\theta yFz}$ driving-point (top plots) and transfer (bottom plots) mobilities for a plate having all four edges simply supported. Solid line: positive values, dotted line: negative values.*

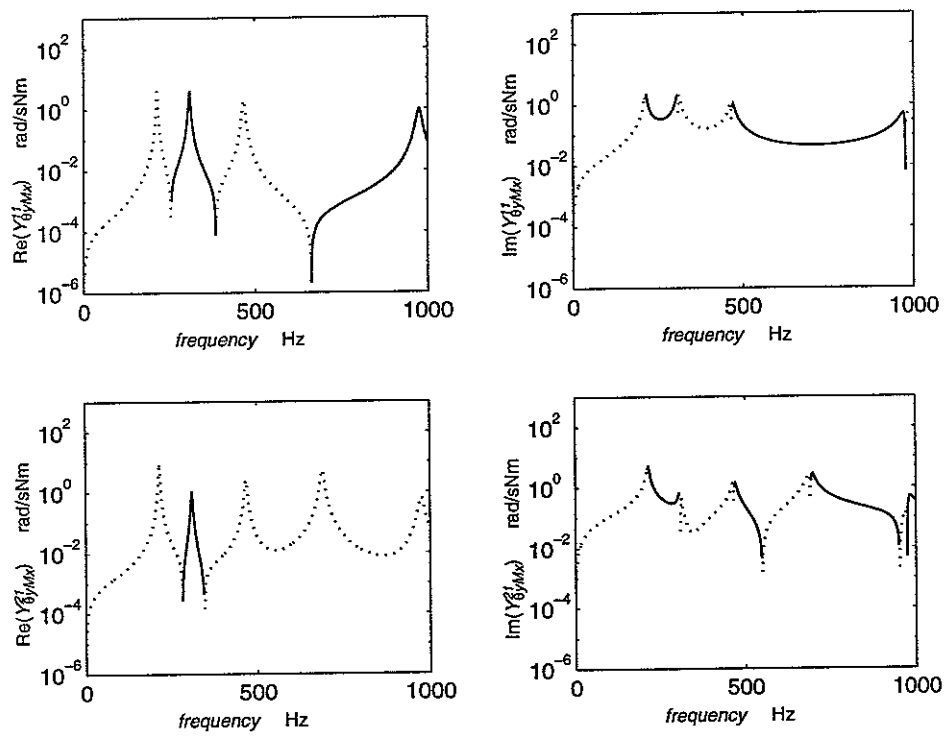

Fig. 28: *Real (left-side plots) and imaginary (right-side plots) part of the $Y_{\theta yMx}$ driving-point (top plots) and transfer (bottom plots) mobilities for a plate having all four edges simply supported. Solid line: positive values, dotted line: negative values.*

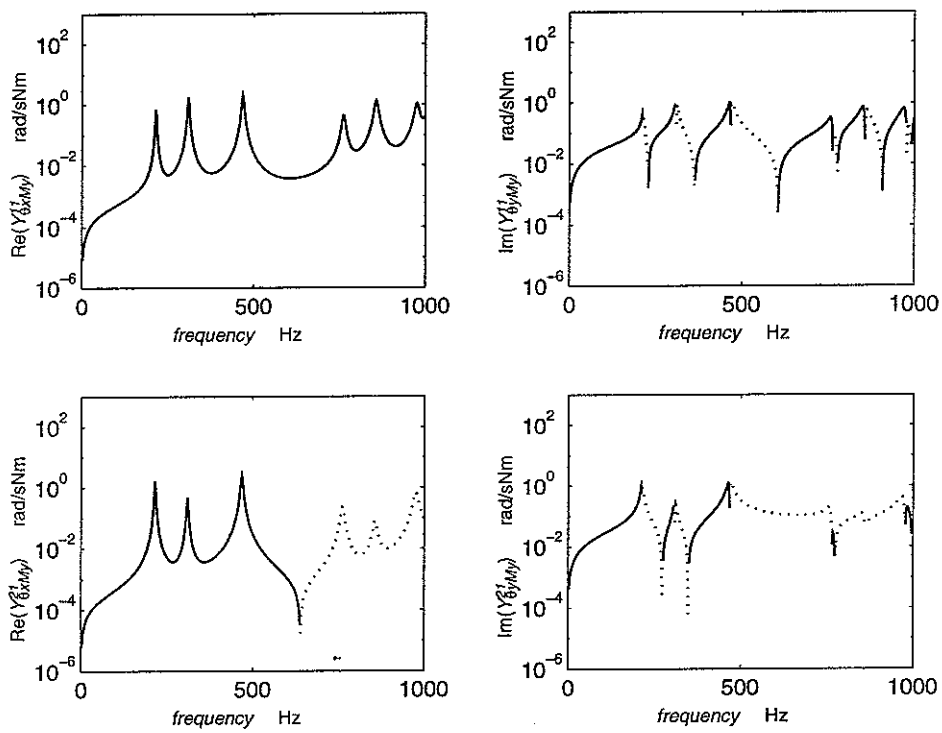

Fig. 29: *Real (left-side plots) and imaginary (right-side plots) part of the $Y_{\theta yMy}$ driving-point (top plots) and transfer (bottom plots) mobilities for a plate having all four edges simply supported. Solid line: positive values, dotted line: negative values.*

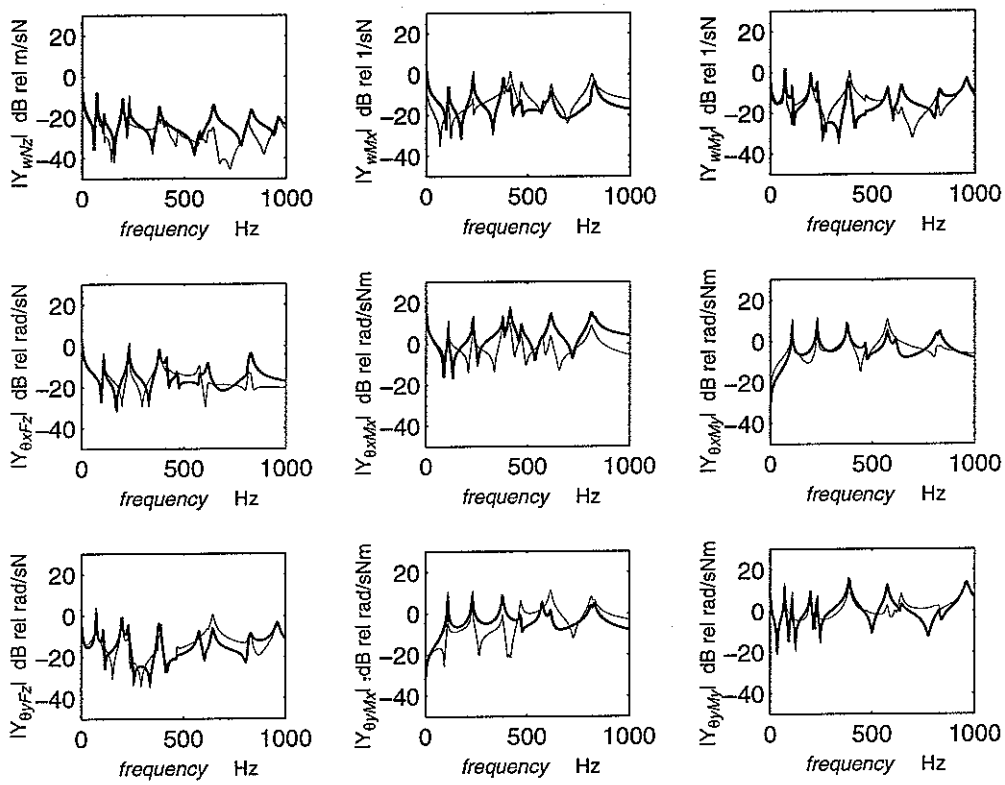

Fig. 30: *Modulus of the nine driving-point (solid line) and transfer (faint line) mobilities for a plate having all four edges free.*

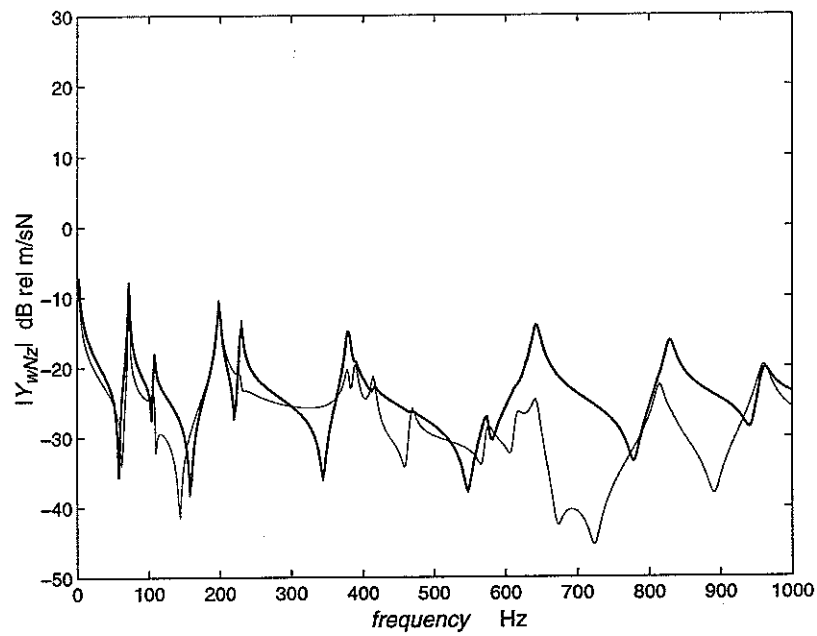

Fig. 31: *Modulus of the Y_{wFz} driving-point (solid line) and transfer (faint line) mobilities for a plate having all four edges free.*

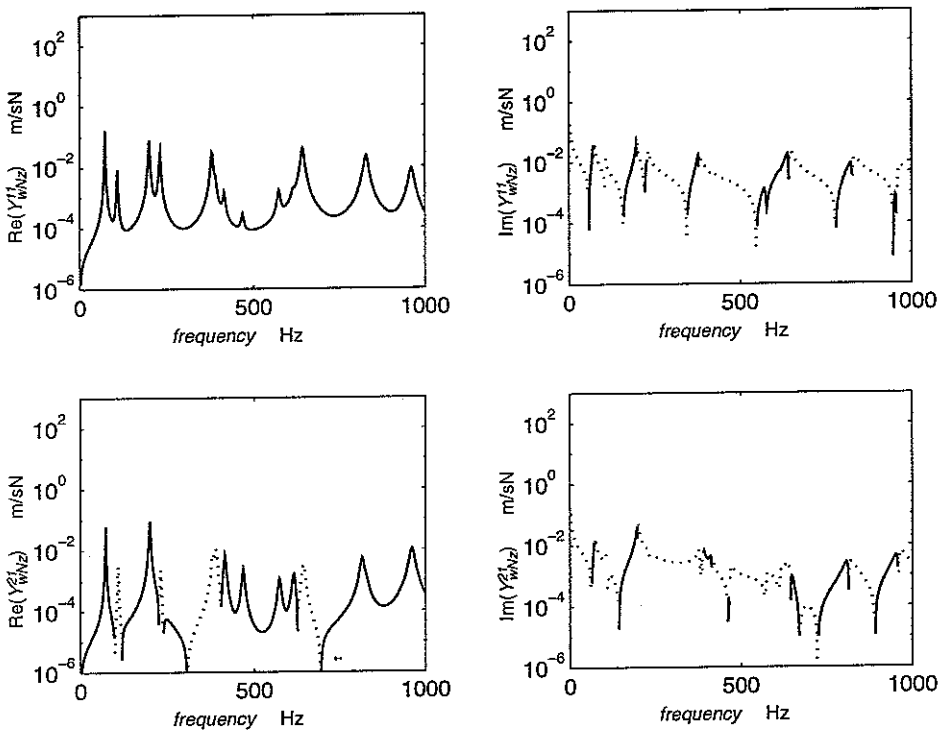

Fig. 32: *Real (left-side plots) and imaginary (right-side plots) part of the Y_{wFz} driving-point (top plots) and transfer (bottom plots) mobilities for a plate having all four edges free. Solid line: positive values, dotted line: negative values.*

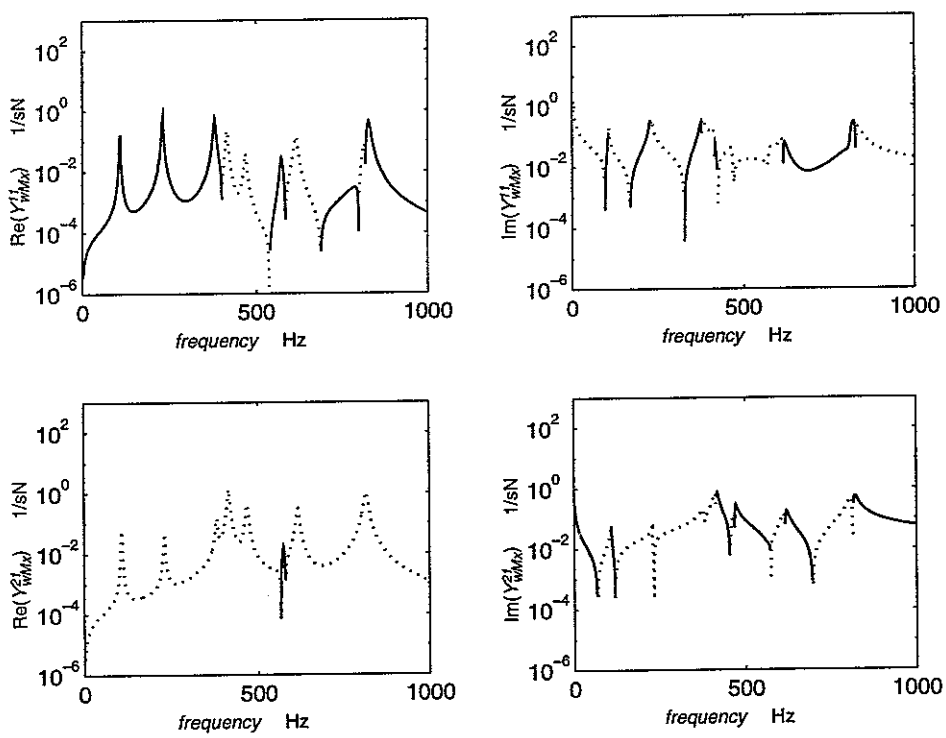

Fig. 33: *Real (left-side plots) and imaginary (right-side plots) part of the Y_{wMx} driving-point (top plots) and transfer (bottom plots) mobilities for a plate having all four edges free. Solid line: positive values, dotted line: negative values.*

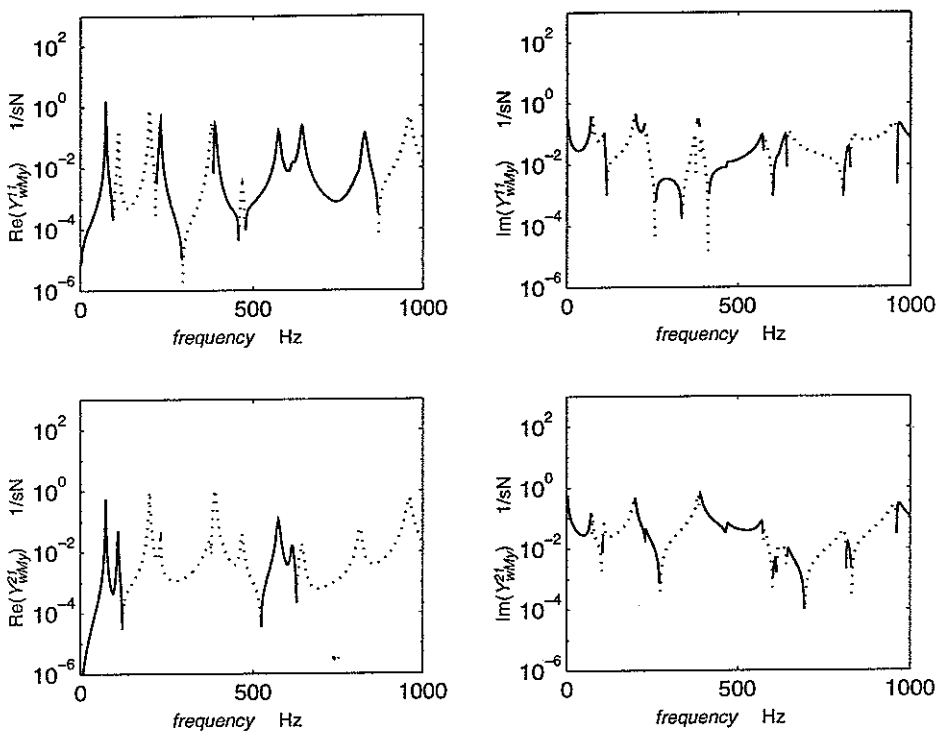

Fig. 34: *Real (left-side plots) and imaginary (right-side plots) part of the Y_{wMy} driving-point (top plots) and transfer (bottom plots) mobilities for a plate having all four edges free. Solid line: positive values, dotted line: negative values.*

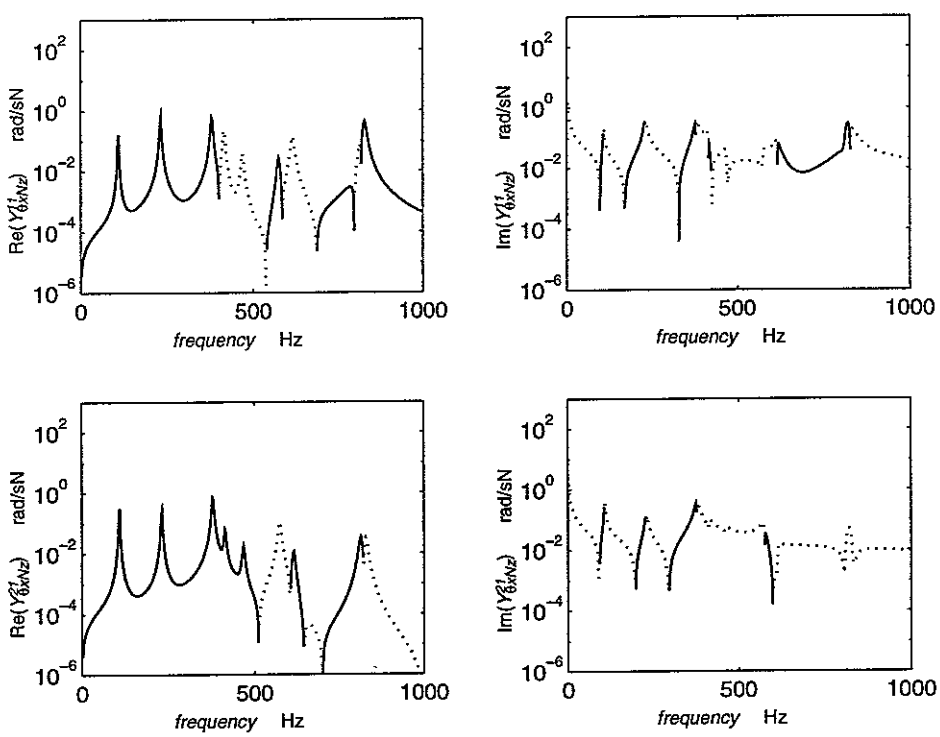

Fig. 35: *Real (left-side plots) and imaginary (right-side plots) part of the $Y_{\theta xFz}$ driving-point (top plots) and transfer (bottom plots) mobilities for a plate having all four edges free. Solid line: positive values, dotted line: negative values.*

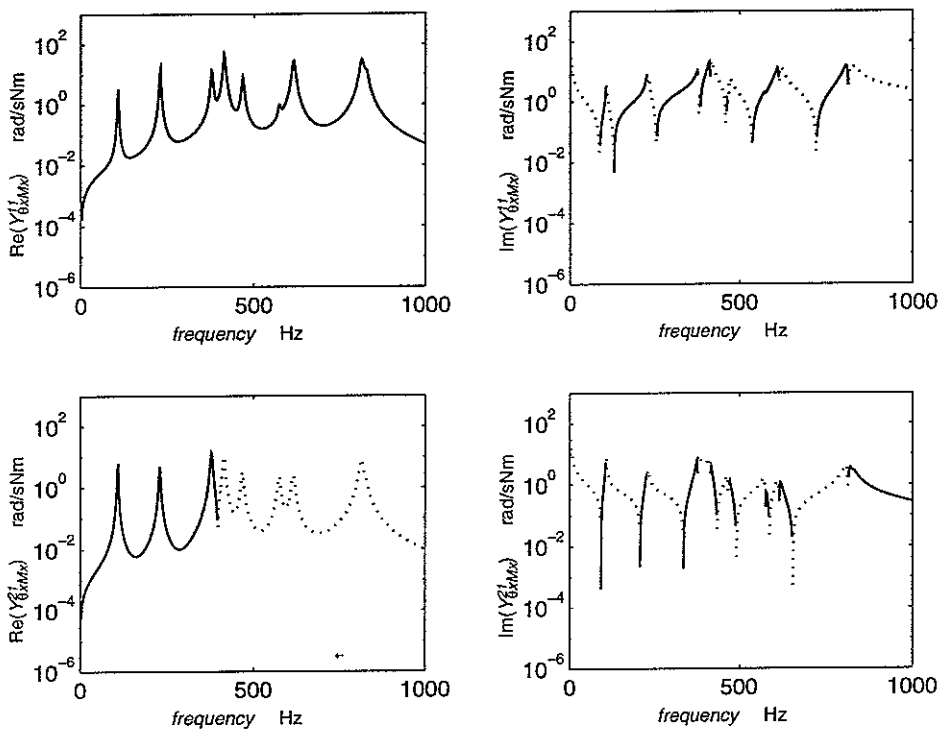

Fig. 36: *Real (left-side plots) and imaginary (right-side plots) part of the $Y_{\theta xMx}$ driving-point (top plots) and transfer (bottom plots) mobilities for a plate having all four edges free. Solid line: positive values, dotted line: negative values.*

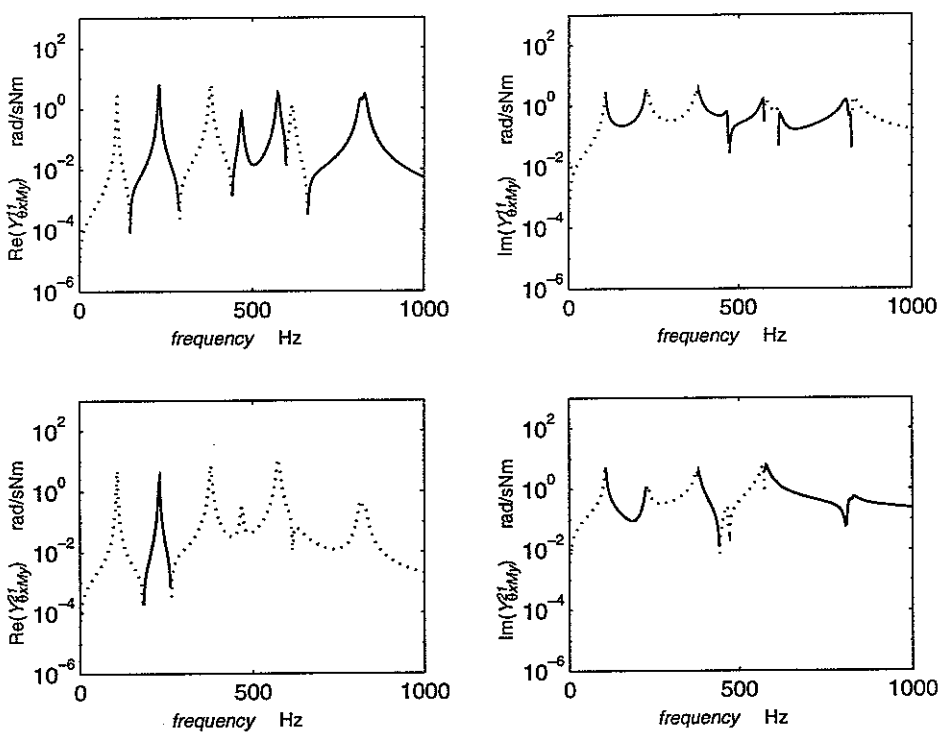

Fig. 37: *Real (left-side plots) and imaginary (right-side plots) part of the $Y_{\theta xMy}$ driving-point (top plots) and transfer (bottom plots) mobilities for a plate having all four edges free. Solid line: positive values, dotted line: negative values.*

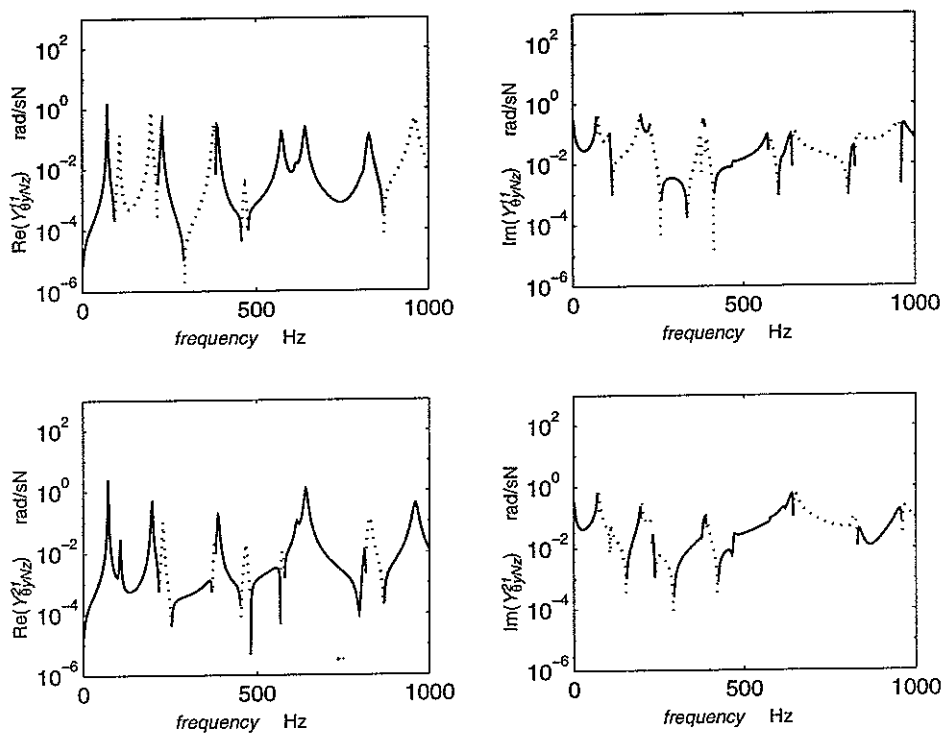

Fig. 38: *Real (left-side plots) and imaginary (right-side plots) part of the $Y_{\theta yFz}$ driving-point (top plots) and transfer (bottom plots) mobilities for a plate having all four edges free. Solid line: positive values, dotted line: negative values.*

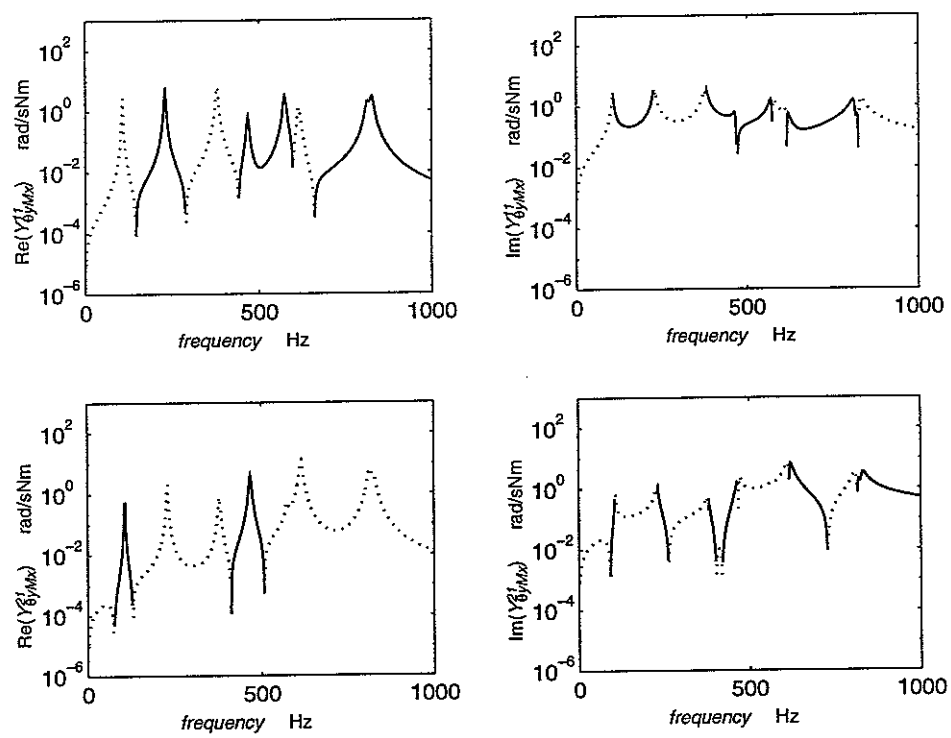

Fig. 39: *Real (left-side plots) and imaginary (right-side plots) part of the $Y_{\theta yMx}$ driving-point (top plots) and transfer (bottom plots) mobilities for a plate having all four edges free. Solid line: positive values, dotted line: negative values.*

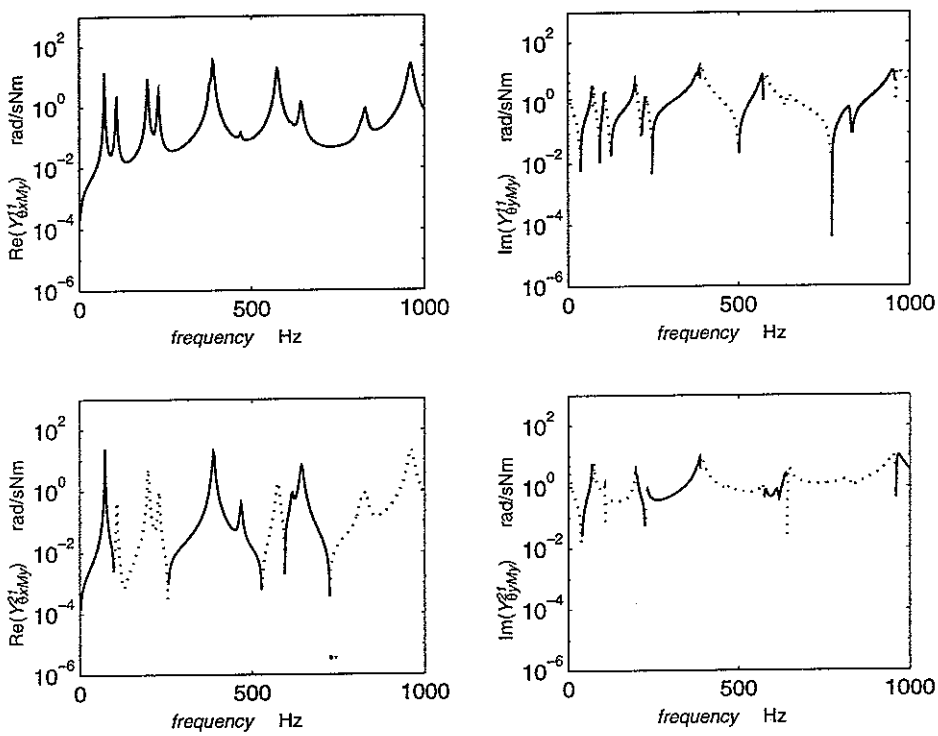

Fig. 40: *Real (left-side plots) and imaginary (right-side plots) part of the $Y_{\theta_y My}$ driving-point (top plots) and transfer (bottom plots) mobilities for a plate having all four edges free. Solid line: positive values, dotted line: negative values.*

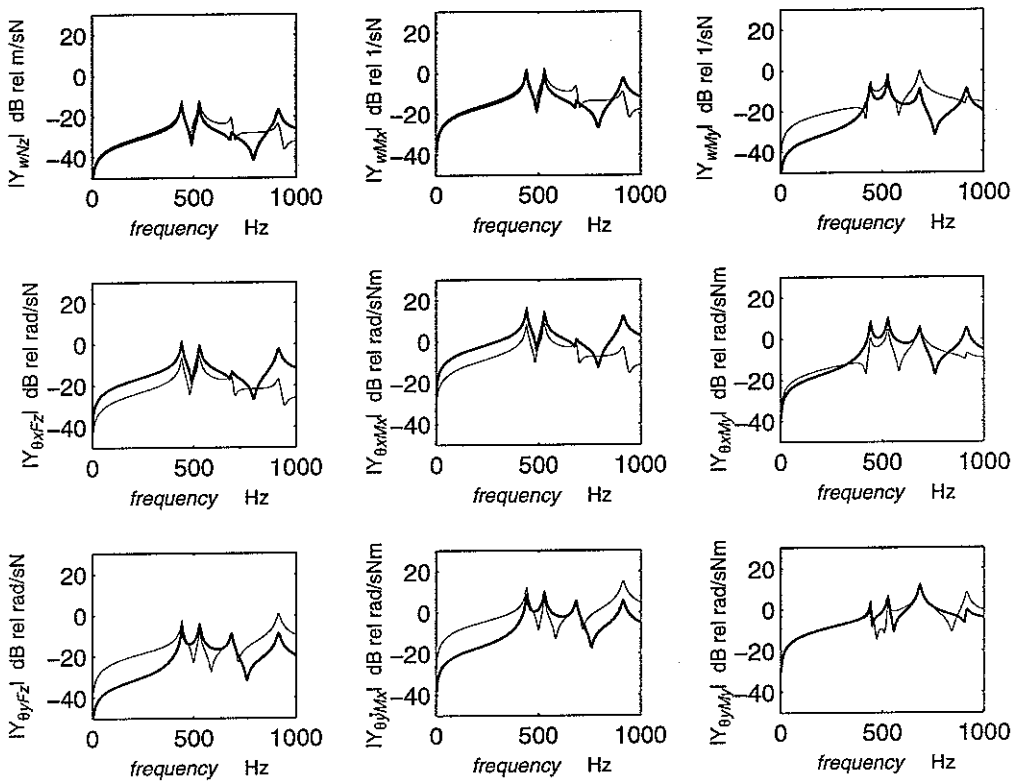

Fig. 41: *Modulus of the nine driving-point (solid line) and transfer (faint line) mobilities for a plate having all four edges clamped.*

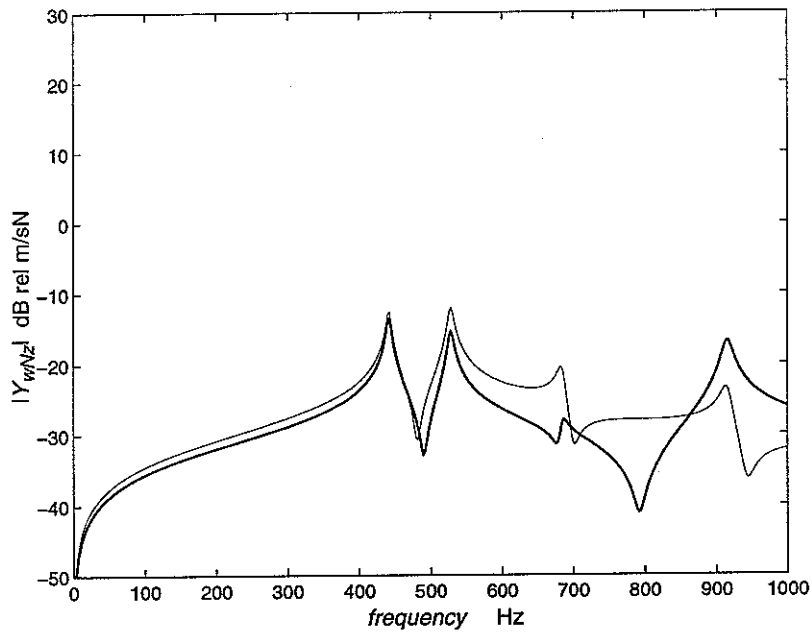

Fig. 42: *Modulus of the Y_{wFz} driving-point (solid line) and transfer (faint line) mobilities for a plate having all four edges clamped.*

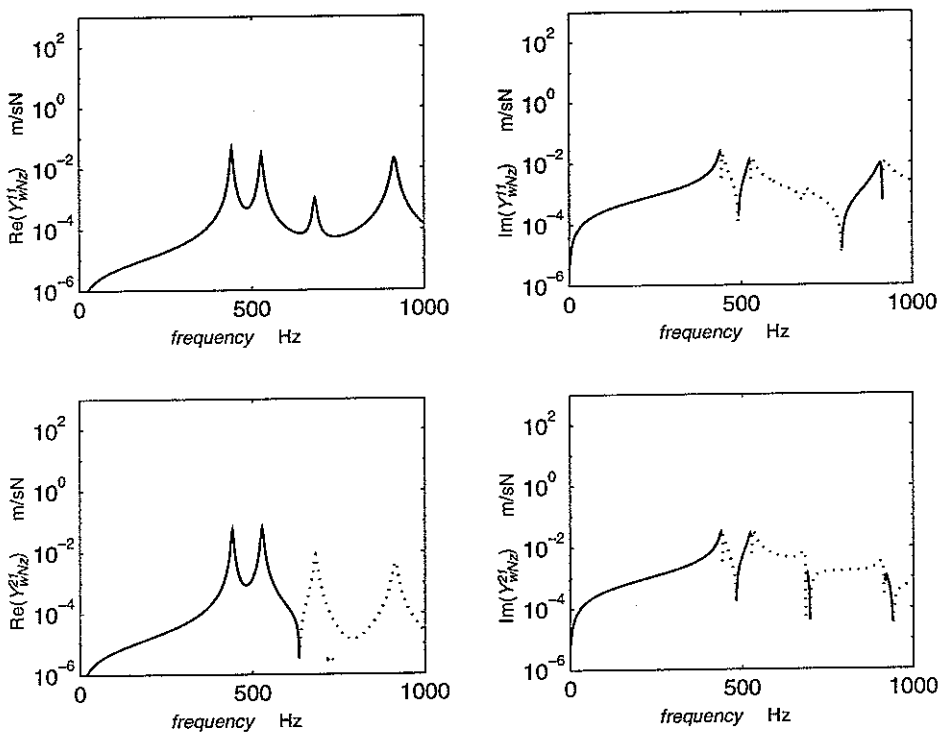

Fig. 43: *Real (left-side plots) and imaginary (right-side plots) part of the Y_{wFz} driving-point (top plots) and transfer (bottom plots) mobilities for a plate having all four edges clamp. Solid line: positive values, dotted line: negative values.*

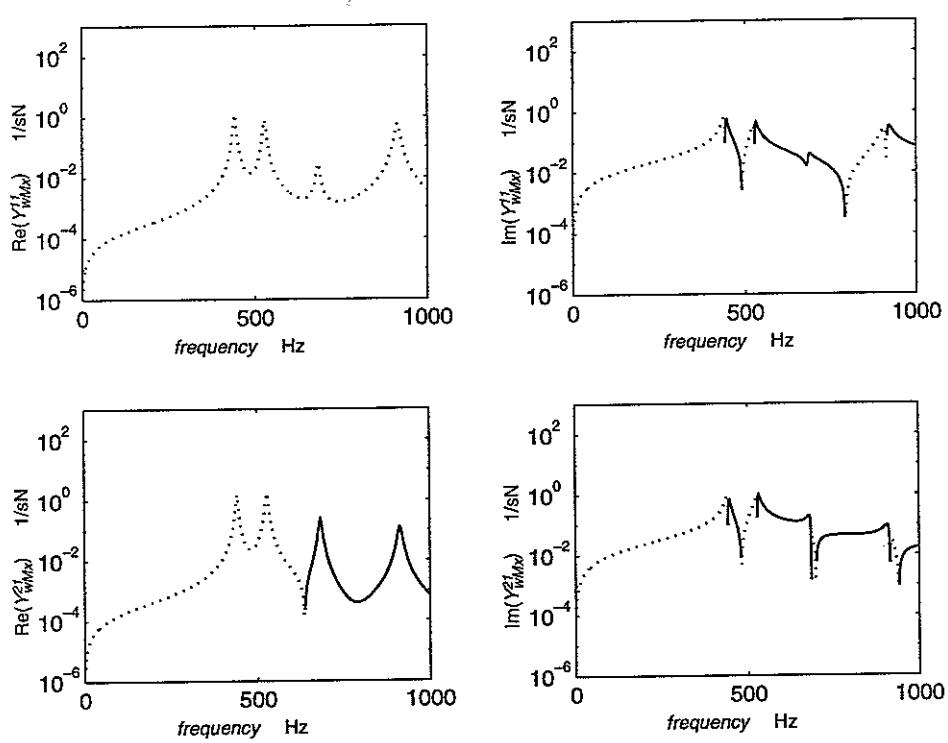

Fig. 44: *Real (left-side plots) and imaginary (right-side plots) part of the Y_{wMx} driving-point (top plots) and transfer (bottom plots) mobilities for a plate having all four edges clamp. Solid line: positive values, dotted line: negative values.*

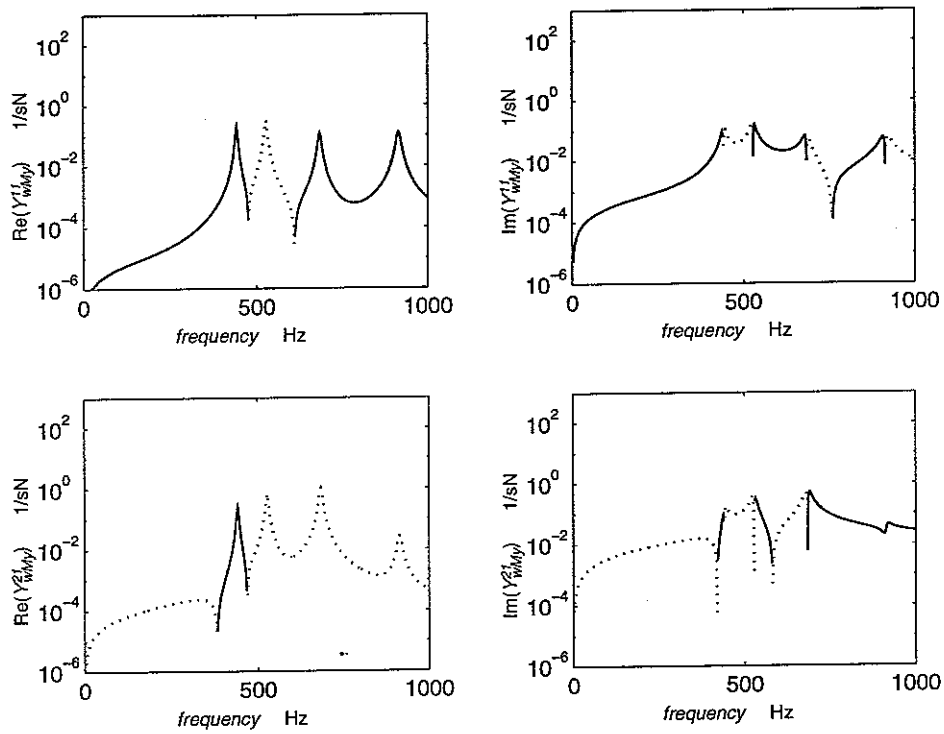

Fig. 45: *Real (left-side plots) and imaginary (right-side plots) part of the Y_{wMy} driving-point (top plots) and transfer (bottom plots) mobilities for a plate having all four edges clamp. Solid line: positive values, dotted line: negative values.*

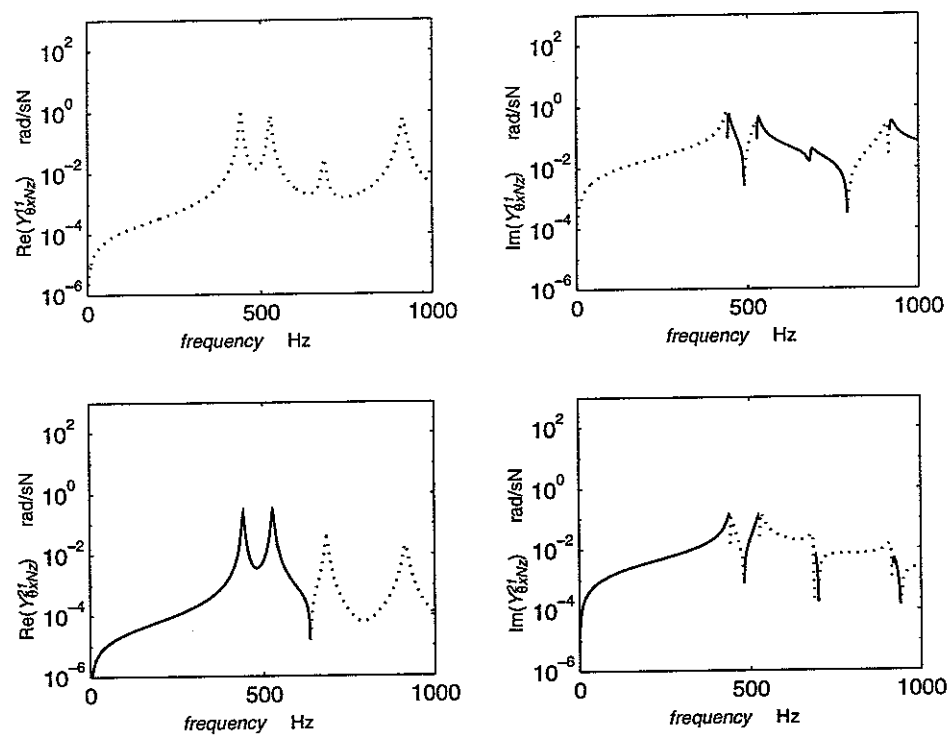

Fig. 46: *Real (left-side plots) and imaginary (right-side plots) part of the $Y_{\theta xFz}$ driving-point (top plots) and transfer (bottom plots) mobilities for a plate having all four edges clamp. Solid line: positive values, dotted line: negative values.*

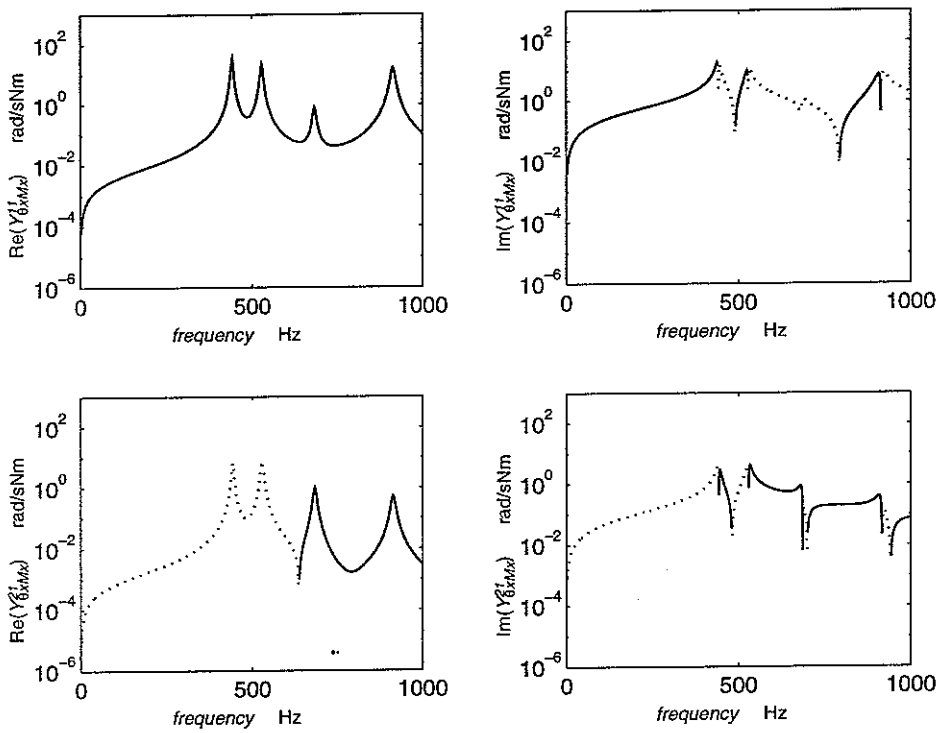

Fig. 47: *Real (left-side plots) and imaginary (right-side plots) part of the $Y_{\theta xMx}$ driving-point (top plots) and transfer (bottom plots) mobilities for a plate having all four edges clamp. Solid line: positive values, dotted line: negative values.*

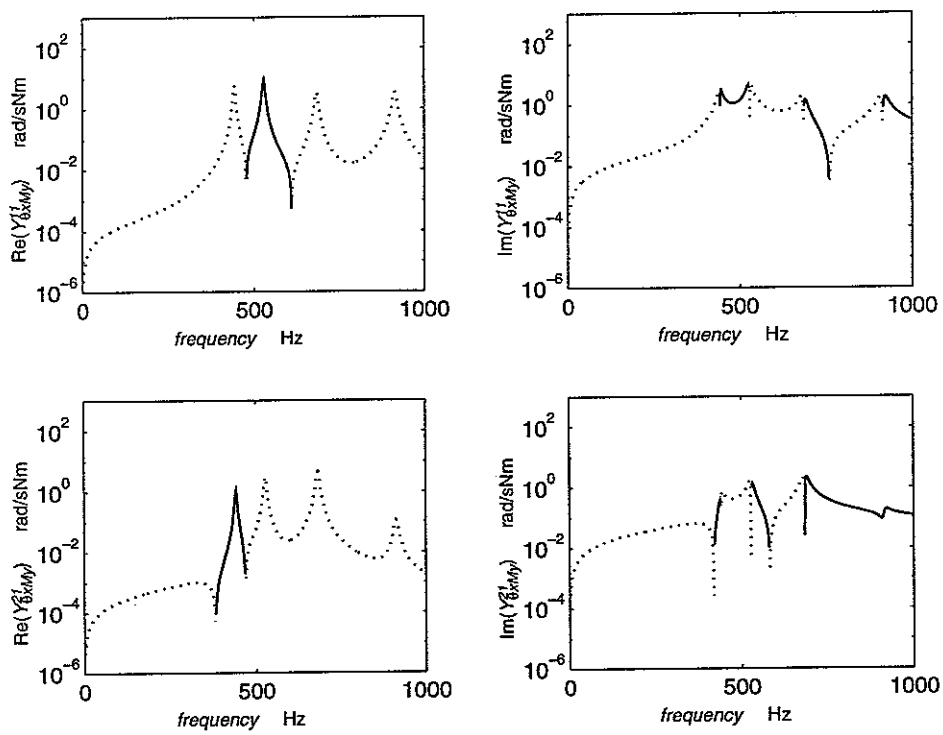

Fig. 48: *Real (left-side plots) and imaginary (right-side plots) part of the $Y_{\theta xMy}$ driving-point (top plots) and transfer (bottom plots) mobilities for a plate having all four edges clamp. Solid line: positive values, dotted line: negative values.*

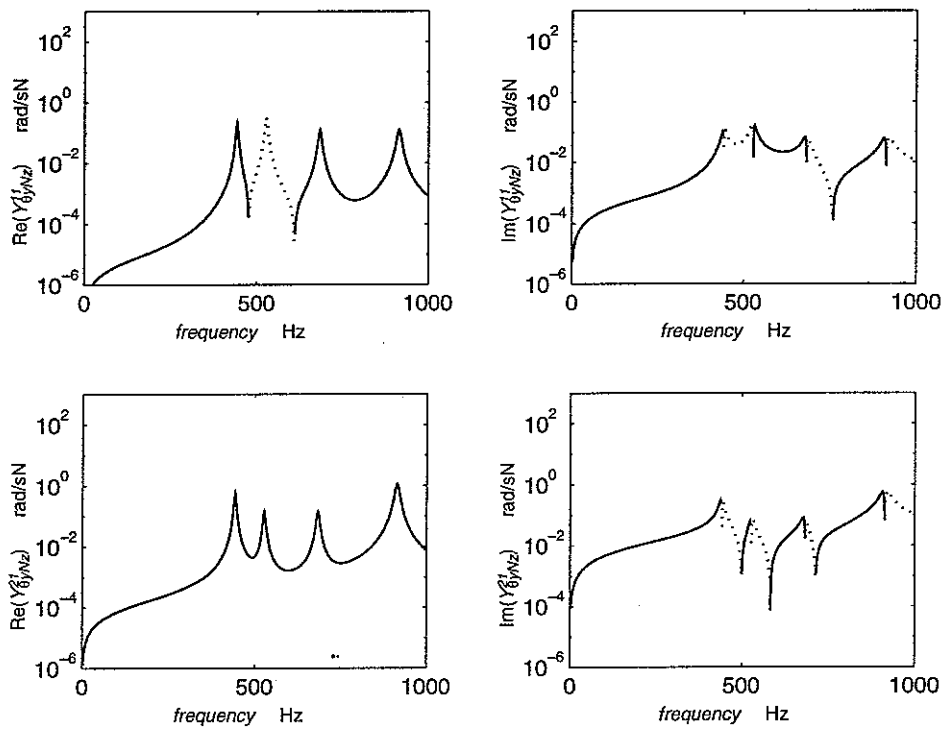

Fig. 49: *Real (left-side plots) and imaginary (right-side plots) part of the $Y_{\theta_y F_z}$ driving-point (top plots) and transfer (bottom plots) mobilities for a plate having all four edges clamp. Solid line: positive values, dotted line: negative values.*

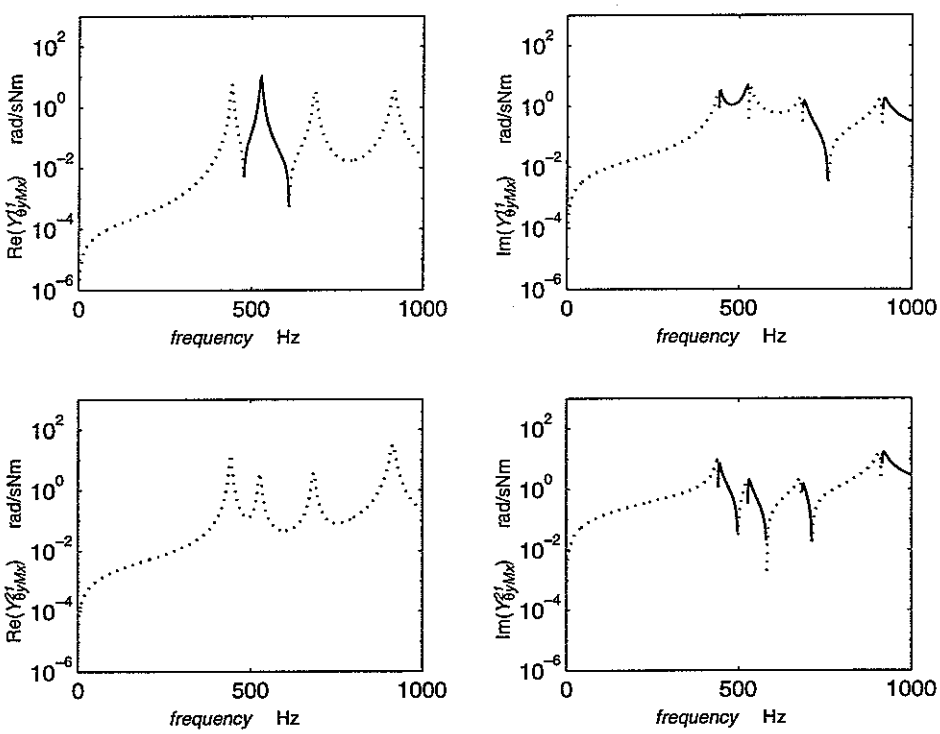

Fig. 50: *Real (left-side plots) and imaginary (right-side plots) part of the $Y_{\theta_y M_x}$ driving-point (top plots) and transfer (bottom plots) mobilities for a plate having all four edges clamp. Solid line: positive values, dotted line: negative values.*

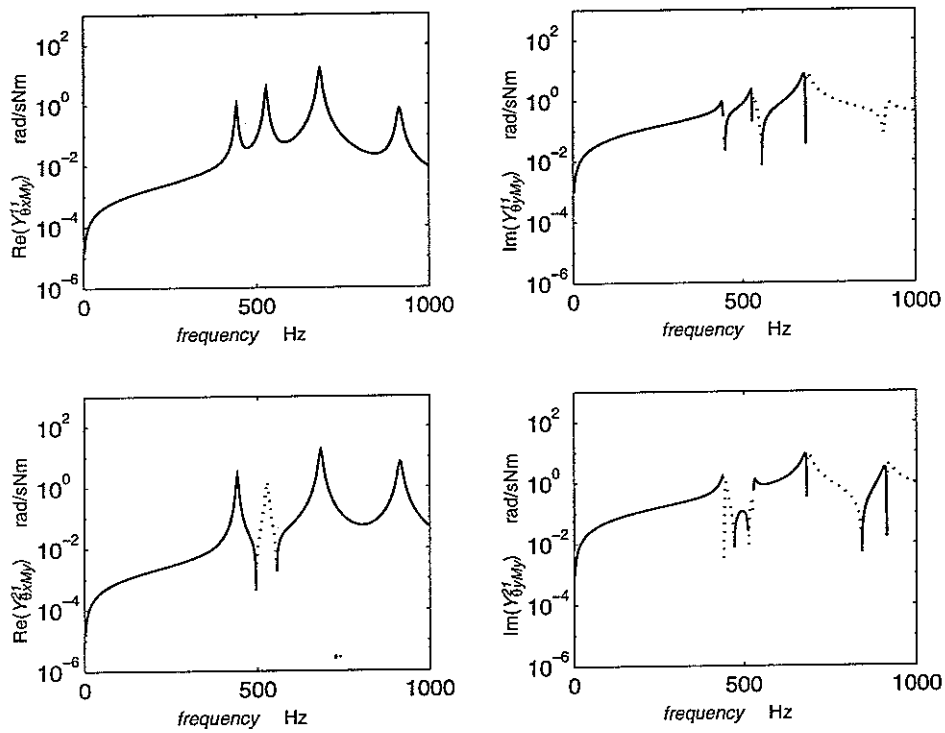

Fig. 51: *Real (left-side plots) and imaginary (right-side plots) part of the $Y_{\theta yMy}$ driving-point (top plots) and transfer (bottom plots) mobilities for a plate having all four edges clamp. Solid line: positive values, dotted line: negative values.*

4. PROPERTIES OF MOBILITY MATRICES

In this section the main properties of the mobility matrices derived in sections 2 and 3 are analysed. As will be shown, the driving point and transfer mobility matrices have some peculiar characteristics that could be used as a check of the driving point and transfer mobility formulae used.

4.1. Relation between infinite and finite driving point mobilities

First of all the driving point mobilities of infinite and finite plates are compared. Skudrzyk [33] has investigated the relationship between systems with a finite and an infinite number of resonances. He has shown that a finite structure may be approximated by an equivalent structure of infinite extent without discontinuities generating reflections. Hence, it could be assumed that waves generated by the source propagate and decay away under the dissipative effect of structural hysteresis and sound radiation damping. Alternatively this is equivalent to assuming that there are many modes of vibration contributing to the motion at any one frequency without one mode being dominant. At low frequencies where the resonances are well separated, Skudrzyk's approximation is less accurate although it is still valuable since it gives the average level of the response. As shown in reference [34], when a distributed system is excited by a harmonic force, the spectrum of the steady state response measured at the excitation point is characterised by a sequence of peaks and "troughs" due respectively to resonance and antiresonance phenomena. At the resonance frequencies the waves generated by the excitation are reflected at the boundaries and arrive at the excitation point in phase with the outgoing wave so that maximum power is transmitted to the system. Alternatively at the antiresonance frequencies the reflected waves arrive at the excitation point out of phase and they destructively interfere with the outgoing waves so that the power generated by the source is minimum. As the hysteretic dissipative effect of the structure rises or the sound radiation damping rises the maxima (at resonance) vibrational amplitude decrease and the minima (at antiresonance) vibrational amplitude increase. The dissipative effect rises as the vibrational frequency response tends towards an average response which is characterised by a smooth line. Since this mean curve has neither maxima nor minima it may be considered to represent the response that would be generated by the excitation if the system is sufficiently damped so that no reflections occur at the boundary of the system. The mean line, then, obviously represents the amplitude of the wave generated when the structure is of infinite extend.

This property could be used to check for example that the natural modes $\phi(x,y)$, the natural frequencies ω_{fmn} and the norm Λ_{mn} used to evaluate the mobilities of a finite plate give an average level of the same order of magnitude of that calculated using the mobilities formulae for infinite plate.

Figures 52, 55 and 58 show the spectrum of the driving point mobilities $Y^{ii}_{wN_z}(\omega) = \dot{\tilde{w}}_{zi}(\omega)/\tilde{N}_{zi}(\omega)$ for an infinite plate given by equation (2.31) (faint line) and for finite plates having the three types of boundary condition considered in this report calculated with equation (3.40). As can be seen the driving point mobility of the infinite plate is constant in frequency and gives approximately the mean response of the finite system with the three types of boundary conditions examined.
Moving to the mobility relating a moment to an angular velocity, figures 53, 56 and 59 compare the driving point mobility formula for infinite plates given by equation (2.62) with

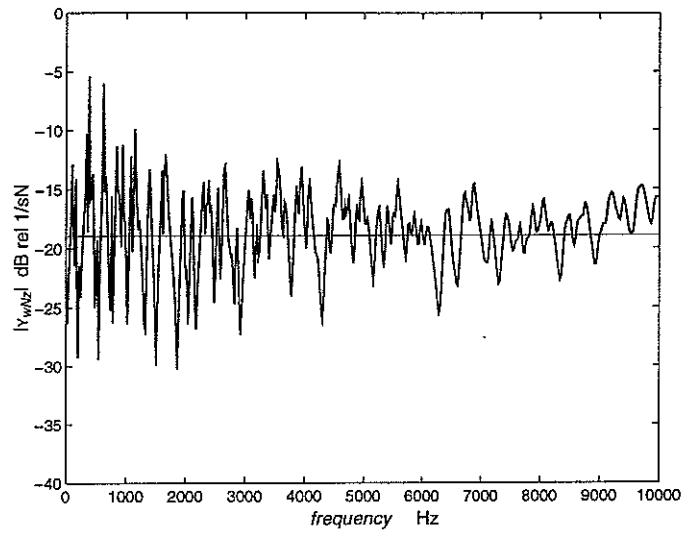

Fig.: 52: *Modulus of the Y_{wF_z} driving-point mobility considering either a finite simply supported plate (solid line) or an infinite plate (faint line).*

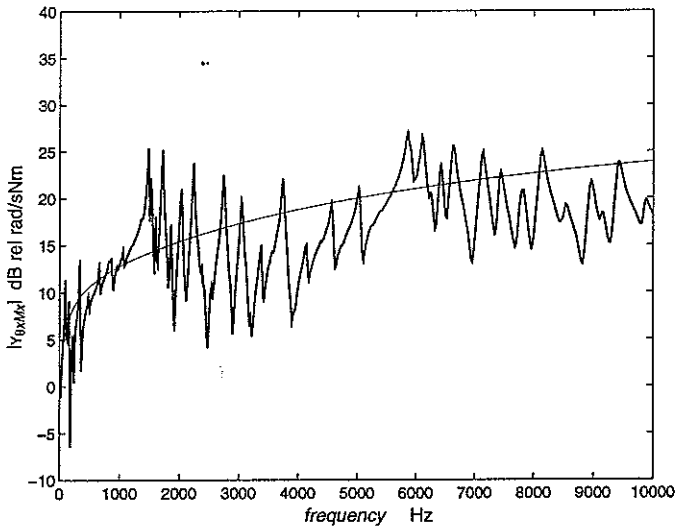

Fig.: 53: *Modulus of the $Y_{\theta xMx}$ driving-point mobility considering either a finite simply supported plate (solid line) or an infinite plate (faint line).*

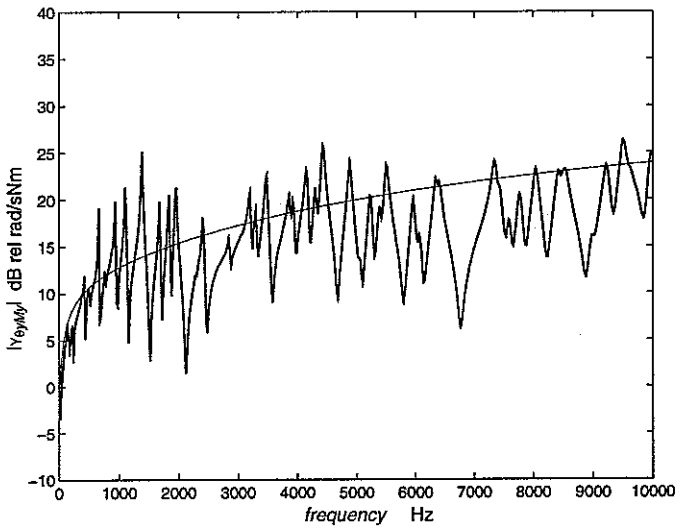

Fig.: 54: *Modulus of the $Y_{\theta yMy}$ driving-point mobility considering either a finite simply supported plate (solid line) or an infinite plate (faint line).*

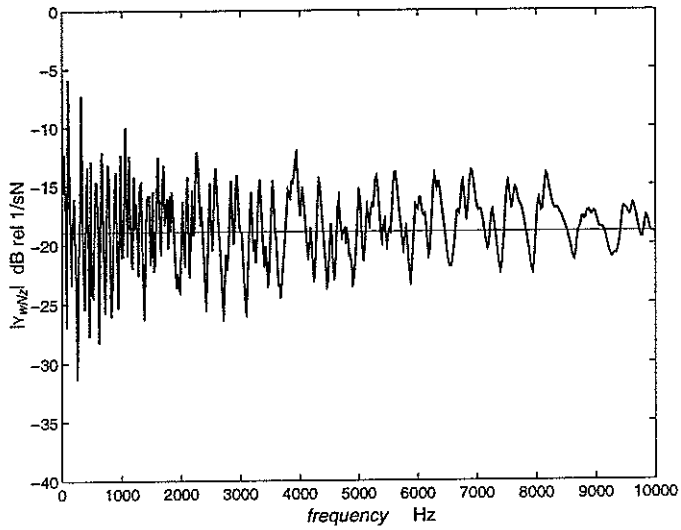

Fig.: 55: *Modulus of the Y_{wFz} driving-point mobility considering either a finite freely suspended plate (solid line) or an infinite plate (faint line).*

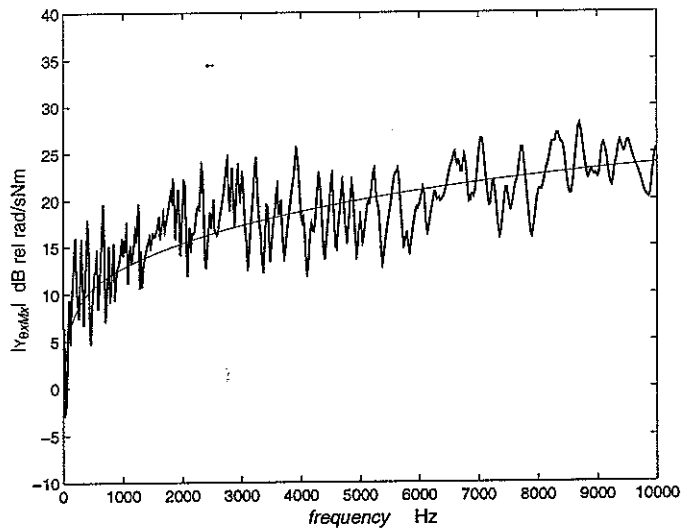

Fig.: 56: *Modulus of the $Y_{\theta xMx}$ driving-point mobility considering either a finite freely suspended plate (solid line) or an infinite plate (faint line).*

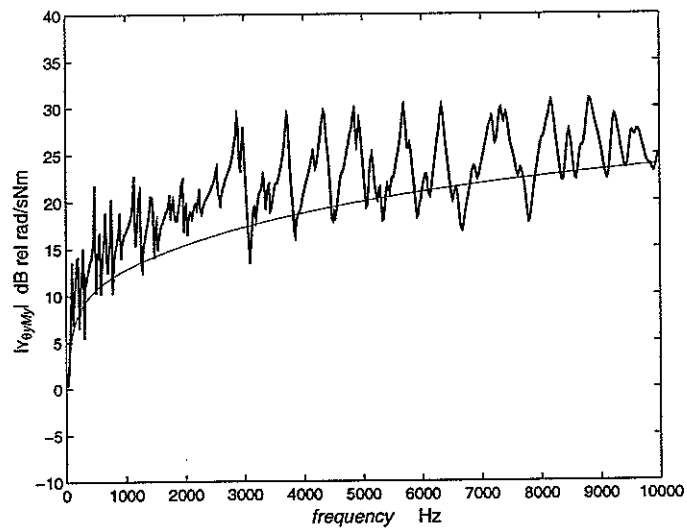

Fig.: 57: *Modulus of the $Y_{\theta yMy}$ driving-point mobility considering either a finite freely suspended plate (solid line) or an infinite plate (faint line).*

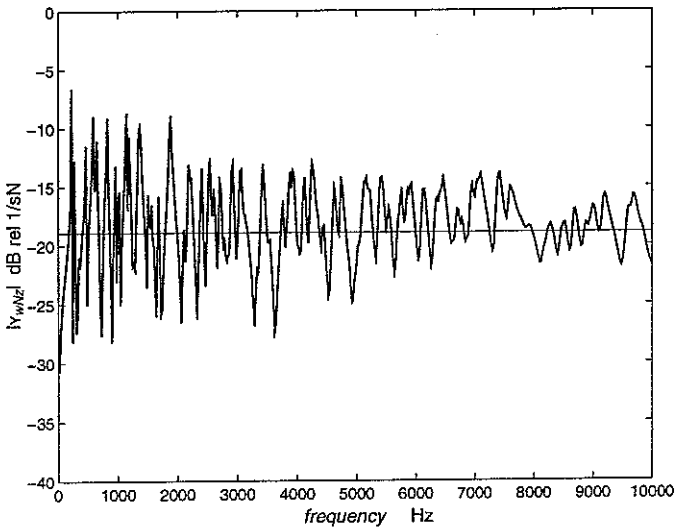

Fig.: 58: *Modulus of the Y_{wFz} driving-point mobility considering either a finite clamped plate (solid line) or an infinite plate (faint line).*

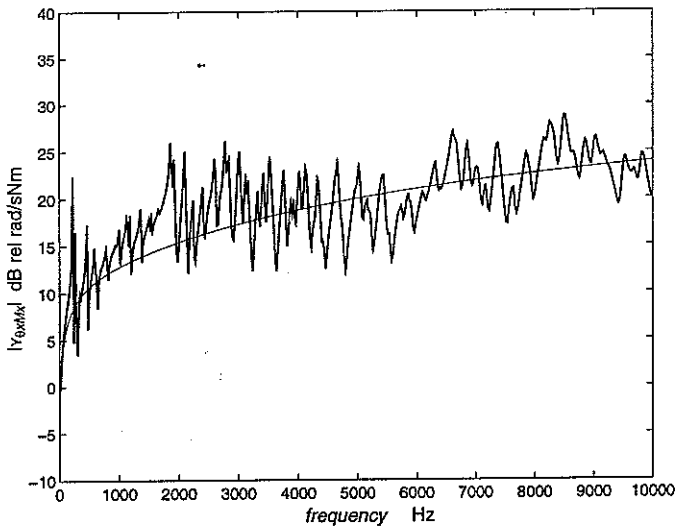

Fig.: 59: *Modulus of the $Y_{\theta xMx}$ driving-point mobility considering either a finite clamped plate (solid line) or an infinite plate (faint line).*

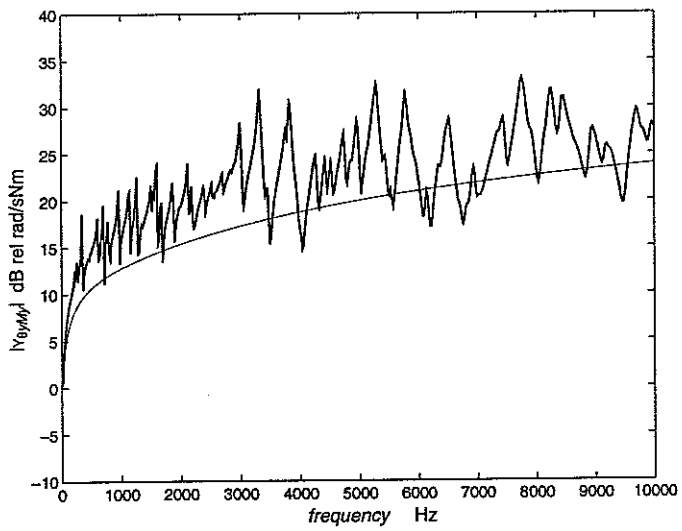

Fig.: 60: *Modulus of the $Y_{\theta yMy}$ driving-point mobility considering either a finite clamped plate (solid line) or an infinite plate (faint line).*

the driving point mobility $Y^{ii}_{\theta_x M_x}(\omega)=\dot{\tilde{\theta}}_{xi}(\omega)/\tilde{M}_{xi}(\omega)$ given by equation (3.47) while figures 54, 57 and 60 compare the driving point mobility formula for infinite plates given by equation (2.62) with the driving point mobility $Y^{ii}_{\theta_y M_y}(\omega)=\dot{\tilde{\theta}}_{yi}(\omega)/\tilde{M}_{yi}(\omega)$ given by equation (3.50). Also in this case the driving point mobility of the infinite plate gives approximately the mean response of the finite system when the freely suspended plate is considered. It should be noted that, considering the infinite plate driving point mobilities, alternatively to the $Y^{ii}_{wN_z}(\omega)$, the $Y^{ii}_{\theta_y M_y}(\omega)$ driving point mobility rises proportionally to the frequency.

4.2. Driving point mobility evaluated at the centre of a finite plate

When the driving point mobility matrix of a rectangular plate is evaluated at the centre of the plate the validity of the formula for the natural modes, $\phi_{mn}(x,y)$, and their derivatives in x and y, $\psi^{(x)}_{mn}(x,y)$ and $\psi^{(y)}_{mn}(x,y)$, directions used in the mobility equations (3.40-50) could be checked. As figures 60, 61 and 62 show for the three types of plate considered in this report, if the driving point mobility matrix is evaluated at the centre of the plate then it is a diagonal matrix. This peculiar characteristic could be explained as follow: the centre point where the mobility parameters are evaluated stays in both the x and y axes of symmetry of the mode shapes. Therefore at this specific point the three degrees of freedom related to bending waves (w, θ_x, θ_y) are uncoupled as can be deduced from the modal amplitude and modal slope plots of figures 16, 17 and 18. As a consequence of this the coupling driving point mobilities are zero. So, in the particular case of a driving point mobility matrix of a finite rectangular plate evaluated at the centre of the plate, $P_i=\left(l_x/2,\ l_y/2\right)$, the mobility parameters of equations (3.7-3.15) are given by:

$$\begin{array}{lll} Y^{ii}_{w_z N_z}(\omega)\neq 0 & Y^{ii}_{w_z M_x}(\omega)=0 & Y^{ii}_{w_z M_y}(\omega)=0 \\ Y^{ii}_{\theta_x N_z}(\omega)=0 & Y^{ii}_{\theta_x M_x}(\omega)\neq 0 & Y^{ii}_{\theta_x M_y}(\omega)=0. \\ Y^{ii}_{\theta_y N_z}(\omega)=0 & Y^{ii}_{\theta_y M_x}(\omega)=0 & Y^{ii}_{\theta_y M_y}(\omega)\neq 0 \end{array} \qquad (4.1\text{-}9)$$

As shown in figures 60,61 and 62, this property is not valid for the transfer mobility matrix even if evaluated between the centre of the plate and at an off centre position.
This property of the finite rectangular plate could be applied for other plate shapes that have two axes of symmetry so that the driving point mobilities at the centre of the plate are as in equations (4.1-9).

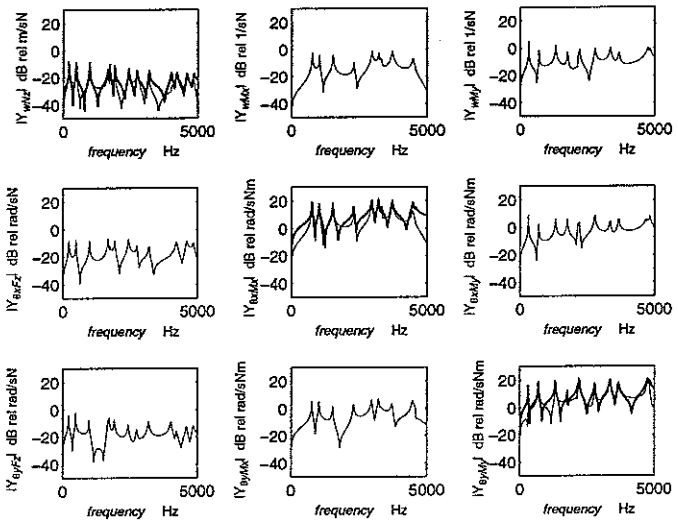

Fig.: 61: *Modulus of the nine driving-point (solid line) and transfer (faint line) mobilities for a plate having all four edges simply supported. $P_1=(l_x/2,l_y/2)$, $P_2=(0.35,0.09)$.*

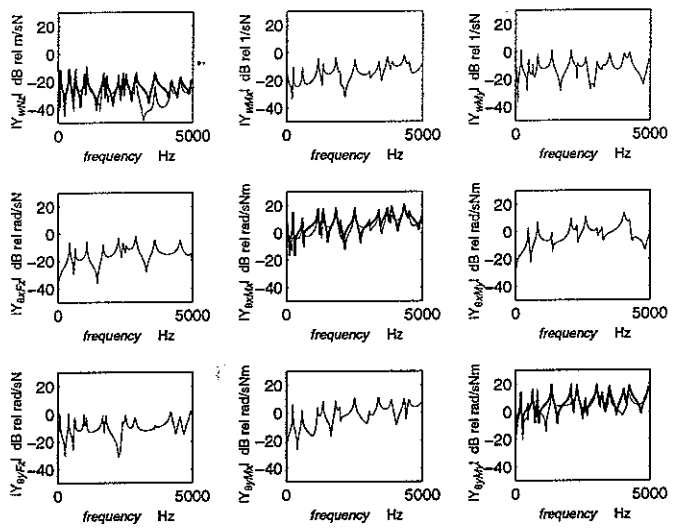

Fig.: 62: *Modulus of the nine driving-point (solid line) and transfer (faint line) mobilities for a plate having all four edges free. $P_1=(l_x/2,l_y/2)$, $P_2=(0.35,0.09)$.*

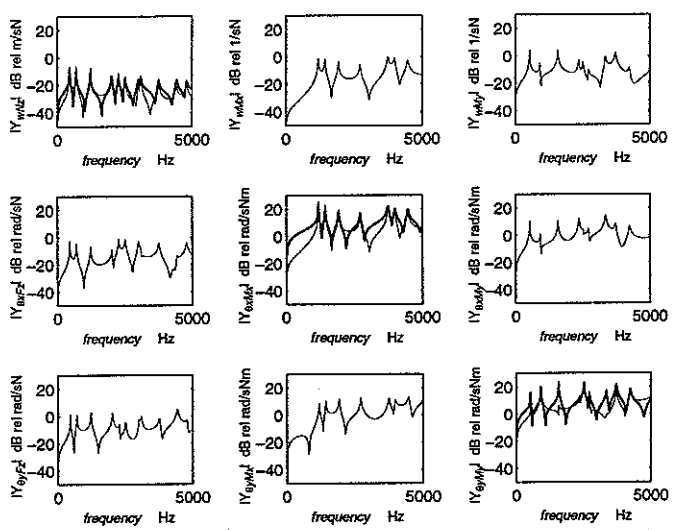

Fig.: 63: *Modulus of the nine driving-point (solid line) and transfer (faint line) mobilities for a plate having all four edges clamped. $P_1=(l_x/2,l_y/2)$, P2=(0.35,0.09).*

4.3. Diagonal terms of the driving point and transfer mobility matrices

Another property that could be used to check the validity of the mobility parameters of finite plates derived from equations (3.40-3.50) can be found by considering the real part of the diagonal terms of the driving point mobility matrix $\mathbf{Y}^{ii}(\omega)$. Figures 64, 65 and 66 show that the three driving point mobilities $\mathrm{Re}\left\{Y^{ii}_{w_zN_z}(\omega)\right\}$, $\mathrm{Re}\left\{Y^{ii}_{\theta_xM_x}(\omega)\right\}$ and $\mathrm{Re}\left\{Y^{ii}_{\theta_yM_y}(\omega)\right\}$ are always greater than zero while the real part of the coupling mobility parameters of the driving point mobility matrix could be either greater or lower than zero. This is a peculiar property of the driving point mobility matrix and could be explained in terms of energy. The *time-averaged vibrational power* injected into the plate by an harmonic point force $N_{zi}(t)$ acting in isolation is given by:

$$P_{N_z}(\omega)=\frac{1}{2}\mathrm{Re}\left\{\tilde{N}^{*}_{zi}(\omega)\dot{\tilde{w}}_i(\omega)\right\}, \tag{4.10}$$

where * indicates the complex conjugate. Therefore, remembering that $\dot{\tilde{w}}_i(\omega)=Y^{ii}_{wNz}(\omega)N_{zi}(\omega)$ equation (4.10) can be written as follows:

$$P_{N_z}(\omega)=\frac{1}{2}\left|\tilde{N}_{zi}(\omega)\right|^2\mathrm{Re}\left\{Y^{ii}_{wNz}(\omega)\right\}. \tag{4.11}$$

Because the point force is acting in isolation on the plate, in order to have power transmission to the plate and not absorption the real part of $Y^{ii}_{wN_z}(\omega)$ has to be positive. A similar conclusion can be drawn when a point moment in the x direction $M_{xi}(t)$ or in the y direction $M_{yi}(t)$ is acting in isolation. In fact the *time-averaged vibrational power* injected into the plate by an harmonic point moment $M_{xi}(t)$ or $M_{yi}(t)$ acting in isolation is given respectively by:

$$P_{M_x}(\omega)=\frac{1}{2}\mathrm{Re}\left\{\tilde{M}^{*}_{xi}(\omega)\dot{\tilde{\theta}}_{xi}(\omega)\right\}, \qquad P_{M_y}(\omega)=\frac{1}{2}\mathrm{Re}\left\{\tilde{M}^{*}_{yi}(\omega)\dot{\tilde{\theta}}_{yi}(\omega)\right\}. \tag{4.12,13}$$

Because $\dot{\tilde{\theta}}_{xi}(\omega)=Y^{ii}_{\theta xMy}(\omega)M_{xi}(\omega)$ and $\dot{\tilde{\theta}}_{yi}(\omega)=Y^{ii}_{\theta yMy}(\omega)M_{yi}(\omega)$ equations (4.12) and (4.13) can be written as follows:

$$P_{M_x}(\omega)=\frac{1}{2}\left|\tilde{M}_{xi}(\omega)\right|^2\mathrm{Re}\left\{Y^{ii}_{\theta xMx}(\omega)\right\}, \qquad P_{M_y}(\omega)=\frac{1}{2}\left|\tilde{M}_{yi}(\omega)\right|^2\mathrm{Re}\left\{Y^{ii}_{\theta yMy}(\omega)\right\}. \tag{4.14,15}$$

Thus, also when the two moment excitations are acting in isolation power is injected to the plate only if the real part of $Y^{ii}_{\theta xMx}(\omega)$ or $Y^{ii}_{\theta yMy}(\omega)$ are positive.

This type of property does not hold when a transfer mobility matrix $\mathbf{Y}^{ji}(\omega)$ is calculated as shown in figures 67 - 69.

It should be noted that the properties above described for the diagonal terms of the driving point mobility matrix of a finite rectangular plate hold as well for the diagonal terms of the driving point mobility matrix of an infinite plate. In fact the real part of the driving point mobilities $Y^{ii}_{w_zN_z}(\omega)$, $Y^{ii}_{\theta_xM_x}(\omega)$ and $Y^{ii}_{\theta_yM_y}(\omega)$ given by equations (2.88) and (2.89) are all positive by definition.

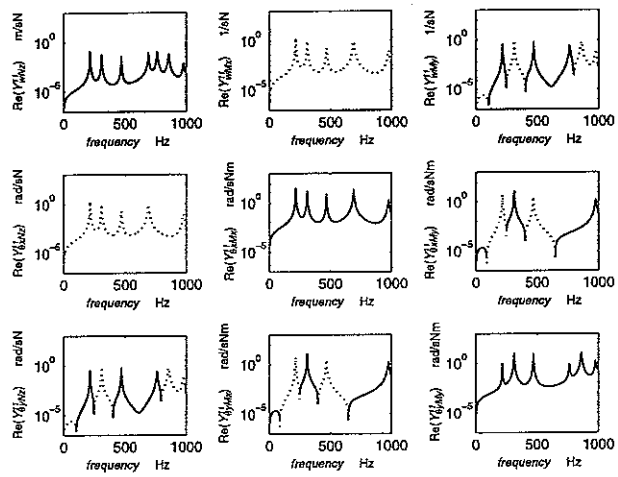

Fig.: 64: *Real part of the nine driving-point mobilities for a plate having all four edges simply supported. Solid line: positive values, dotted line: negative values.*

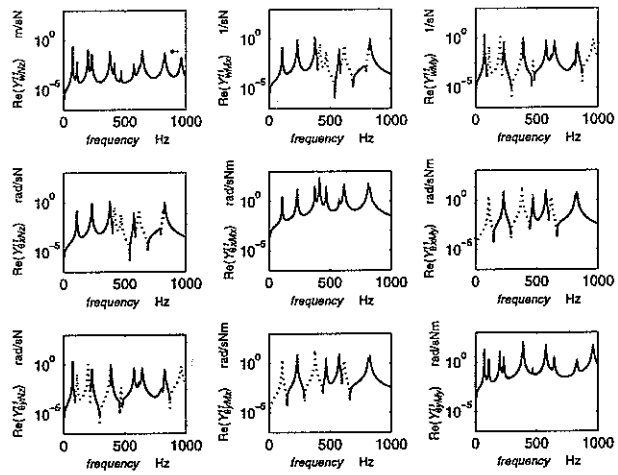

Fig.: 65: *Real part of the nine driving-point mobilities for a plate having all four edges freely suspended. Solid line: positive values, dotted line: negative values.*

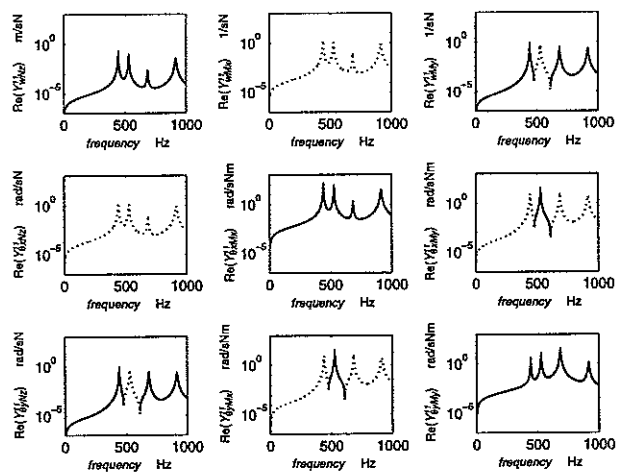

Fig.: 66: *Real part of the nine driving-point mobilities for a plate having all four edges clamped. Solid line: positive values, dotted line: negative values.*

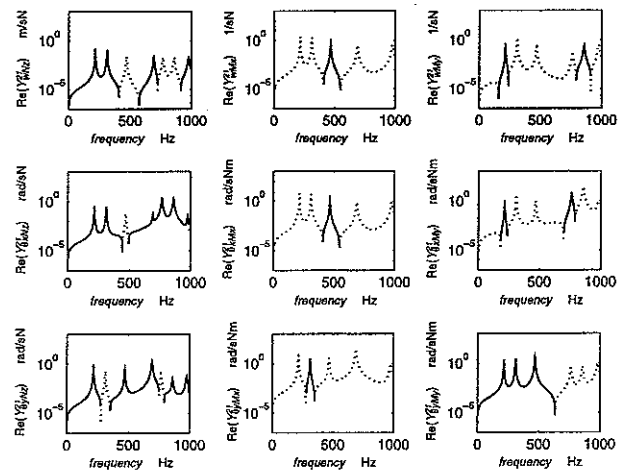

Fig.: 67: *Real part of the nine transfer mobilities for a plate having all four edges simply supported. Solid line: positive values, dotted line: negative values.*

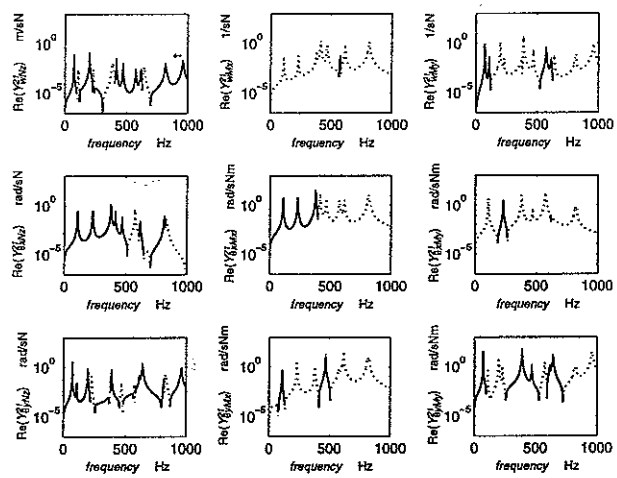

Fig.: 68: *Real part of the nine transfer mobilities for a plate having all four edges freely suspended. Solid line: positive values, dotted line: negative values.*

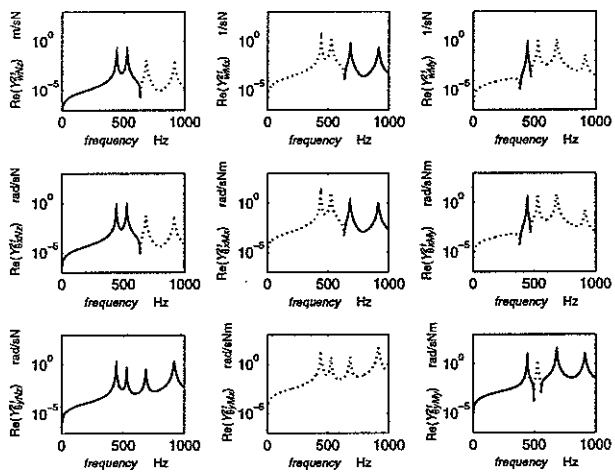

Fig.: 69: *Real part of the nine transfer mobilities for a plate having all four edges clamped. Solid line: positive values, dotted line: negative values.*

4.4. Symmetry and positive definition properties for driving point and driving multi-point mobility matrices

With reference to a finite rectangular plate the following properties of the driving point and transfer mobility matrices can be verified. From the modal formulae of equations (3.40) to (3.50), assuming $P_i = P_j$ so that $\phi_{mn}(P_i) = \phi_{mn}(P_j)$, $\psi_{mn}^{(x)}(P_i) = \psi_{mn}^{(x)}(P_j)$ and $\psi_{mn}^{(y)}(P_i) = \psi_{mn}^{(y)}(P_j)$, it can be seen that

$$Y^{ii}_{\theta_x N_z}(\omega) = Y^{ii}_{w_z M_x}(\omega) \qquad Y^{ii}_{\theta_y N_z}(\omega) = Y^{ii}_{w_z M_y}(\omega) \qquad Y^{ii}_{\theta_y M_x}(\omega) = Y^{ii}_{\theta_x M_y}(\omega). \quad (4.16\text{-}18)$$

Therefore the driving point mobility matrix $\mathbf{Y}^{ii}(\omega)$ is symmetric:

$$(\mathbf{Y}^{ii})^T = \mathbf{Y}^{ii}. \quad (4.19)$$

The transfer mobility matrices between two positions $P_i \neq P_j$ are not symmetric but, because of reciprocity are related to each other so that:

$$(\mathbf{Y}^{ji})^T = \mathbf{Y}^{ij}. \quad (4.20)$$

Equations (4.19) and (4.20) hold also when the driving point and transfer mobility matrices are calculated with reference to an infinite plate as can be directly verified by the definition of the driving point mobility matrix given in equation (2.74) and from the mobility equations (2.90-2.98). Therefore the two properties of equations (4.19) and (4.20) can be used as a check of driving and transfer mobilities for both infinite and finite plates.

If a plate is excited at two positions $P_1 = (x_1, y_1)$ and $P_2 = (x_2, y_2)$ and $\mathbf{Y}^{11}(\omega)$, $\mathbf{Y}^{22}(\omega)$ are the driving point mobility matrices at P_1 and P_2 while $\mathbf{Y}^{21}(\omega)$, $\mathbf{Y}^{12}(\omega)$ are the transfer mobility matrices between P_1 and P_2 the following mobility matrix could be defined:

$$\mathbf{Y}^{1-21-2}(\omega) = \begin{bmatrix} \mathbf{Y}^{11}(\omega) & \mathbf{Y}^{12}(\omega) \\ \mathbf{Y}^{21}(\omega) & \mathbf{Y}^{22}(\omega) \end{bmatrix}, \quad (4.21)$$

so that the excitation vector $\mathbf{f}(\omega) = \left\{ \tilde{N}_{z1} \quad \tilde{M}_{x1} \quad \tilde{M}_{y1} \quad \tilde{N}_{z2} \quad \tilde{M}_{x2} \quad \tilde{M}_{y2} \right\}^T$ is related to the velocity vector $\mathbf{v}(\omega) = \left\{ \dot{\tilde{w}}_1 \quad \dot{\tilde{\theta}}_{x1} \quad \dot{\tilde{\theta}}_{y1} \quad \dot{\tilde{w}}_2 \quad \dot{\tilde{\theta}}_{x2} \quad \dot{\tilde{\theta}}_{y2} \right\}^T$ through the usual relation:

$$\mathbf{v}(\omega) = \mathbf{Y}^{1-21-2}(\omega) \cdot \mathbf{f}(\omega). \quad (4.22)$$

This type of matrix could be defined as a *driving multi-point mobility matrix* since it relates the kinematic parameters $\dot{\tilde{w}}$, $\dot{\tilde{\theta}}_x$, $\dot{\tilde{\theta}}_y$ at a set of positions $P_1, P_2, \ldots, P_n$ to the dynamic parameters $\tilde{N}_z$, $\tilde{M}_x$, $\tilde{M}_y$ at the same positions $P_1, P_2, \ldots, P_n$. This type of driving point mobility matrix is often used to model the dynamics of a mechanical system composed of several sub-systems which are connected to each other at a set of point junctions

$P_1, P_2, \ldots, P_n$. For each sub-system a driving multi point mobility matrix is derived and used in a mobility matrix formulation as described in reference [29].
Now, considering the two conditions of equations (4.19), for a driving point mobility matrix, and (4.20), for a transfer mobility matrix, it comes out that also the driving multi-point mobility matrix is symmetric.
Figures 70, 72, 74 show the real part while figures 71, 73, 75 show the imaginary part of the driving multi point mobility matrix $\mathbf{Y}^{1-21-2}(\omega)$ evaluated considering two positions $P_1 = (0.3,\ 0.15)$ and $P_2 = (0.35,\ 0.09)$ for the three types of finite plates considered in this report. The symmetry condition is verified in all three cases and considering the real part of the diagonal terms it can be seen that they are all positive. In fact they are all diagonal terms of either the $\mathbf{Y}^{11}(\omega)$ or $\mathbf{Y}^{22}(\omega)$ driving point mobility whose diagonal terms' real part are all positive as seen in section 4.3.

In conclusion the real part of any driving point $\mathbf{Y}^{ii}(\omega)$ or driving multi-point $\mathbf{Y}^{1-N1-N}(\omega)$ mobility matrix for either a finite or an infinite are positive definite since they are symmetric and their diagonal terms are always positive. So for any vector $\mathbf{x}$ the following conditions are verified:

$$\mathbf{x}^T \mathrm{Re}(\mathbf{Y}^{ii})\mathbf{x} > 0, \qquad \mathbf{x}^T \mathrm{Re}(\mathbf{Y}^{1-N1-N})\mathbf{x} > 0 \tag{4.23,24}$$

This condition can be explained in terms of power, in fact for any vector of excitations $\mathbf{f}(t)$ the time-averaged vibrational power injected to the structure is given by:

$$P(\omega) = \frac{1}{2}\mathrm{Re}\left\{\mathbf{f}^H(\omega)\mathbf{v}(\omega)\right\}, \tag{4.25}$$

where H indicates the complex conjugate transpose. Therefore, remembering that $\mathbf{v}(\omega) = \mathbf{Y}^{1-N1-N}(\omega)\cdot\mathbf{f}(\omega)$ equation (4.25) can be written as:

$$P(\omega) = \frac{1}{2}\mathrm{Re}\left\{\mathbf{f}^H(\omega)\mathbf{Y}^{1-N1-N}(\omega)\mathbf{f}(\omega)\right\} = \frac{1}{2}\mathbf{f}^H(\omega)\,\mathrm{Re}\left\{\mathbf{Y}^{1-N1-N}(\omega)\right\}\mathbf{f}(\omega) \tag{4.26}$$

and, because the system is passive, power is only injected to the structure, i.e. power must be positive, which means that the real part of the driving multi point mobility matrix has to be positive definite.

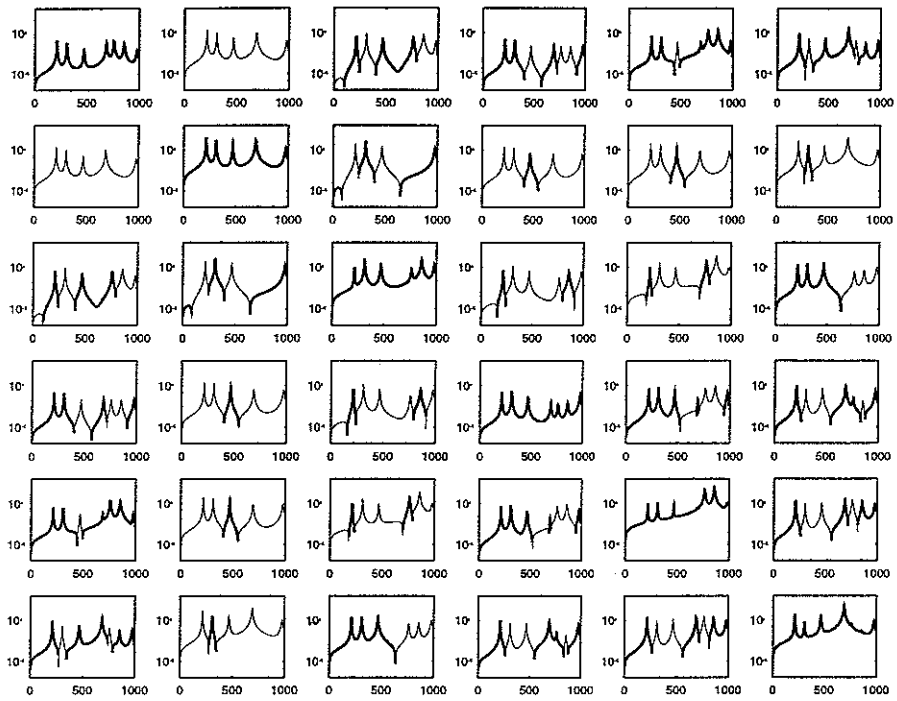

Fig.: 70: *Real part of the 36 driving point and transfer mobilities for a plate having all four edges simply supported. Solid line: positive values, faint line: negative values.*

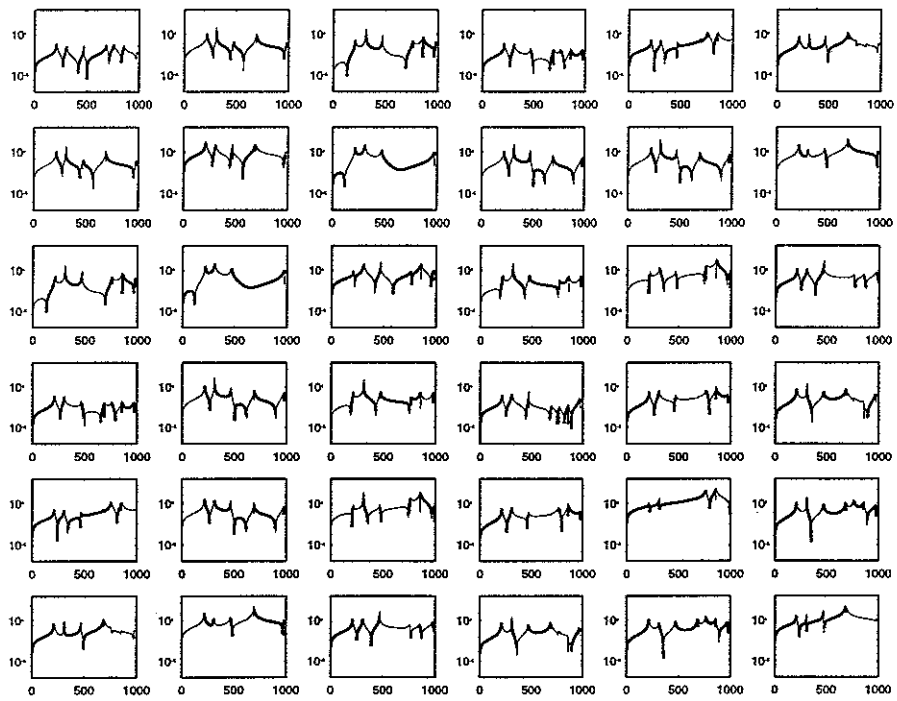

Fig.: 71: *Imaginary part of the 36 driving point and transfer mobilities for a plate having all four edges simply supported. Solid line: positive values, faint line: negative values.*

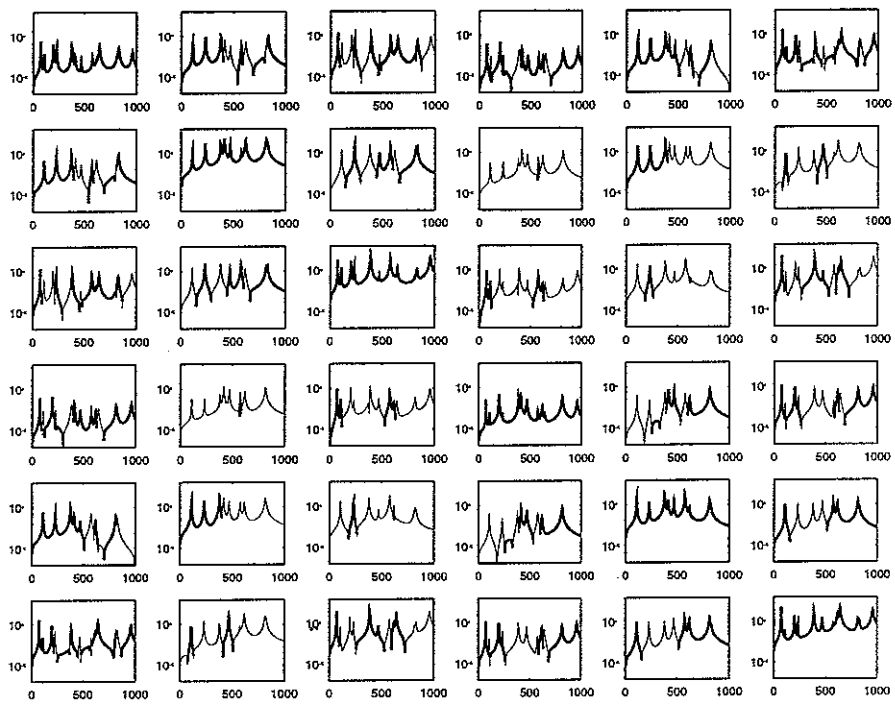

Fig.: 72: *Real part of the 36 driving point and transfer mobilities for a plate having all four edges freely suspended. Solid line: positive values, faint line: negative values.*

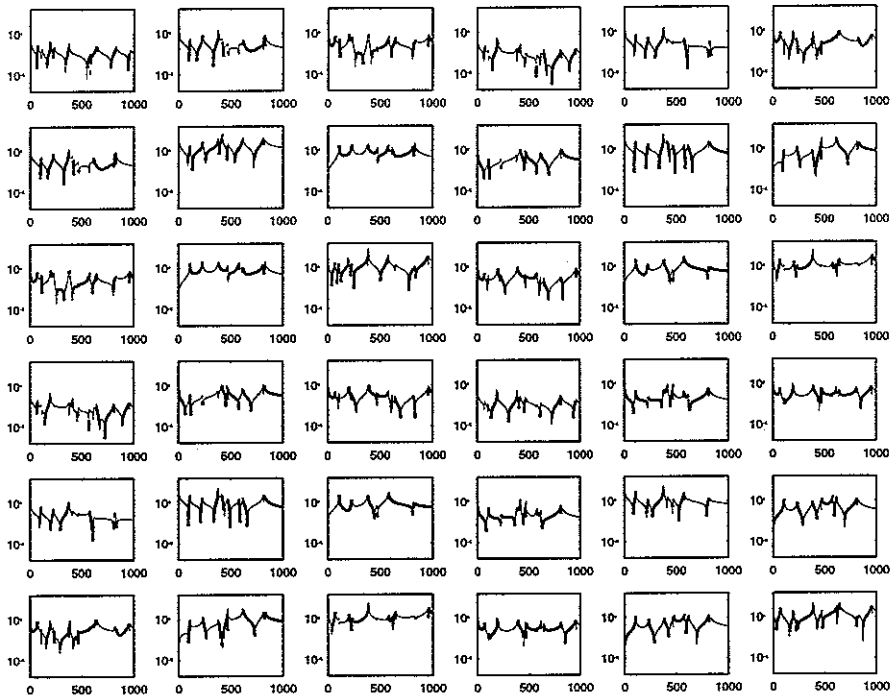

Fig.: 73: *Imaginary part of the 36 driving point and transfer mobilities for a plate having all four edges freely suspended. Solid line: positive values, faint line: negative values.*

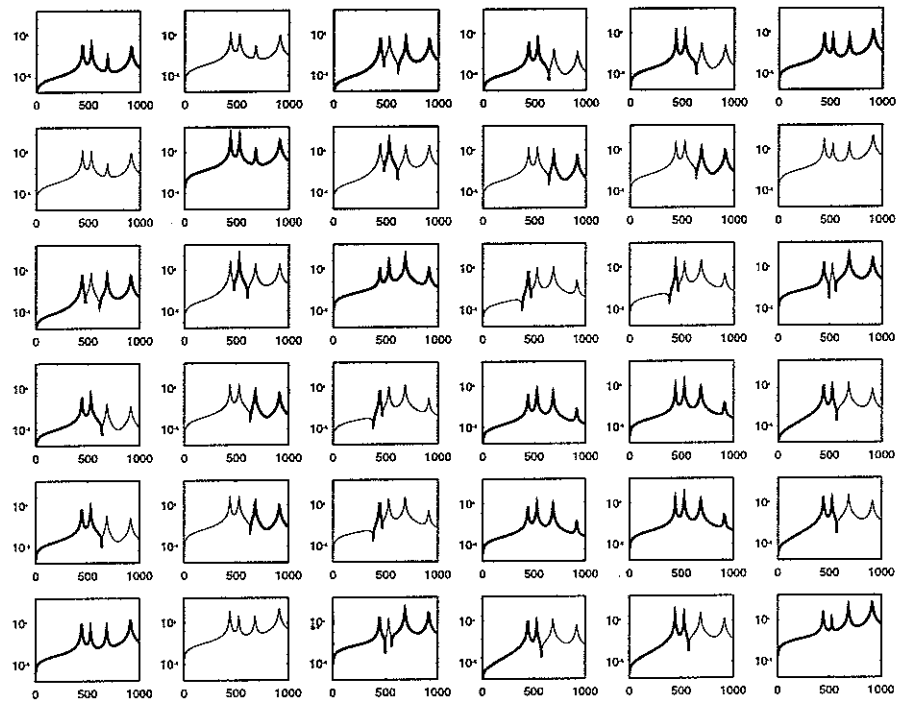

Fig.: 74: *Real part of the 36 driving point and transfer mobilities for a plate having all four edges clamped. Solid line: positive values, faint line: negative values.*

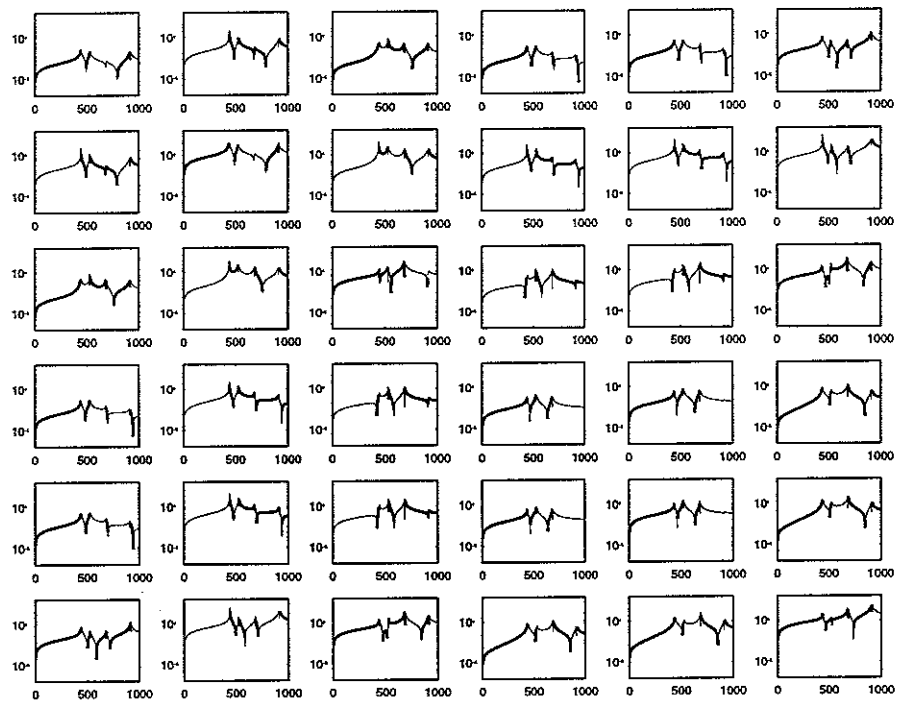

Fig.: 75: *Imaginary part of the 36 driving point and transfer mobilities for a plate having all four edges clamped. Solid line: positive values, faint line: negative values.*

5. CONCLUSIONS

This report presents a detailed description of the driving, point and transfer mobility matrices derived for thin plates excited in flexure. Both mobilities formulae related to an infinite plate and a finite rectangular plate are analysed. The details of the mathematical formulation are given and the procedure presented could be used for other types of bi-dimensional structure like, for example, cylindrical shells. In particular the procedure to derive the mobility formulae for a rectangular plate with any type of boundary condition is shown.

The main properties of the driving-point and transfer mobility matrices are analysed and it is shown that:

a the driving point mobility of an infinite plate gives approximately the mean response of the driving point mobility of a finite rectangular plate;

b the driving point mobility matrix of an infinite plate is a 3×3 diagonal matrix while the driving point mobility matrix of a finite rectangular plate is a fully populated 3×3 matrix except in the particular case of considering the centre position of the plate in which case also for a finite plate the driving point mobility matrix is diagonal;

c the real part of the diagonal terms of the driving point mobility matrix of a finite rectangular plate are all positive;

d for reciprocity, if the system is linear, the transfer matrices between position P_1 and P_2 is equal to the transpose of the transfer mobility matrix between positions P_2 and P_1;

e as a consequence of point *c* and *d* the driving point or driving multi-point mobility matrix is positive definite.

6. REFERENCES

[1] L. Cremer, M. Heckl and E. E. Ungar. *Structure-borne Sound* Springer-Verlag, Berlin 1988 (second edition).

[2] S. S. Rao. *Mechanical Vibrations*. Addison-Wesley Publyshing Company, Wokingham England 1986.

[3] W. T. Thomson. *Theory of Vibration*. Prentice-Hall, Inc., Englewood Cliffs, NJ 1981.

[4] R.E.D. Bishop and D.C. Johnson. *The Mechanics of Vibrations*. Cambridge University Press, London 1960.

[5] D. J. Ewins. *Modal Testing: Theory and Practice*. John Wiley & Sons, Chichester, West Sussex, England 1984.

[6] C. R. Wylie and L. C. Barrett. *Advanced Engineering Mathematics*. McGraw-Hill International Book Company, London 1982 (fifth edition).

[7] J. W. S. Rayleigh. *The Theory of Sound*. Dover Publications, New York 1945 (Vol I, II).

[8] P. M. Morse and K. U. Ingard. *Theoretical Acoustics*. McGraw-Hill International Book Company, New York 1968.

[9] K. F. Graff. *Wave motion in elastic*. Clarendon Press, Oxford 1975.

[10] F. A. Firestone A new analogy between mechanical and electrical systems. *Journal Acoustical Society of America* **4**, 249-267, 1933.

[11] F. A. Firestone. The mobility method of computing the vibration of linear mechanical and acoustical systems: mechanical-electrical analogies *Journal of Applied Physics* **9**, pp 373-387, 1938.

[12] F. A. Firestone. Twixt earth and sky with road and tube; the mobility and classical impedance analogies. *Journal Acoustical Society of America* **28**(6), pp 1117-1153, 1956.

[13] S. Rubin. Transmission matrices for vibration and their relation to admittance and impedance. *Transaction of the ASME Journal of Engineering for Industry*, **86**(1), pp 9-21, 1964.

[14] S. Rubin. Mechanical immitance- and transmission-matrix concepts. *Journal of the Acoustical Society of America*, **41**(5), pp 1171-1179, 1967.

[15] G.J. O'Hara. Mechanical impedance and mobility concepts. *Journal of the Acoustical Society of America* **41**(5), pp 1180-1184, 1966.

[16] C. T. Molloy. Use of four-pole parameters in vibration calculations. *Journal of the Acoustical Society of America* **29**(7), pp 842-853, 1957.

[17] J. C. Snowdon. Mechanical four-pole parameters and their application. *Journal of sound and vibration* **15**(3), pp 307-323, 1971.

[18] V. H. Neubert. *Mechanical impedance: Modelling/Analysis of Structures*. Jostens Printing and Publishing Company, Science Park Road, State College, PA 16801, 1987..

[19] C.M. Harris and C.E. Crede. *Shock and Vibration Handbook*. McGraw-Hill Inc. New York 1976 (Chapter 10 *Mechanical Impedance* by E.L. Hixson).

[20] E. Skudrzyk. *Simple and complex vibratory systems*. The Pennsylvania State University Press, London 1968.

[21] W. Soedel. *Vibrations of Shells and Plates*. Marcel Dekker Inc. New York, 1993 (second edition).

[22] R. G. White and J. G. Walker. *Noise and Vibration*. John Wiley & Sons 1986 (second edition).

[23] R.J. Pinnington. *Approximate mobilities of built up structures*. ISVR Technical Report No 162, University of Southampton 1988.

[24] S. Ljunggren. *Force and Moment Impedance of Infinite Plates*. Swedish Council for Building Research, Stockholm. Internal Report : D3, 1978.

[25] E. Kreyszig. *Advanced engineering mathematics* (seventh edition). New York; John Wiley & Sons 1993.

[26] M.L. Boas. *Mathematical Methods in the Physical Sciences* (second edition). John Wiley & Sons; New York 1983.

[27] M. Abramowitz and I.A. Stegun. *Handbook of Mathematical Functions* (ninth edition). Dover Publications Inc., New York 1972.

[28] O. Bardou, P. Gardonio, S.J. Elliott, R.J. Pinnington Active power minimisation and power absorption in a plate with force and moment excitation. *Journal of Sound and Vibration* **208**(1), pp 111-152. 1997.

[29] P. Gardonio, S.J. Elliott, R.J. Pinnington, Active isolation of structural vibration on multiple degree of freedom systems. Part I: Dynamics of the system. *Journal of Sound and Vibration* **207**(1) pp 61-93. 1997.

[30] Y. K. Koh and R. G. White. Analysis and control of vibrational power transmission to machinery supporting structures subjected to a multi-excitation system, part I: driving point mobility matrix of beams and rectangular plates. *Journal of Sound and Vibration* **196**(4), pp 469-493. 1996.

[31] G.B. Warburton. The vibration of rectangular plates. *Proceedings of the Institute of Mechanical Engineering* Vol **168**, pp 371-384. 1951

[32] A.W. Leissa. *Vibration of plates*. Washington D.C. Office of Technology Utilization, National Aeronautics and Space Administration, Nasa SP-160. 1969.

[33] E.J. Skudrzyk. Vibrations of a system with a finite or an infinite number of resonances. *Journal of the Acoustical Society of America* **30**(12), pp 1140-1152. 1958.

[34] E.J. Skudrzyk. The mean-value method of predicting the dynamic response of complex vibrators. *Journal Acoustical Society of America* **67**(4), pp 1105-1135. 1980.

[35] I. Dyer. Moment Impedance of Plates. *Journal of the Acoustical Society of America* **32**(10), pp 1290-1297. 1960.